INFORMATION TO USERS

This dissertation was produced from a microfilm copy of the original document. While the most advanced technological means to photograph and reproduce this document have been used, the quality is heavily dependent upon the quality of the original submitted.

The following explanation of techniques is provided to help you understand markings or patterns which may appear on this reproduction.

1. The sign or "target" for pages apparently lacking from the document photographed is "Missing Page(s)". If it was possible to obtain the missing page(s) or section, they are spliced into the film along with adjacent pages. This may have necessitated cutting thru an image and duplicating adjacent pages to insure you complete continuity.

2. When an image on the film is obliterated with a large round black mark, it is an indication that the photographer suspected that the copy may have moved during exposure and thus cause a blurred image. You will find a good image of the page in the adjacent frame.

3. When a map, drawing or chart, etc., was part of the material being photographed the photographer followed a definite method in "sectioning" the material. It is customary to begin photoing at the upper left hand corner of a large sheet and to continue photoing from left to right in equal sections with a small overlap. If necessary, sectioning is continued again — beginning below the first row and continuing on until complete.

4. The majority of users indicate that the textual content is of greatest value, however, a somewhat higher quality reproduction could be made from "photographs" if essential to the understanding of the dissertation. Silver prints of "photographs" may be ordered at additional charge by writing the Order Department, giving the catalog number, title, author and specific pages you wish reproduced.

University Microfilms

300 North Zeeb Road
Ann Arbor, Michigan 48106

A Xerox Education Company

73-11,062

CAIN, Charles Alan, 1943-
A CONTROL SYSTEMS STUDY OF THE HUMAN OCULOMOTOR PREDICTIVE TRACKING MECHANISM.

The University of Michigan, Ph.D., 1972
Engineering, biomedical

University Microfilms, A XEROX Company, Ann Arbor, Michigan

THIS DISSERTATION HAS BEEN MICROFILMED EXACTLY AS RECEIVED.

A CONTROL SYSTEMS STUDY OF THE HUMAN OCULOMOTOR PREDICTIVE TRACKING MECHANISM

by
Charles Alan Cain

A dissertation submitted in partial fulfillment
of the requirements for the degree of
Doctor of Philosophy
(Electrical Engineering)
in The University of Michigan
1972

Doctoral Committee:

Professor William J. Williams, Chairman
Professor Spencer L. BeMent
Professor Daniel G. Green
Professor James M. Miller

PLEASE NOTE:

Some pages may have

indistinct print.

Filmed as received.

University Microfilms, A Xerox Education Company

ACKNOWLEDGMENTS

I wish to express my sincere appreciation to my thesis advisor, Professor William J. Williams, for his continuing interest and guidance during the course of this research. Without his encouragement, this work might never have been completed.

I wish to thank Professor BeMent for his many useful suggestions and help in editing the manuscript. I am grateful to Professor Daniel G. Green and Professor James M. Miller for their participation on my thesis committee.

The patience and willingness of my subjects is hereby gratefully acknowledged. The use of computer programs written by John Gesink and Mike Stern was a big help. The help of Aneta Glover in editing and typing the manuscript is appreciated.

I would like to express special appreciation to my wife, Maria, for her encouragement and for the many contributions she has made to the preparation of the manuscript. I would also like to thank my sons, Kent and Jimmy, for the help they gave by being such delightful children.

This research was carried out while I was receiving an N.D.E.A. fellowship (1968-1971) and a fellowship from the Institute for Environmental Quality (1971-1972).

TABLE OF CONTENTS

	Page
ACKNOWLEDGMENTS	ii
LIST OF TABLES	v
LIST OF FIGURES	vi
CHAPTER I: INTRODUCTION	1
1.1 Research Objectives	2
1.2 Applications	4
CHAPTER II: PHYSIOLOGY AND ANATOMY OF THE EYE	6
2.1 The Eye	6
2.2 The Visual Pathways	12
2.3 The Extraocular Muscles	19
2.4 Position Sense and Proprioception	25
CHAPTER III: EYE MOVEMENTS	27
3.1 Types of Eye Movements	27
3.2 Oculomotor Control System Studies	33
CHAPTER IV: EXPERIMENTAL EQUIPMENT AND GENERAL METHODS	38
4.1 Methods of Oculography	38
4.2 Eye Movement Monitor	42
4.3 Target Projection System	46
4.4 Data Recording	49
4.5 Data Analysis	50
CHAPTER V: GENERAL EXPERIMENTAL OBJECTIVES	53
CHAPTER VI: EXPERIMENT 1	58
6.1 Purpose of the Experiment	58
6.2 Description of the Experiment	58
6.3 Experimental Methods	59
6.4 Results of Experiment 1	63
CHAPTER VII: EXPERIMENT 2	68
7.1 Purpose of the Experiment	68
7.2 Description of Experiment 2a	69
7.3 Results of Experiment 2a	70
7.4 Description of Experiment 2b	72
7.5 Experimental Methods (Experiment 2b)	73
7.6 Expected Results for Experiment 2b	74
7.7 Results of Experiment 2b	77
7.8 Discussion of Results	85

Page

CHAPTER VIII: EXPERIMENT 3 89
8.1 Purpose of the Experiment 89
8.2 Description of the Experiment 91
8.3 Experimental Methods 97
8.4 Expected Results 98
8.5 Results 99

CHAPTER IX: EXPERIMENT 4 105
9.1 Purpose of the Experiment 105
9.2 Description of the Experiment 106
9.3 Results 109
9.4 Discussion of Results 142

CHAPTER X: CONCLUSIONS 147
10.1 Summary of Results 147
10.2 Suggestions for Further Research 148

APPENDIX A 152

APPENDIX B 156

APPENDIX C 159

APPENDIX D 162

APPENDIX E 170

APPENDIX F 174

APPENDIX G 178

APPENDIX H 184

BIBLIOGRAPHY 188

LIST OF TABLES

Table		Page
9.1	Controller Parameters for Subject W.W.	133
9.2	Controller Parameters for Subject M.C.	141
E.1	Phase vs. S/N Ratio: Subject W.W.	171
E.2	Phase vs. S/N Ratio: Subject M.F.	172
E.3	Phase vs. S/N Ratio: Subject T.Y.	173
F.1	Magnitude vs. S/N Ratio: Subject W.W.	175
F.2	Magnitude vs. S/N Ratio: Subject M.F.	176
F.3	Magnitude vs. S/N Ratio: Subject T.Y.	177
G.1	Closed Loop Bode Plot Data - Subject W.W.	179
G.2	Closed Loop Bode Plot Data - Subject W.W.	180
G.3	Closed Loop Bode Plot Data - Subject W.W.	181
G.4	Closed Loop Bode Plot Data - Subject W.W.	182
G.5	Closed Loop Bode Plot Data - Subject W.W.	183

LIST OF FIGURES

Figure		Page
1.1	Basic System Configuration	2
2.1	Horizontal Section of the Right Eye	7
2.2	Horizontal Sections Through the Orbit Showing Orbital Contents	8
2.3	Retinal Neural Connections	10
2.4	Visual Pathways	13
2.5	Diagram of the Extraocular Muscles from Above	21
2.6	Diagram of the Muscles from Above Showing the Origin and Insertion of the Superior Oblique	23
2.7	Diagrams Showing the Action of the Extraocular Muscles	24
3.1	Young's Revised Stochastic Model	37
4.1	Schematic Diagram of Eye Movement Detection System	43
4.2	Schematic Diagram of Eye Position Monitor Electronics	45
4.3	Diagram of Target Projection System	47
4.4	Bode Plot of Target Projecton System	48
4.5	A System Frequency Response Extraction Technique	52
6.1	Bode Plot (Single Sinusoids)-Subject W.W.	64
6.2	Bode Plot (Single Sinusoids)-Subject M.C.	65
6.3	Bode Plot - Data and Model Subject M.C.	67
7.1	Amplitude Effects - Subject M.D.	71
7.2	Power Density Spectrum of Noise	74
7.3	Constant Amplitude Signal Corrupted with Increasing Amounts of Noise (S/N Ratios are Ratios of Mean Square Amplitude	75
7.4	Phase vs. S/N Ratio - Subject M.F.	78
7.5	Phase vs. S/N Ratio - Subject W.W.	79
7.6	Phase vs. S/N Ratio - Subject T.Y.	80
7.7	Magnitude vs. S/N Ratio - Subject M.F.	82

Figure		Page
7.8	Magnitude vs. S/N Ratio - Subject W.W.	83
7.9	Magnitude vs. S/N Ratio - Subject T.Y.	84
8.1	Swept Sinusoid Input Waveform and the Eye Tracking Response	92
8.2	Band-limited Random Input Waveform and the Eye Tracking Response	93
8.3	Matched Power Density Spectra for the Swept Sinusoid and the Random Noise Input Waveform	94
8.4	Matched Autocorrelation Functions for the Swept Sinusoid and the Random Noise Input Waveforms	96
8.5	Bode Plots - Subject W.W.	100
8.6	Bode Plots - Subject M.C.	101
8.7	Input-output Crosscorrelation Functions for Subject M.E.	103
9.1	Basic System Configuration	108
9.2	Open and Closed Loop Bode Plots (0% Noise)	110
9.3	Open and Closed Loop Bode Plots (25% Noise)	111
9.4	Open and Closed Loop Bode Plots (50% Noise)	112
9.5	Open and Closed Loop Bode Plots (75% Noise)	113
9.6	Open and Closed Loop Bode Plots (100% Noise)	114
9.7	Open Loop Controller Bode Plot (0% Noise); $C_1(S)$	117
9.8	Open Loop Controller Bode Plot (25% Noise); $C_2(S)$	118
9.9	Open Loop Controller Bode Plot (50% Noise); $C_3(S)$	119
9.10	Open Loop Controller Bode Plot (75% Noise); $C_4(S)$	120
9.11	Open Loop Controller Bode Plot (100% Noise); $C_5(S)$	121
9.12	Open Loop Data and Model (100% Noise)	125
9.13	Open Loop Data and Model (75% Noise)	126
9.14	Open Loop Data and Model (50% Noise)	127
9.15	Open Loop Data and Model (25% Noise)	128
9.16	Open Loop Data and Model (0% Noise)	129
9.17	Phase Plots for $C_\alpha(S)$ when $\alpha = 1, 2$	131
9.18	Plot of Changes in the Parameter τ for Various Random Content	135

Figure		Page
9.19	Root Position Diagram for the Oculomotor Controller Given by Equation (9.4)	136
9.20	Plot of Changes in the Open Loop Zero Frequency Gain with Varying Amounts of Noise	137
9.21	Two Measures of the Controller Gain Bandwidth Product . . .	139
9.22	Single Sine and Swept Bode Plots	146
A.1	Linear System	152
B.1	Linear System	156
D.1	Mechanical Schema of the Oculomotor Plant	163
D.2	Normalized Bode Plot of the Torque Angle Transfer Function of the Oculomotor Plant	166

CHAPTER I

INTRODUCTION

This dissertation is an attempt to examine some aspects of the human oculomotor control system. Eye movements have been studied by numerous investigators for almost a century. However, early investigators could use only subjective methods to measure eye movements. More detailed quantitative studies had to await the development of suitable instrumentation, photographic and electronic recording techniques.

During the past twenty years, engineers and physiologists have applied systems and control engineering theory to the study of eye movements. Fortunately, the oculomotor system is a physiological control system which is relatively easy to excite and observe. System output, eye position and movement, is relatively easy to measure, and its input, motion of a target, can be well specified. Unfortunately, the intermediate sections between input and output are not readily accessible in man. However, by a suitable choice of experiments much can be inferred about internal function through study of input-output relationships.

1.1 Research Objectives

Figure 1.1 is an overall block diagram of the oculomotor control system for continuous inputs. An engineering control

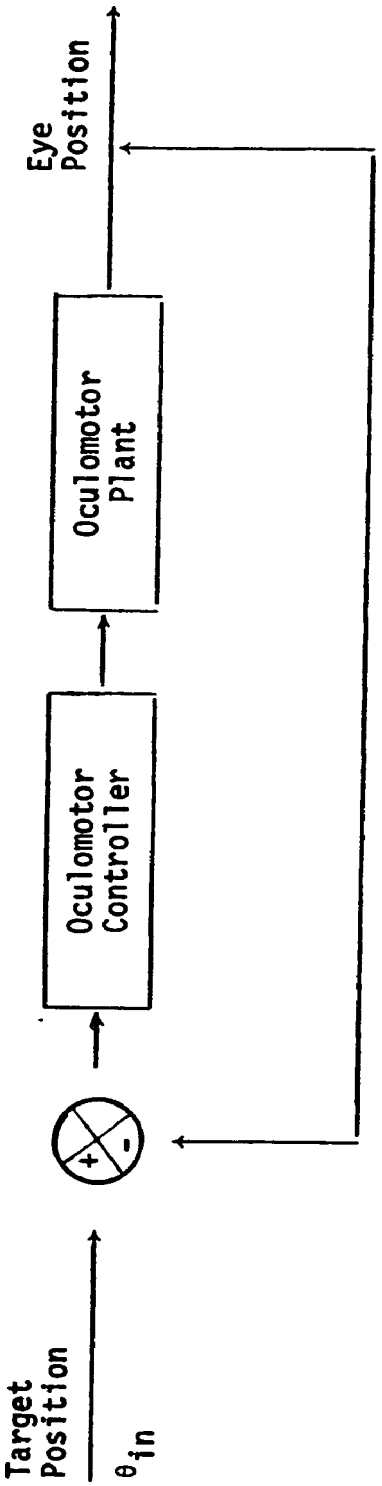

FIGURE 1.1. Basic System Configuration.

system is often described as consisting of two parts, the plant and the controller. The plant is generally assumed to be fixed and may only be controlled by certain control signals. The controller determines how the plant shall be controlled based on information received from the environment and from the plant.

In this thesis, the controlled system (the plant) consists of the eyeball, extraocular muscles and the restraining orbital tissues. The controlling system, which consists of certain elements of the human brain, is called the controller.

One purpose of this dissertation is to discover some aspects of how the eye movement controller adapts itself to changing input parameters. For example, it has been shown (14, 15) that the overall transfer function for the oculomotor control system obtained with certain predictive signals (sinusoids) is different from that obtained using non-predictive inputs. In general, transfer functions obtained with non-predictive inputs have resulted in decreased gain and increased phase lag of the oculomotor control system. However, the non-predictive inputs used in past studies have considerably wider power spectral densities that those of the single sinusoids used as the predictive inputs. Therefore, it is debatable (53, 54) whether the differences in transfer functions are due to differences in spectral content of the signals or to differences in signal predictivity. Experiments described later help solve this particular quandry.

If the system can adapt itself to "predictive" inputs to provide for more optimum outputs, then the dynamics of how the controller changes from a non-predictive mode are of interest. Experimental results concerned with this interesting aspect of oculomotor control will be presented.

This thesis is primarily concerned with the behavior of the oculomotor control system when the inputs to the system are predictive, i.e., when the input target motion waveform contains some pattern which imparts information to the brain concerning future trajectories of the target spot. Of particular interest is how such patterns are used by the brain to cancel normal neural transport delays and the phase lag associated with the dynamics of the oculomotor plant.

Given the system configuration of Figure 1.1, and given a transfer function for the oculomotor plant (eyeball, extra-ocular muscles, orbital tissues, etc.), a mathematical operator approximating the input-output characteristics of the controller can be computed based on the response of the eye (system output) to target motion waveforms (system input). If the system is adaptive, then one can determine how the parameters of the mathematical operator used to describe the oculomotor controller change as certain statistics of the input waveform change.

1.2 Applications

The study of eye movements has engineering importance as well as importance to the physiologist or opthalmologist concerned with vision and the visual process. An accurate description of

the oculomotor control system helps the designer of man-machine systems to determine upper limits on the ability of the human operator to gather information with the eye. The operation of high velocity aircraft and space vehicles are two examples where dynamics of the human operator, and consequently eye dynamics, have extremely important engineering aspects.

Aside from utilitarian considerations, the fact that systems such as the eye movement mechanism exist and are part of our bodies makes them worthy of study. Hopefully such studies will contribute to our knowledge of human information processing and the functioning of that most complex of all systems, the human brain.

CHAPTER II

PHYSIOLOGY AND ANATOMY OF THE EYE

2.1 The Eye

The eye (Figure 2.1) is a globular organ, approximately 12mm in radius, suspended in the orbital cavity by various ligaments and fascial expansions which surround it (Figure 2.2). It is comprised of three coats, from exterior inward: (1) sclera and cornea; (2) choroid layer, ciliary body and iris; and and (3) retina. Light enters the eye through the cornea, the most powerful refractive interface of the optical system. The cornea and the lens focus the incoming light onto the retina, the location of the photoreceptive elements. The shape of the lens is altered during accommodation to change its focal length. The amount of light entering the eye is controlled by the iris, a highly pigmented muscular organ with an opening of variable diameter, the pupil.

The sclera, or white of the eye, is the tough connective tissue skeleton of the globe. It is continuous with the cornea, a transparent window without any blood vessels to hamper the passage of light. The choroid layer is a black-pigmented highly vascularized layer which is both nutritive and light absorbing.

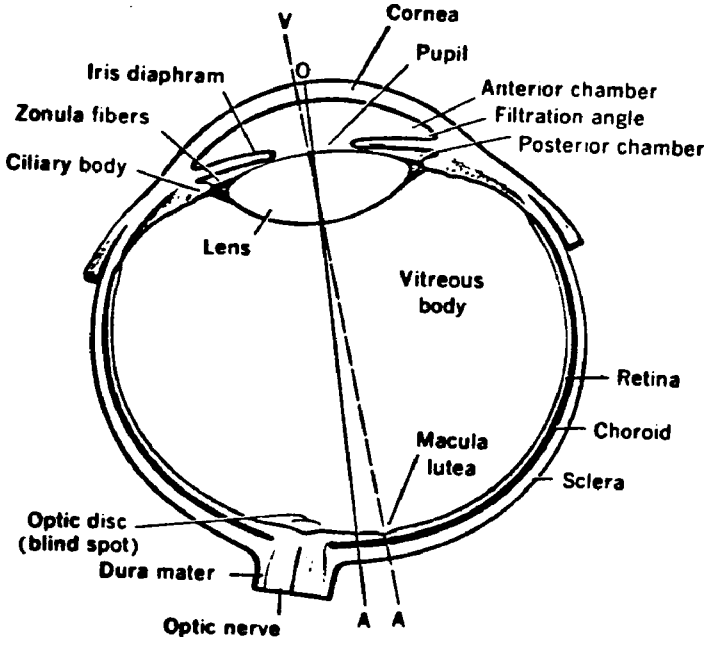

Diagram of a horizontal meridional section through the right eye of man. V.A., visual axis; O.A., optical axis.

FIGURE 2.1. Horizontal Section of the Right Eye.
Source: Noback, C. R., The Human Nervous System, New York: McGraw Hill, 1967.

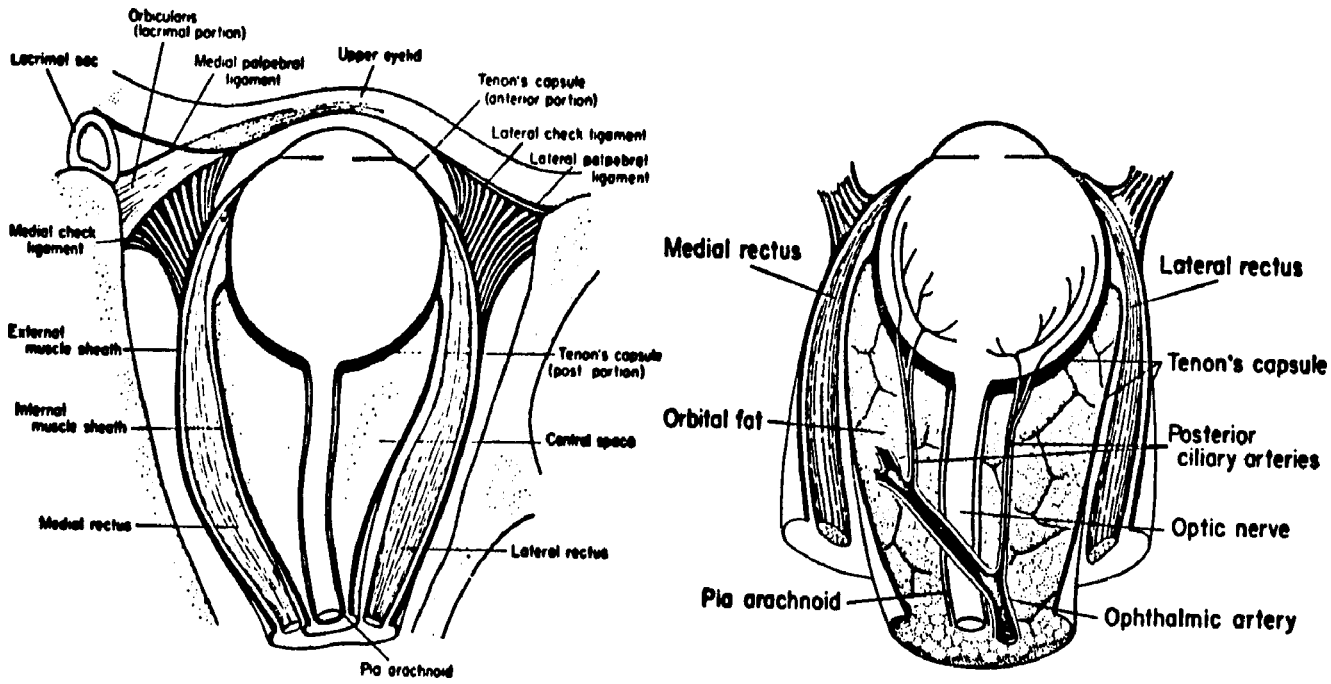

FIGURE 2.2 Horizontal Sections Through the Orbit Showing Orbital Contents.
Source: Francis Heed Adler, Physiology of the Eye, 4th ed. St. Louis, Missouri: The C. V. Mosby Co., 1965.

The ciliary body contains involuntary muscles which control tension exerted on the lens through the zonula fibers (Figure 2.1).

The junction between sclera and cornea forms the limbus, a band-shaped zone 0.75mm to 1.0mm in width. The limbus represents a sharp junction of the white sclera to the colored iris beneath the transparent cornea. Thus the limbus, a convenient landmark on the surface of the eye, is the basis for several techniques for measuring eye movements.

The retina (41, 42), embryologically part of the brain, is composed of several distinct layers (Figure 2.3). Some of the complexity of organization of receptors and nerve cells in the retina is indicated in Figure 2.3. Visual information is transmitted from the rods and cones via the bipolar cells to the ganglian cells whose axons form the optic nerve. In addition, the rods and cones are interconnected by horizontal cells. The bipolar and ganglion cells are interconnected by various amacrine or association type neurons. The system is further complicated by efferent (centrifugal) fibers which direct neural activity back to the receptor and bipolar cells. These complex neural interconnections allow a great deal of information processing to occur in the retina.

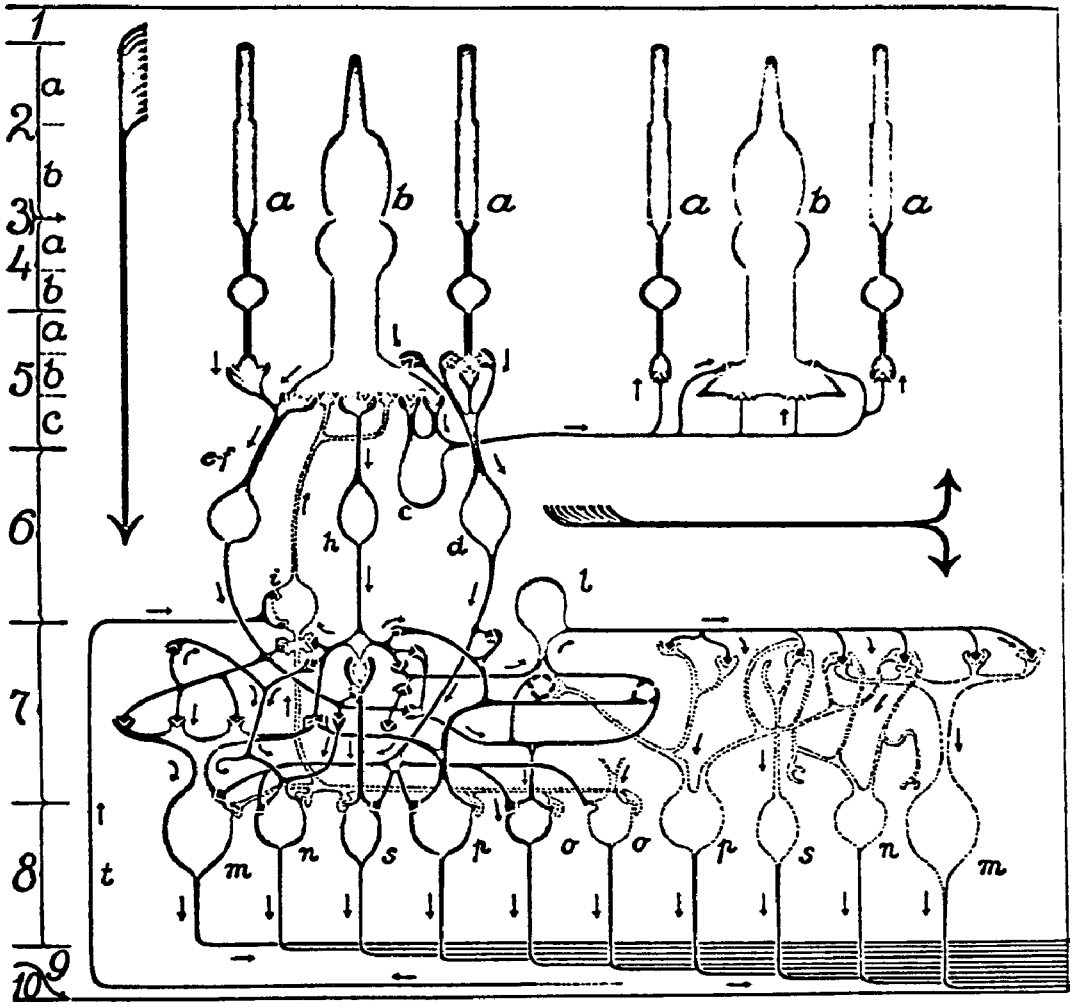

Structure of the primate retina reduced to its essentials, including the synopsis of the propagation of the retinal impulses from the photoreceptors to other parts of the retina, to the brain, and from the brain back to the retina (direction indicated by arrows). The marking of the layers and the zones the same as in (below). Labeling of the cells: a and b rods and cones or the photoreceptors where the nervous impulses are generated by physical light (in the scheme only the left group of the photoreceptors is assumed to be stimulated by light); c, horizontal cells by means of which the impulses are transmitted to the surrounding rods and cones; d, e, f, and h, centripetal bipolar cells of the mop, brush, flat, and midget varieties, which transmit the impulses from the photoreceptors to the ganglion cells, the bipolars serving as analyzers; i, centrifugal bipolar cell, a variety of amacrine cells, which probably receives the impulses from the centripetal bipolars, from the ganglion cells, and also from the brain by way of the centrifugal or efferent fibers, t, and transmits them back upon the photoreceptors, a and b); l, an amacrine cell which possibly intercepts a part of the bipolar impulses and spreads them over the surrounding territory; m, n, o, p, and s, ganglion cells which receive impulses from the centripetal bipolars and transmit them to the brain along their axons celled optic nerve fibers. (From Polyak, S.: The retina, Chicago, 1941, University of Chicago Press.)

Layers are: *1*, pigment epithelium; *2a*, outer segment of rods and cones; *2b*, inner segment of rods and cones; *3*, outer limiting membrane; *4*, outer nuclear layer; *5*, outer plexiform layer (cone-pedicles and rod-spherules); *6*, inner nuclear layer; *7*, inner plexiform layers; *8*, ganglion cells (origin of optic nerve fibers); *9*, layers of optic nerve fibers; *10*, inner limiting membrane. Various cell types are: *c*, horizontal cells; *d*, *e*, *f*, diffuse or polysynaptic bipolar cells; *h*, individual cone (midget) bipolar cell; *i*, *l*, "amacrine cells"; *m*, *n*, *o*, *p*, *r*, *s*, ganglion cells, of which *s* is the individual or monosynaptic ganglion cell. (From Polyak, *The retina*, Chicago, University of Chicago Press, 1941.)

FIGURE 2.3. Retinal Neural Connections.

The light sensitive ends of the receptors are oriented toward the back of the eye. Therefore, light must first pass through the fibers from the ganglion cells, and on through intermediate layers of bipolar cells, amacrine cells, blood vessels, etc., before impinging on the light sensitive rods and cones backed by a layer of flattened light absorbing pigmented cells.

The rods and cones are the visual photoreceptors. The rods, which are more senstive than the cones, have a peak spectral sensitivity to light at a wavelength of about 5050 angstroms (1). The cones, responsible for color vision, are subdivided into three types according to the color of light to which they are most sensitive. The cones' differential sensitivity to light in the red, blue and green portions of the visible spectrum is the basis for the trichromatic theory of color vision (38).

Vision has maximum acuity when the image falls within the fovea, an area on the retina which subtends approximately one degree of the visual field and contains only cones. To illustrate the importance of the fovea, the human fovea contains approximately one cone per two ganglion cells, i.e., for each optic nerve fiber. Across the remainder of the retina there is convergence which in the periphery is enormous. This becomes most evident when one considers that the retina contains 125 million rods and approximately 6 million cones for about 1 million myelinated optic nerve fibers (1).

The existence of a small central area of maximum visual acuity is of prime importance to the evolution of the oculomotor control system in man and other animals. The survival value of a system which accurately and rapidly fixates the image of an object of interest onto a foveal-like area of the retina is readily appreciated.

2.2 The Visual Pathways

The major afferent pathways of the visual system are well known and relatively simple (Figure 2.4). The path of information flow can be outlined as follows: retina-optic nerve-optic chiasm-optic tracts-lateral geniculate body-optic radiations-striate cortex (area 17)-other "higher" cortical visual centers (areas 18 and 19).

In lower vertebrates the entire optic nerve from one retina goes to the contralateral side of the brain, i.e., a complete cross-over of the optic nerve fibers occurs at the optic chiasma. Where some degree of binocular vision exists, as in some higher vertebrates, a portion of each optic nerve projects to the ipsilateral side of the brain. In man (Figure 2.4) the optic nerve fibers from the right half of the retina (representing the left half of the visual field) project to the right lateral geniculate body of the thalamus. Likewise, fibers from the left half of each retina project to the left lateral geniculate body. The fibers cross over at the optic chiasm, the point where the two optic nerves come together.

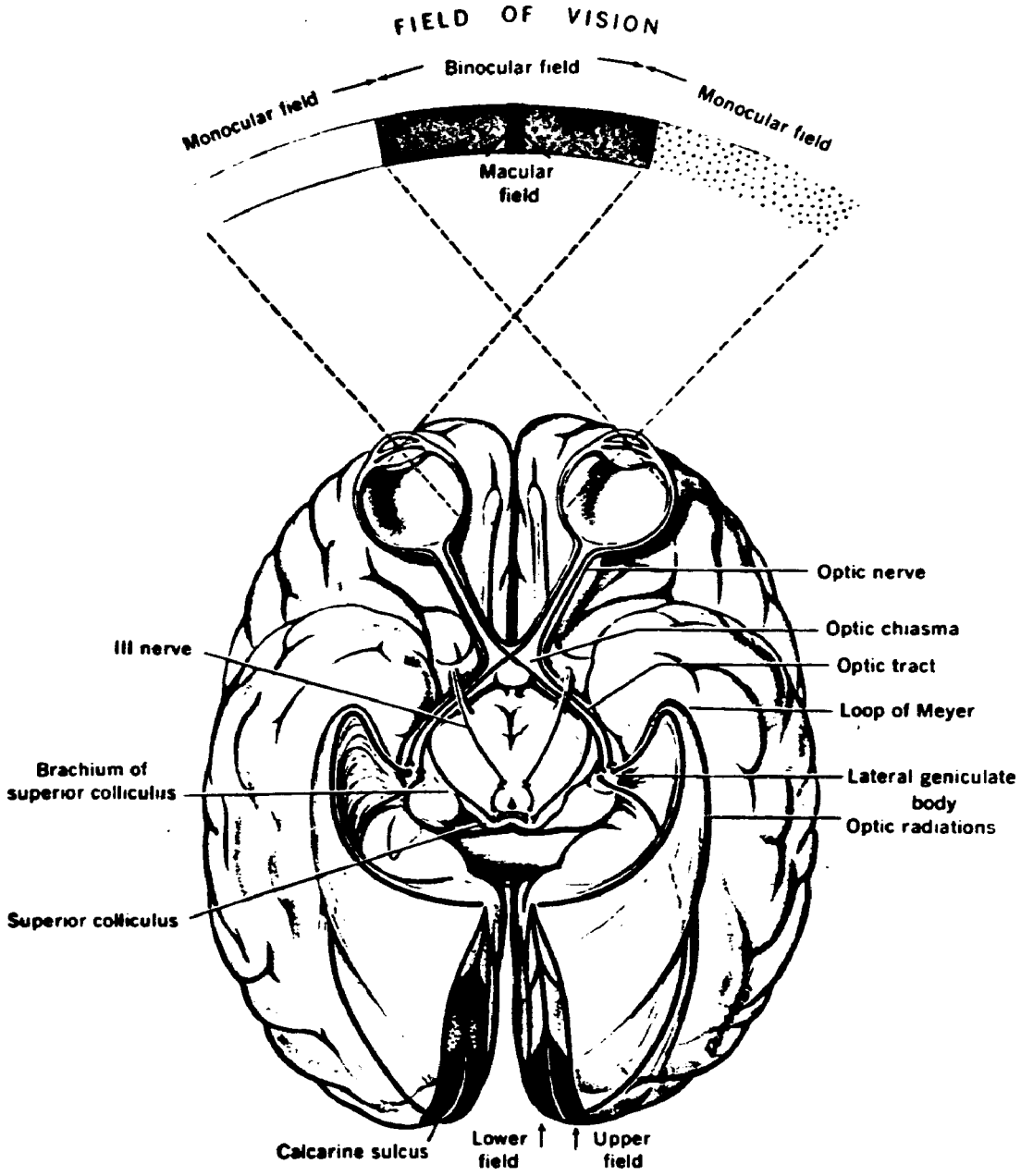

Fig. 2-4. Diagram of the visual pathways from the retina to lateral geniculate bodies and to the primary visual cortex on either side of the calcarine sulcus. The right visual field is projected to the left primary visual cortex (left visual field to right primary visual cortex). The macular field projects to the posterior aspect of the primary visual cortex (solid black). The rest of the binocular field projects to the visual cortex just rostral to the "macular visual cortex." The monocular field projects to the most rostral portion of the primary visual cortex. The upper half of the visual field projects to the primary visual cortex below the calcarine sulcus. The lower half of the visual field projects to the primary visual cortex above the calcarine sulcus.

FIGURE 2.4. Visual Pathways.

By convention, the fibers projecting from the chiasm to the lateral geniculate are called the optic tracts. It should be kept in mind, however, that the visual afferents do not synapse in the chiasm. Optic nerve and optic tract fibers are both retinal ganglion cell axons which synapse primarily at the lateral geniculate body in man. However, some optic tract fibers do project to the superior colliculus and pretectal areas of the midbrain.

In man, the lateral geniculate body (Figure 2.4) consists of six layers (numbered from ventral to dorsal). Layers 1, 4 and 6 receive projections from the contralateral eye and layers 2, 3 and 5 from the ipsilateral eye. Apparently, each fiber in the optic tract projecting to the lateral geniculate body synapses with five or six adjacent neurons within a layer. Some overlapping occurs because the number of neurons in the lateral geniculate is not greater than the number of optic tract fibers (40).

The geniculocalcarine tract (optic radiations, Figure 2.4) is the pathway from the lateral geniculate body to the primary visual cortex (area 17 or striate cortex). Apparently all the geniculate neurons project to the visual cerebral cortex (40).

From the lateral geniculate body to the visual cortex a process of divergence begins, as opposed to the primarily convergent process observed in the retina. Hence, the number of neurons in the striate cortex receiving inputs from geniculate neurons far exceeds the number of neurons in the lateral

geniculate body. There appears to be general agreement today that a precise point-to-point projection of the retinal surface on the visual cortex exists. As might be expected, the small macular (foveal) areas of the retina have a disproportionately large cortical representation (see Figure 2.4).

The striate, or visual cortex (Brodmann's area 17), located in the extreme occipital lobes, represents the primary sensory receiving area for visual stimuli. As illustrated in Figure 2.4, the left and right visual fields are represented in the right and left occipital lobes, respectively. In man, area 17 appears to be a crucial relay station in the visual pathways leading to perception and higher visual functions. Thus, complete destruction of area 17 in man leads to total loss of vision. It should also be noted that area 17 is the site of the initial integration of the information from half of each eye, i.e., the act of fusion of the visual fields from both eyes commences in the striate cortex. Hence, a specific neuron in the striate cortex can be stimulated by a spot of light on a specific site of one retina as well as by a spot of light focused only on the equivalent site in the other eye. The concept of fusion of the visual fields is important to the consideration of binocular vision, depth perception, vergence eye movements and conjugate eye movements.

The primary visual cortex (area 17) is integrated with other regions of the cortex, primarily area 18 and area 19 of the

hemispheres of the same and of opposite sides through the corpus callosium. Area 18 is most often described as having an associative function. People with lesions in area 18 might see an object clearly, but are unable to name the object or to describe its function (visual agnosia). Also, areas 18 and 19 are thought to have motor functions. In particular, they are thought to be involved in following movements and fixation of the eye. Stimulation of area 18 causes eye movements often accompanied by movements of the head. Area 18 receives efferent fibers from area 17 and produces afferents going to area 19 and the frontal structures which are thought to be involved in voluntary eye movements. Area 18, in the right hemisphere, is connected by means of cross-commissural fibers to area 18 of the left hemisphere, and vice versa (63). The functions associated with area 19 in general, are similar to those of area 18, i.e., largely associative and motor.

Much of what is known about the visual sensory system is the result of studies of the organization of receptive fields of cells in the retina, fibers in the optic nerve, Lateral Geniculate Body (LGB) neurons and cells in the visual cortex. If, while exploring the retina with a small spot of light one records from single cells at any place in the visual system, whenever the light falls within a certain small well defined area of the retina, the firing pattern of the cell from which one is recording will be modified. This retinal area comprises the

receptive field of the cell. By probing the retina with light and recording from single cells at various levels in the visual pathway, it is possible to map out receptive fields.

In general, receptive fields for retinal ganglion cells and LGB neurons are relatively simple and are formed from circular or concentric fields. Most commonly, stimulation of the central portion of the field induces cell firing ("on" discharges), and in the peripheral portion inhibits activity or causes discharges when the stimulus light is extinguished ("off" discharges). Illumination of the entire receptive field usually activates cells, as does a diffuse light flashed to the entire visual field.

In contrast to the above, most cells in the visual cortex do not respond at all to large or diffuse spots of light. In general, the receptive fields of cells in the visual cortex are not concentric or circular but tend instead to be rectangular or edge shaped. In addition to shape, the orientation of the receptive field and movement of the appropriate shape across the field, are important variables.

Particularly striking are the studies of Hubel and Wiesel (27, 28, 29, 30, 31) of receptive fields of cortical neurons in the cat. They found that cells of the visual cortex respond to edges or boundaries of particular shapes, sizes, positions, and orientations, only if the stimulus shapes move in particular directions.

Hubel and Wiesel made a distinction between "simple" and "complex" receptive fields. In general, complex fields differ

from simple fields in that a stimulus is effective whenever it is placed in the field, provided that the orientation is appropriate. Simple fields require the stimulus to have a specific location as well.

It is thought that complex cells receive their inputs from many simple cells. The cellular structure of the visual cortex seems to support this hypothesis. Hubel and Wiesel found that neurons of the visual cortex are grouped with precision into columnar segments which extend through the entire thickness of the cerebral cortex perpendicular to the surface (30, 31). Apparently, each vertical segment receives connections from a small group of lateral geniculate neurons via the optic radiations. An "on" field (or an "off" field) is comprised of the long narrow columnar segments with an "on" region adjoining an "off" region. It is not difficult to imagine how a group of neurons in the lateral geniculate body all having concentric receptive fields (oriented along a straight line on the retina) could connect with a columnar segment to form an edge shaped receptive field in the cortex. By similar reasoning, columnar segments having cells with "complex" receptive fields could be constructed from outputs of neurons having "simple" receptive fields. In this way increasingly complex and abstract aspects of stimulus quality could be coded by single nerve cells, each such cell dependent on a whole hierarchy of connections proceeding

from cells with complex receptive fields down to cells having the simple circular fields.

Hubel and Wiesel (31) studied the stimulus properties that will activate cells in areas 18 and 19. A majority of the cells in these areas were found to be of the "complex" type. In addition, some cells in area 18 and many in area 19 were given the designation "hypercomplex." Apparently, hypercomplex cells not only require a given orientation for a stimulus lying within a visual field but also a given length of the stimulus edge. Some "higher order hypercomplex" cells were even responsive to given lengths of lines forming corners or angles. Further study of this increasing order of complexity in the neural processing of visual information is bound to play a fundamental role in the ultimate understanding of the abstract concept of visual "perception."

2.3 The Extraocular Muscles (1, 17, 63)

Each eyeball is moved by six extrinsic striated muscles innervated by three cranial nerves. The abducens nerve (VI) innervates only the lateral rectus muscle while the trochlear nerve (IV) innervates only the superior oblique muscle. The oculomotor nerve (III) innervates the four remaining extraocular muscles: the medial rectus, inferior oblique, superior rectus, and inferior rectus. These muscles act in reciprocally innervated pairs to move the eyeball about its approximate geometric

center; the stimulated agonist contracting to pull the eye while the more inhibited antagonist opposes the motion with less force. The extraocular muscles are capable of rotating the globe approximately 45° left or right, 40° up, 60° down, and 30° in torsion (rotational motion around the optic axis).

The axes of rotation of the individual muscle pairs do not lie in mutually perpendicular planes. When the line of sight is in the horizontal plane looking straight ahead (the primary position of the eye), the lateral and medial rectus mediate purely horizontal movements. However, from the primary position, the action resulting from use of either of the two remaining muscle pairs is a complex composite of vertical, horizontal and torsional (rotational) movements. Hence most eye movements result from a complex interaction of more than one muscle pair.

The superior and inferior recti are involved primarily in vertical eye movements. Their insertions are very nearly in the vertical plane of the eye. However, their lines of action make an angle of about 23° with this plane (see Figure 2.5). Thus movements resulting from the contraction of these muscles can only be purely vertical when the the globe is turned through an angle of 23° to the temporal side. Otherwise, the action of this muscle pair results in a movement with vertical, horizontal and torsional components.

The superior and inferior oblique muscles are the only extraocular muscles having insertions in the posterior hemisphere

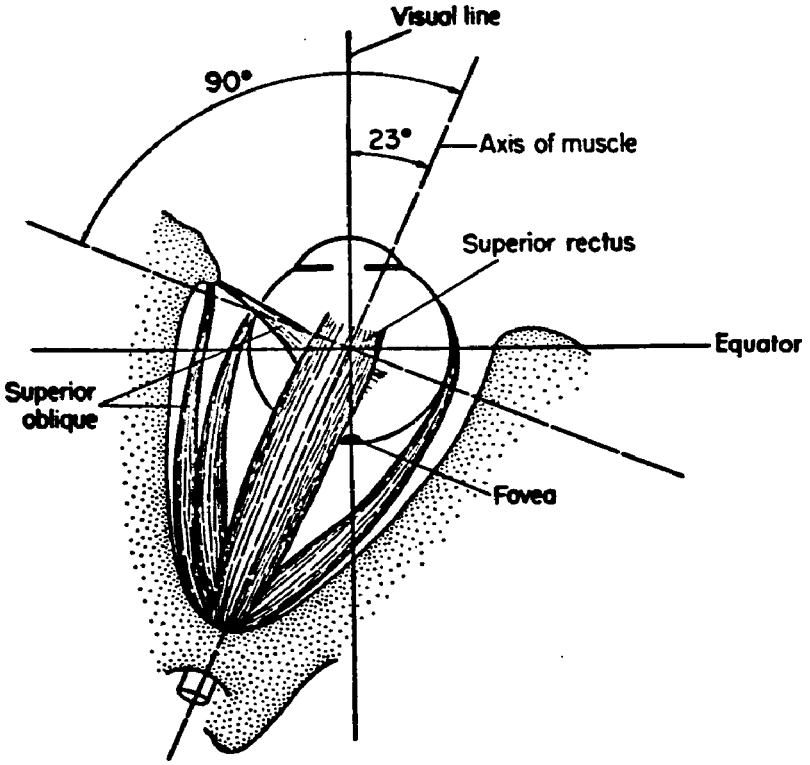

Diagram of the muscles seen from above, showing the origin and insertion of the superior rectus.

FIGURE 2.5. Diagram of the Extraocular Muscles from Above.
Source: Francis Heed Adler, Physiology of the Eye, 4th ed., St. Louis, Missouri: The C. V. Mosby Co., 1965.

of the globe in a plane forming an angle of 51° with the vertical plane of the eye (see Figure 2.6). If the eye of Figure 2.6 is turned 51° nasally, such that the line of action is parallel to the line of sight, the muscles will produce purely vertical motions. Likewise, the action of the obliques is purely torsional if the line of action of the muscles is normal to the line of sight (eye turned temporally through 39°). Since none of these special conditions is normally encountered, the actions of the obliques almost always have vertical, torsional and horizontal components.

The activity of each of the ocular muscles is depicted diagrammatically in Figure 2.7. In this Figure, the arrows are drawn to depict the movement components resulting from the contraction of each muscle when the line of sight is in the primary position. The direction of the arrows gives the direction of the movement. The length of the arrows gives some idea of the comparative effectiveness of each of the various components.

The extraocular muscles are extremely fast acting, having the shortest reaction time of any muscles in the body, and are relatively large in comparison with the mass they must move. Furthermore, one motoneuron innervates from two to five extraocular muscle fibers, whereas in the larger skeletal muscles the ratio of nerve fibers to muscle fibers is about 1:120 (1). The skill and precision of the movements performed by an neuromuscular system vary inversely with the size of the motor unit.

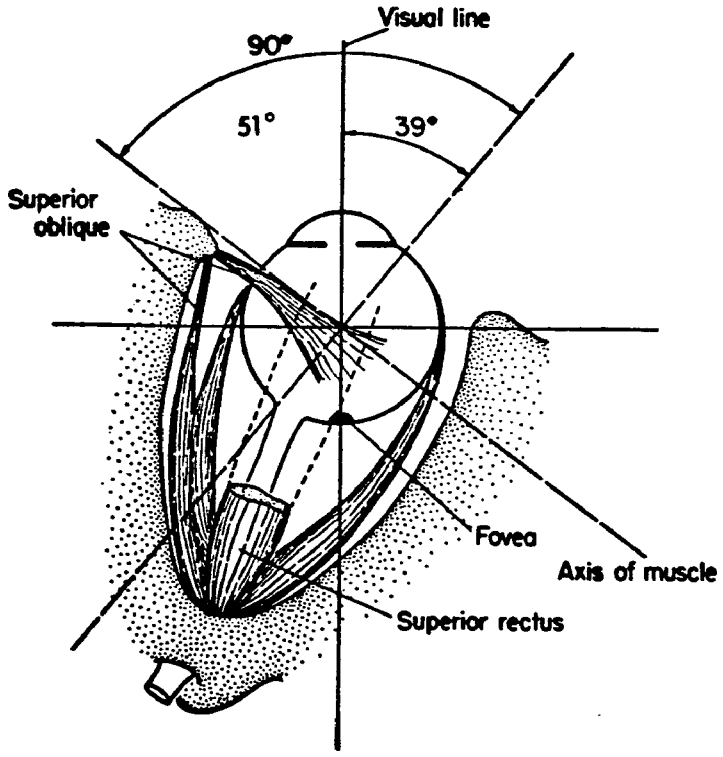

Diagram showing the origin and insertion of the muscles from above, with the superior rectus cut away. The physiologic origin of the superior oblique is at the trochlea.

FIGURE 2.6. Diagram of the Muscles from Above Showing the Origin and Insertion of the Superior Oblique.
Source: Francis Heed Adler, Physiology of the Eye, 4th ed., St. Louis, Missouri: The C. V. Mosby, 1965.

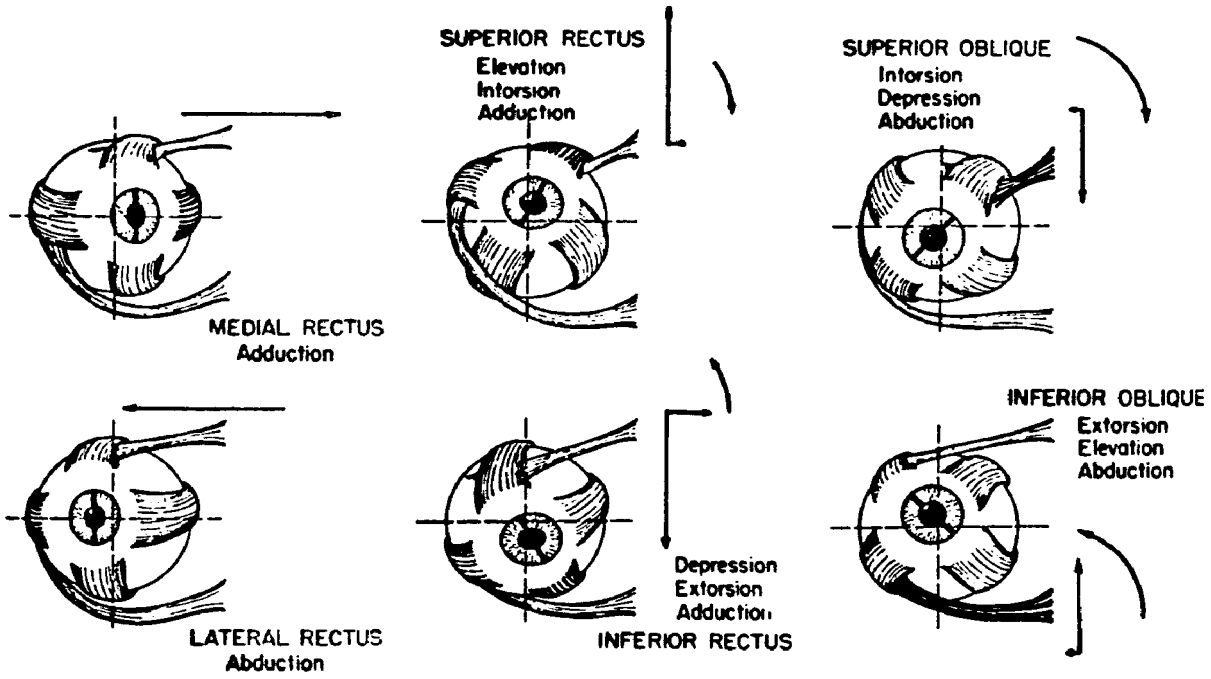

A. Diagram illustrating the antagonistic action of the lateral and medial recti.

B. Diagram illustrating the antagonistic action of the superior and inferior recti.

C. Diagram illustrating the antagonistic action of the superior and inferior obliques.

FIGURE 2.7 Diagrams Showing the Action of the Extraocular Muscles. Source: Francis Heed Adler, Physiology of the Eye, 4th ed., St. Louis, Missouri: The C. V. Mosby, Co., 1965.

Hence, the extraocular muscles are fast acting, not easily fatigued and capable of very precise finely graduated movements.

2.4 Position Sense and Proprioception

The subject of proprioception in the extraocular muscles has been one of considerable interest in the history of eye movement physiology. It is of obvious interest to those using feedback control system theory in the study of oculomotor functions.

Helmholtz believed that awareness of eye movements results from knowledge of the efferent commands sent to the eye muscles. This central monitoring of eye movements has been called the "outflow" or "efference copy" theory of eye position sense. However, Sherrington felt that awareness of eye position results from sensory afferent discharges from proprioception in the muscles themselves; this is termed the "inflow theory."

Some investigators claim to have found nerve endings resembling muscle spindles, tendon-organs and other types of sensory receptors in human extraocular muscles (9, 10, 16, 60). However, the question is complicated by the fact that no muscle spindles can be found in the ocular muscles of the cat, rabbit or dog (17).

In darkness, it is generally considered that man lacks conscious eye position sense. The anesthetized eye can be rotated up to 40° by external manipulation in the dark with the subject unaware of the motion. Therefore, if proprioceptive feedback exists, it is thought to provide unconscious reflexive feedback to the CNS about extraocular muscle tension and velocity of contraction. In fact, proprioception is an essential factor in all phases of a muscle's activity and, in the case of the delicate movements performed by the eye, proprioception would seem even more necessary than in other types of muscle performing more gross functions.

CHAPTER III

EYE MOVEMENTS

3.1 Types of Eye Movements

Eye movements can be separated into four classifications: reflexive movements, versional (or conjugate) eye movements, vergence movements, and movements which occur during fixation of staionary targets.

Reflex, or compensatory, eye movements may be produced by movements of the head or by direct stimulation of the semi-circular canals (1). Compensatory movements produced by vestibular stimulation move the eye in a direction opposite to head motion and, therefore, tend to provide a stable platform for the visual system. Constant stimulation of one of the semi-circular canals (as when a subject is rotated on a platform) results in a rhythmic movement of the eyes called vestibular nystagmus. Nystagmus consists of the eye's slow deviation from the primary position opposite to the direction of head rotation followed by a rapid recovery movement (saccade) back to the primary position. This sequence of events is repeated continuously resulting in a almost periodic jerk-like rhythm.

Nystagmoidal eye movements may be elicited by movement of the visual field with respect to the subject. Rotation of a drum with vertical stripes in a subject's field of view will result in an eye movement pattern similar to vestibular nystagmus. Such movements are called optokinetic (or railroad) nystagmus. Regardless of the similarity of the two patterns of eye movements, it appears that two separate mechanisms are involved. Vestibular nystagmus is elicited easily with the eyes closed and may be abolished selectively by means of streptomycin (4) leaving the optokinetic response intact. Furthermore, optokinetic nystagmus ceases immediately upon cessation of movement in the visual field. Vestibular nystagmus, however, continues for a short time after rotation of the subject ceases. This after-nystagmus is responsible for the illusion that the world is in motion about the subject although he is no longer being rotated. The neural pathways responsible for vestibular nystagmus are thought to be simple reflex pathways involving only the sensory organs in the semicircular canals, the vestibular nuclei and the motor nuclei in the brainstem subserving eye movements (63). Optokinetic nystagmus, however, apparently originates in the cerebral cortex (1).

Vergence movements (2, 44, 45) involve motion of the two eyes in opposite directions. They rise in binocular vision in order to maintain the image of an object on corresponding regions of the two retinas as the object-to-eye distance varies.

Convergence is the nasally directed movement of both eyes as a subject attempts to fixate on a target moving in from optical infinity. Divergence movements result when the object of interest moves away from the eyes. These movements are smooth and much slower than other types of eye movements, taking up to a full second to change fusion from a far to a near field object.

Versional (or conjugate) eye movements result when both eyes move simultaneously in the same direction, to maintain binocular fixation of an object of interest (1, 2). In order to maintain perception of a single image it is necessary that the eyes move together, not only in vergences, but also in versions. In general, a moving object approaching the eyes requires both versions and convergences; one receding from the eyes requires versions and divergences. Diplopia, or double vision, results with dysfunction of either version or vergence mechanisms.

The two main types of versional eye movements of primary concern in this study are the saccade and the smooth pursuit movement. The saccade is a rapid versional flick-like movement through which the eyes change from one discrete fixation point to another. The time course of a saccadic response to a step target displacement is composed of a latent period (response

time) of 120-250 ms followed by a period of rapid acceleration and then a longer period of deceleration (66). The velocity of a saccade increases with amplitude and may reach a mixiмum of 600° /sec for very large excursions (60). After the initial saccade, there are often secondary saccades to correct for positional errors (3). The duration of the saccade is approximately linearly related to amplitude, a 15° saccade requires about 45 ms to complete,while a 30° saccade requires around 75 ms. Saccadic movements rarely occur more often than every 200 ms. However, under unusual conditions they can occur as frequently as every 75 ms (49).

During the course of the saccadic motion, the visual threshold is raised by a factor of approximately 3 (57). The visual suppression begins approximately 50-80 ms before the eye begins to move and achieves maximum suppression approximately 20-40 ms before the eye begins to move (70, 35).

Smooth pursuit movements occur when the eye tracks a smoothly moving target having a velocity of less than about 25 to 35°/sec (66). It is interesting to note that smooth pursuit movements normally do not occur in the absence of a moving object of interest. Hence, they are said to be semivoluntary. One study suggests that the necessary prerequisite for pursuit eye movements is an "image" at the cortical level, i.e., a cerebral image rather than a retinal image. This would account for such movements occurring during sleep (18).

Pursuit movements occur following a latent period of about 125 ms and range in velocity from 1 to 30°/sec. Pursuit movements tend to be a series of constant velocity segments when tracking a nonpredictable target. However, the movements become more continuous in nature when the target motion is predictable (14, 50).

In the past, most investigators have agreed that the primary function of pursuit movements is to match angular eye velocity with target velocity (44, 66). Saccadic movements, meanwhile, are thought to correct for position errors resulting from the displacement of the target image from the fovea. However, recent studies indicate that smooth pursuit movements also tend to correct position errors, even in the absence of target motion (55). Furthermore, smooth pursuit movements are not capable of matching target velocity with much accuracy (43). This calls into question certain models (66, 67) which assiduously separate saccadic and smooth pursuit eye movements into separate functional classifications, position error correctors and velocity trackers respectively.

Eye movements during fixation of a stable target, all having amplitudes less than 0.5 deg., fall into three classifications (20, 21, 46, 55).

1) Rapid "flicks" or saccades occurring at intervals as small as 0.2 sec. apart. These flicks tend to maintain the

fixation point within the 1° foveal field, i.e., such movements tend to correct for position errors in fixation. The amplitude of movement ranges from 1 to 25 min. of arc but averages about 6 min. of arc.

2) Slow drifts about the point of fixation with an average amplitude of about 5 min. of arc and with an angular velocity of about 1 min. of arc per sec. Until recently, drifts have been considered a form of noise having no correlation with position error. However, a study by St. Cyr and Fender (55) shows that drifts are not entirely noise but serve to correct vergence errors. The net effect of drifts and flicks is that the image stays within a foveal area roughly 50 microns in diamter (about 10 min. of arc).

3) High frequency tremor, a rapid movement with appreciable power at all frequencies up to about 80 Hz and an amplitude of about 5 to 15 sec. of arc. for horizontal and vertical movements (21, 25).

These involuntary eye movements of steady fixation seem to be a necessary part of normal vision. If they are "stopped" by stabilized image techniques, the fixated object disappears from view (19, 65). Some investigators report a periodic return of the image and relate this to a possible slippage in the stabilization apparatus (19). Others claim evidence that image fading is not purely a factor of the photoreceptor stimuli (37).

However, Yarbus claims a complete fading of the image with a method that eliminates all mechanical slippage (65).

3.2 Oculomotor Control System Studies

In the past fifteen years, the oculomotor control system has been extensively studied by those investigators interested in applying linear systems analysis techniques to biological control systems. This section is a brief review of some of this work.

As early as 1903, Dodge (22) was able to draw a distinction between saccadic and smooth pursuit movements. Since then the evidence has mounted to support the notion that these two types of ocular activity are subserved by two distinct neurological pathways. For example, the inability to make controlled smooth pursuit movements in the absence of moving visual stimuli has already been mentioned. Also, in certain pathological conditions, patients are incapable of smooth pursuit tracking of any target (58) while maintaining saccadic movement capabilities. Rashbass (44) claims to have shown selective pharmacological interference in smooth pursuit movements by barbiturates. Furthermore, by using a step-ramp stimulus, Rashbass (44) has shown that the smooth pursuit system attempts to match eye and target velocity. Although, in so doing, the eye must actually move away from the target position (the target jumps in one direction and simultaneously begins constant velocity movement

in the other). However, Puckett and Steinman (43) have shown that smooth pursuit tracking is a function of subject motivation and subject training. Furthermore, they show that smooth pursuit movements do not track velocity nearly as well as Rashbass claimed. This may imply that, instead of two different neurological pathways, distinctions between smooth pursuit and saccadic movements may be due only to factors affecting subject motivations.

In 1961 Fender and Nye (25) were among the first to model the eye movement control system using feedback control system theory. They postulated three feedback loops: proprioceptive (velocity), oculomotor (position), and retinal image (position). While the nature of oculomotor proprioception in man is open to question, Fender and Nye were the first to employ variable retinal image feedback to the study of the oculomotor control system.

In 1962, Dallos (14, 15) studied the "learning behavior" of the eye motion control system by comparing the frequency response curves obtained from predictable sinusoidal inputs and unpredictable Gaussian random noise target movements. This study was the first to show the effects of target predictability on the oculomotor control system frequency response characteristics.

Also in 1962, Young (52, 66, 67, 68) presented a sampled data system model which appeared to be a good first order approximation to the saccadic tracking system. The model could explain

certain saccadic responses to pulse and step inputs. Young also reported a definite peak in the frequency response curves at about 2.5 Hz for unpredictable target motions. He interprets this peak as representing the power from saccadic eye movements occurring approximately every 200 ms during active tracking. Young's model incorporates several nonlinear elements, including a dead zone, a limiter and saturation elements.

Young assumed that the smooth pursuit system is also a sampled data system and served by the same sampler as the saccadic system. However, Robinson (50), used a double ramp input to show that the pursuit eye movement control system could make changes temporally spaced by the same time as target rate changes for spacings as low as 75 ms. This is much less than the approximately 200 ms sampling period required to explain saccadic phenomena. By eliminating saccadic eye movements from the feedback signal, Robinson also performed variable feedback experiments involving only the pursuit system. He observed only smooth continuous changes in pursuit eye movement response and, therefore, concluded that the pursuit eye movement control system is continuous rather than sampled.

Wheeless (62) found that, in cases where a pulse input elicited no response, the pulse had not gone unnoticed by delayed response to an immediately following step input in the opposite direction by an average of 40 ms. This result is inconsistent with Young's sampled data model.

To meet these and other objections, Young (67) presented a revised stochastic sampled data model for eye tracking movements (Figure 3.1). His revised model, however, fails to explain the eye tracking system's dependence on such input variables as amplitude, spectral content, or target predictability. As Fender (53) points out, Young's inclusion of nonlinear elements in the model would predict significant harmonics not detected by Fender's experiments.

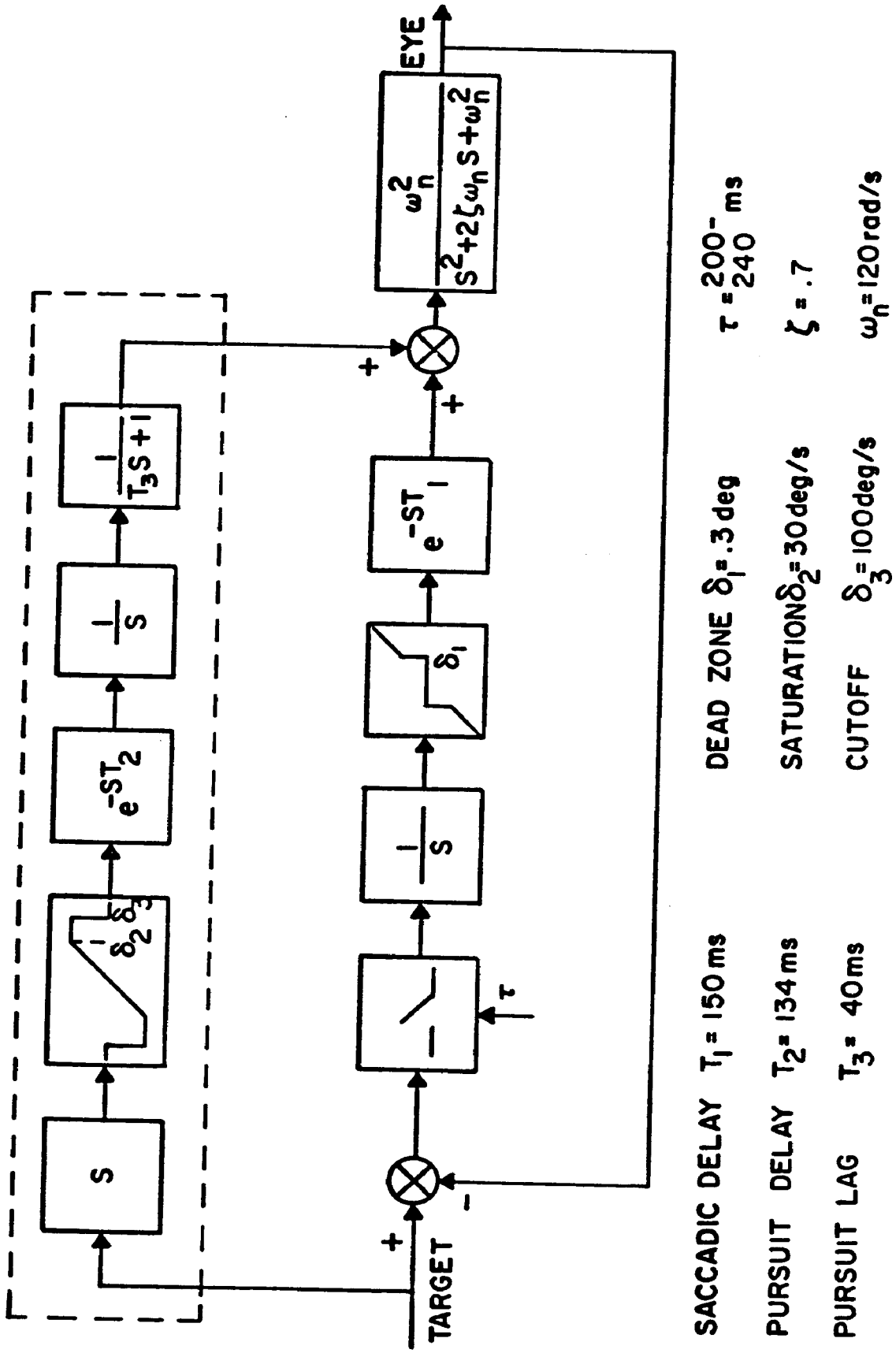

FIGURE 3.1. Young's Revised Stochastic Model.

CHAPTER IV

EXPERIMENTAL EQUIPMENT AND GENERAL METHODS

This dissertation is an engineering study of the oculomotor control system based on information obtainable from observing both the input and the output of the control system. Here, the input is defined as the movement waveform of a spot of light projected onto a circular screen. The output is defined as the observed movement (or response) of the eye as it attempts to track the target spot. This chapter discusses methods of projecting the input and detecting the output. In particular, methods of measuring eye movements (oculography) and apparatus for projecting a moving target spot onto a screen are discussed. A discussion of data recording and data analysis techniques is also presented.

4.1 Methods of Oculography

There are many methods of measuring eye position. Much of the early work was done by directly observing eye movements or by subjective measurements. Early quantitative studies of eye movements used the method of after images on the retina. This very subjective method permitted the detection of eye movements up to ±45° with a resolution of .5°, however, it yielded no permanent or continuous record of eye movements.

At the turn of the century, Huey (32) and Delabarre (13) developed ingenious mechanical recording techniques for the measurement of eye position. Since the process involved fitting a plaster cast to the eyeball, less painful methods were soon devised.

Dodge and Cline (23) were first to develop a photographic technique for measuring eye movements; the photographic techiques have been continuously refined. However, all such methods share the same disadvantages: namely, the tediousness of processing the records and the delay involved in developing the film.

A common photographic method was to obtain a photographic recording of a spot of light reflected off the cornea (21). Since the cornea forms an eccentric bulge on the eyeball, the bright spot on the cornea moves as the eye moves. This method has the advantage of showing vertical as well as horizontal components of eye motion. The method has a linear range of about ±12° with a sensitivity of about 0.2° of arc. However, it is extremely sensitive to head movement, a major disadvantage of the method.

The contact lens method is perhaps the most sensitive way for recording eye motion (11). By placing a small mirror on the contact lens, an incident beam of light can be reflected onto a moving photographic film. The resolution can be as great as 10 sec. of arc.

Robinson (48) embedded a set of coils in a contact lens to measure horizontal, vertical and torsional eye movements simultaneously. The coils were exposed to two magnetic fields in quadrature in order to get an electrical output signal. A sensitivity of 15 sec. of arc with a linear range of ±20° is reported. Suction was used to avoid slippage.

All contact lens methods share the disadvantage of having to place foreign objects on the eye. Furthermore, the contact lens adds to the inertia of the eyeball and is prone to slippage, especially during large saccadic eye movements. Suction techniques (48, 65) avoid lens slippage. However, suction causes the intraocular pressure to rise, limiting the duration of experiments to less than thirty minutes.

A potential difference exists between the cornea and retina of the eyeball (5, 6, 33). If electrodes are placed on the skin around the eye, then rotation of the eyeball "dipole" will cause a detectable potential between the electrodes. However, these potentials, on the order of 100 micro-volts, are often corrupted by artifacts such as large muscle action potentials and varying skin-electrode potentials. Hence, electro-oculography (EOG), as this method is called, is usually restricted to a minimum resolution of approximately .5°. While eye motions of up to ±45° have been recorded using this method, the linear

range is small. Calibration maps must be constructed for such large eye movements. Electro-oculography has certain advantages: namely, it requires no bright lights or foreign object on the eye and strict immobility of the head is not required.

Several electronic eye movement monitoring techniques have been developed in recent years. These methods can usually be classified into two types: 1) sensitive differential reflection techniques using photoelectric devices for position detection and 2) scanning techniques.

All differential reflection techniques (24, 66, 68, 61, 51) depend on the detection of the iris-scleral boundary, the limbus, and converting this information into a voltage via photoelectric devices. Since the iris reflects less light than the sclera, movement of the eye will cause a change in the intensity of light falling on a correctly positioned photodetector. This method has the advantage of providing a continuous output voltage proportional to eye position which can be easily recorded. Also, no foreign objects must be placed on the eye. The method is limited in its frequency response characteristics only by the bandwidth of the associated electronics. The maximum range depends only on the visibility of the limbus. Sensitivity is limited only by electronic noise and variations in ambient light. Although each realization of this method is somewhat different (see above references), most have a linear range of greater than ±15° and a resolution greater than 15 min. of arc.

Several scanning techniques have been devised. Cornsweet (12) developed a system which scans a spot of light rapidly across the eye. A photomultiplier detects the light reflected off the eye. By measuring the time from the onset of a sweep to the time the spot reaches the limbus, eye position can be computed. This timing information is provided by the output of the photodetector since the iris reflects less light than the sclera. Rashbass and Westheimer (45) used a variation of this "flying spot scanner" technique and were able to achieve a resolution of 6 min. of arc.

4.2 Eye Movement Monitor

Except for minor changes, the eye movement monitor used for the experiments in this study was the differential reflection apparatus described by Feinstein (24). This method depends upon detection, as the eye moves, of the difference in diffuse reflected light from the limbus (iris-scleral junction). Figure 4.1 shows the arrangement of the two light source-photodetector pairs. These are mounted on specially constructed eye glass frames worn by the subject. Since the iris is darker than the sclera, it is clear from Figure 4.1 that the amount of reflected light received by each photodetector is a function of the angle of gaze. Also, when the light input to one photodetector increases, the input to the other decreases. By amplifying

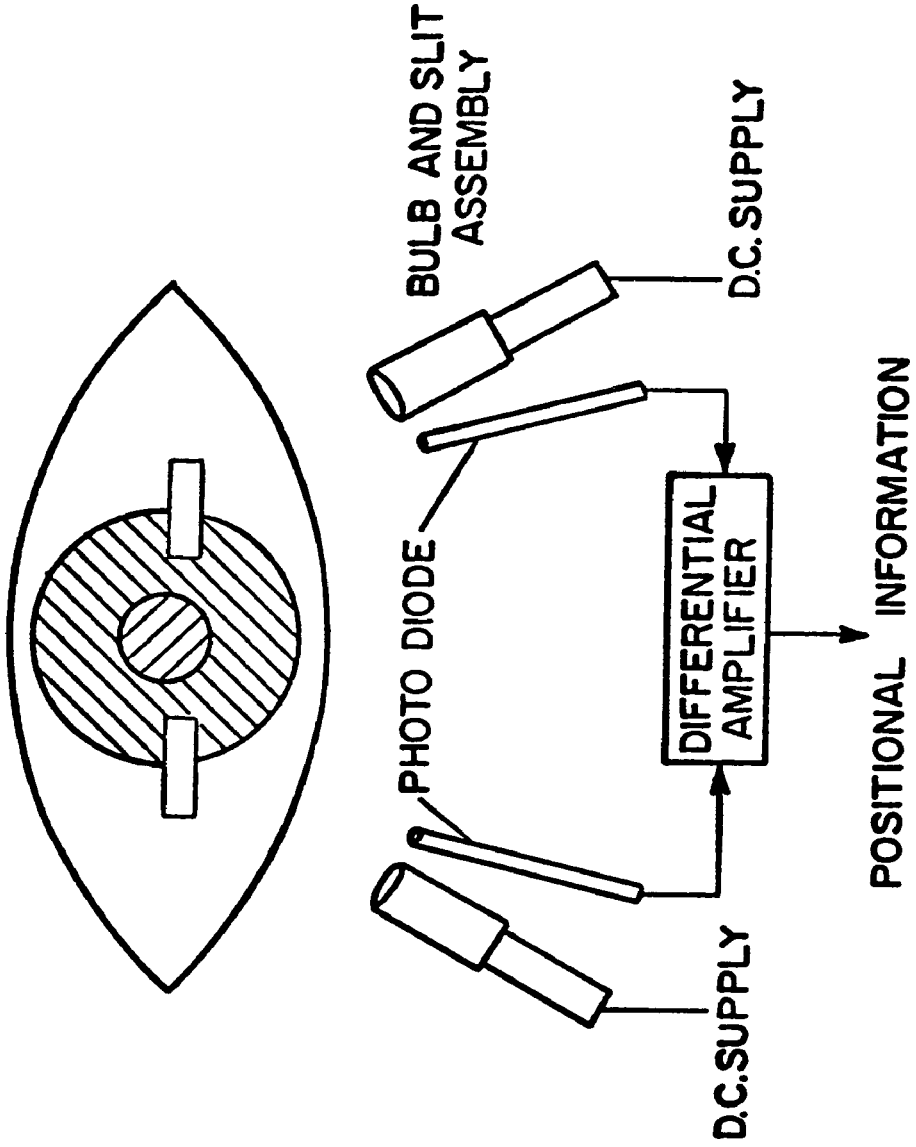

FIGURE 4.1 Schematic Diagram of Eye Movement Detection System.

the output of the two detectors differentially, the effects of any nonlinearities or changes in ambient light or temperature are minimized.

The light sources for the eye monitor glasses were 15 volt grain of wheat bulbs. Each slit projector consisted of a bulb enclosed in a brass tube containing a pinhole and a slit, both optically arranged to project a well defined slit of light onto the limbus.

The photodetectors were photodiodes[1] with maximum sensitivity at 0.9 mu in the infrared. This made it possible to place infrared filters (Kodak Wratten 89B) over the light-slit projectors, thus eliminating any annoying glare on the subject's eye from the light sources. The filters resulted in no effective reduction in detection sensitivity.

Figure 4.2 is a complete schematic of the photodiode detector and amplifier circuit. Each photodiode is reverse biased by 9.5 volts and forms the input to an emitter follower. The outputs of the emitter followers provide the inputs to a differential amplifier. When the light-slit projectors and associated photodiodes are correctly adjusted, the output of the differential amplifiers is a voltage proportional to eye position.

The eye movement monitor has a frequency response from D.C. to greater than 10 kHz. The resolution is a function of the

---

[1]Texas Instrument LS-400.

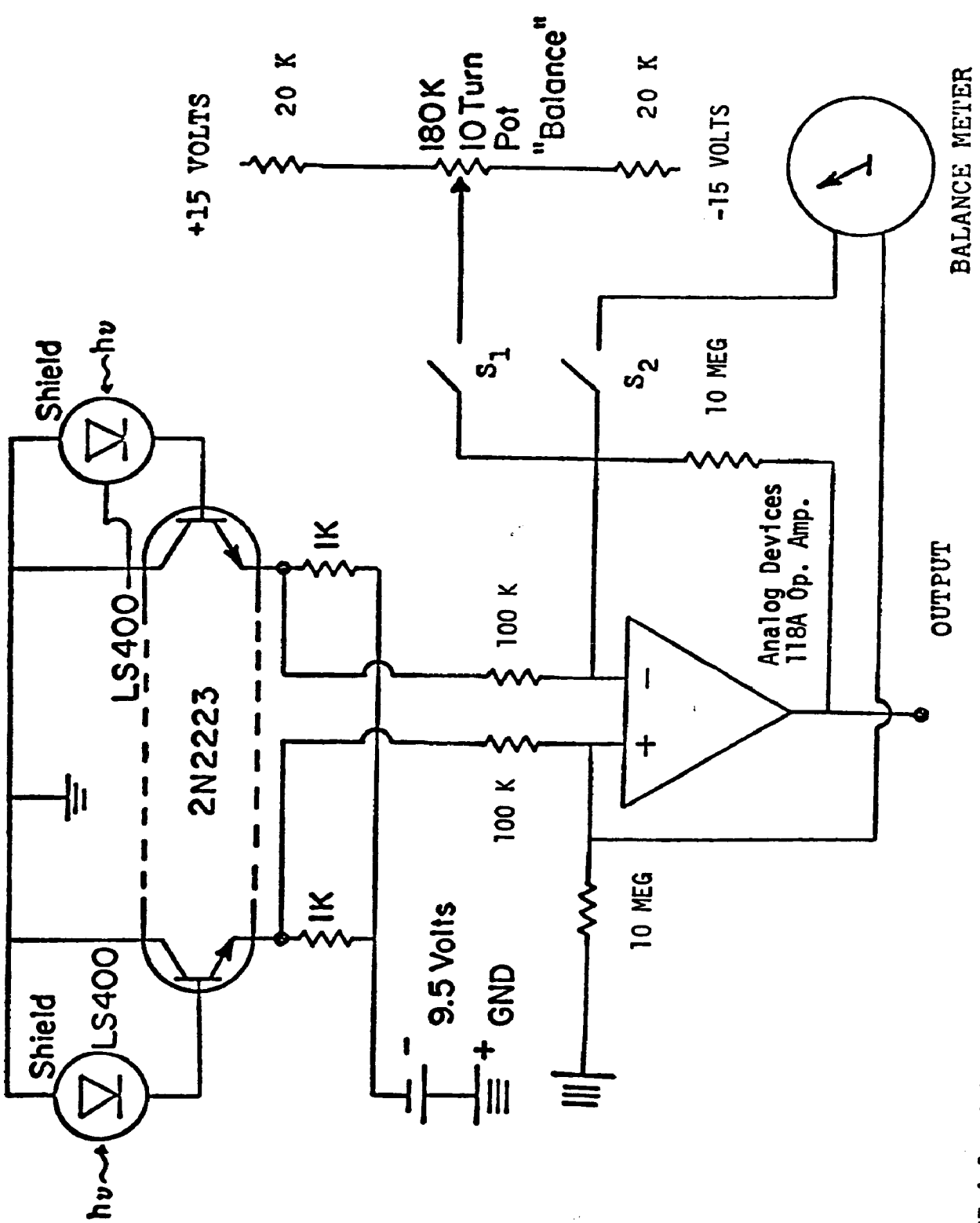

FIGURE 4.2. Schematic Diagram of Eye Position Monitor Electronics.

dynamic range. With a dynamic range of ±28°, resolution is better than .5°. With the monitor adjusted for a dynamic range of about ±5°, horizontal resolution of about 5 min of arc can be obtained. Most of the experiments reported in this study used the latter adjustment.

4.3 Target Projection System

The target projection system consists of a 500 watt slide projector and a Harvard Apparatus #350 recorder galvanometer. A one-inch round front surface mirror mounted on the galvanometer moves the target across a semicircular screen having a radius of 5 feet, located in a darkened booth. The subject sits in a chair located at the screen's center of curvature. Immobility of the subject's head is assured by use of a bite board rigidly supported by the chair. A diagram of the target projection setup is given in Figure 4.3.

The galvanometer is capable of moving the target across the screen with a linear dynamic range of ±40° horizontally. The mirror-galvanometer setup is a third order system with a 3 db cutoff frequency of approximately 60 Hz. A Bode plot of the target projection system is shown in Figure 4.4. The data were obtained for a displacement of ±20° which is equivalent to a target velocity of 2400°/sec at 60 Hz. The size of the target spot in all experiments was 0.25°.

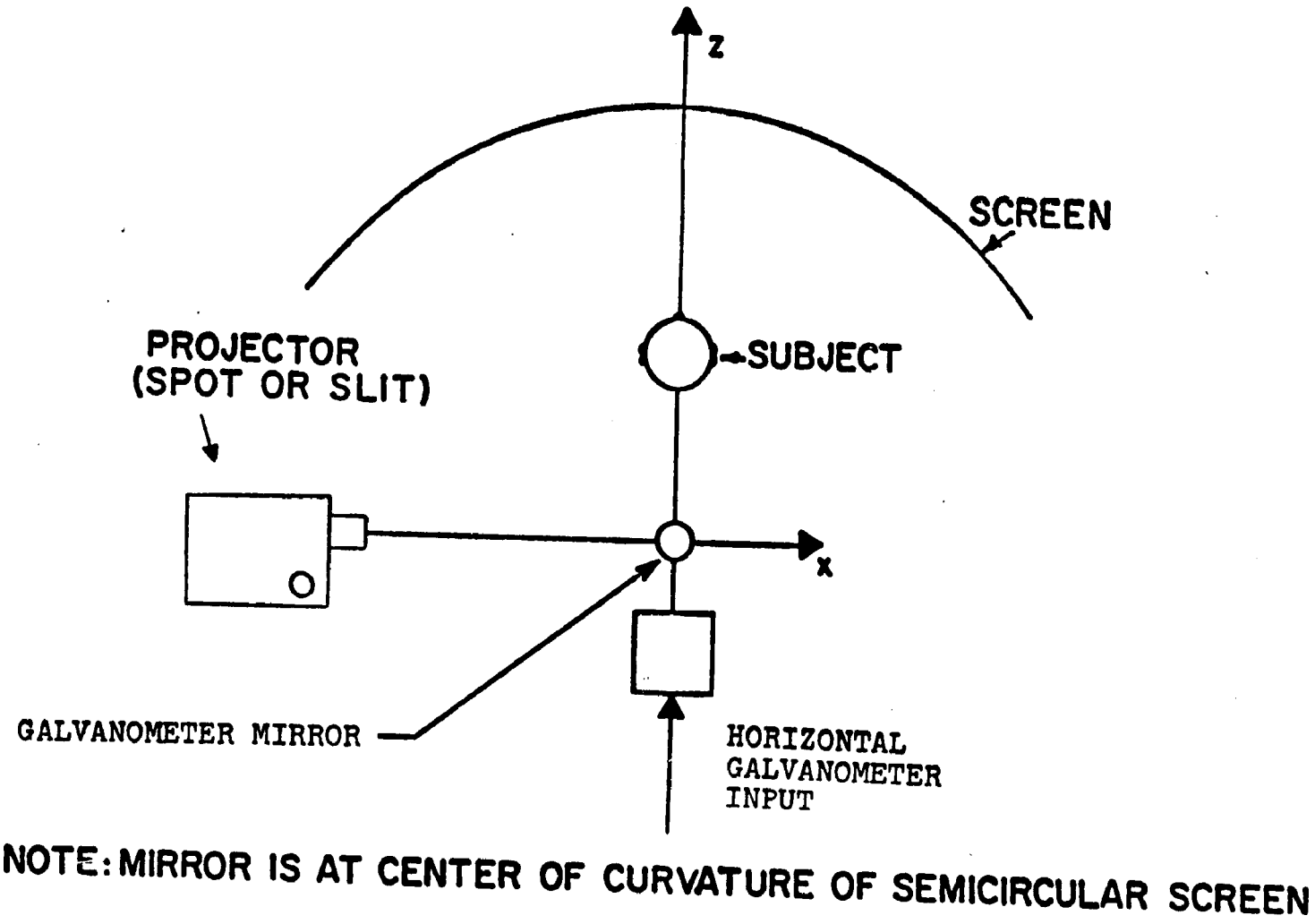

FIGURE 4.3. Diagram of Target Projection System.

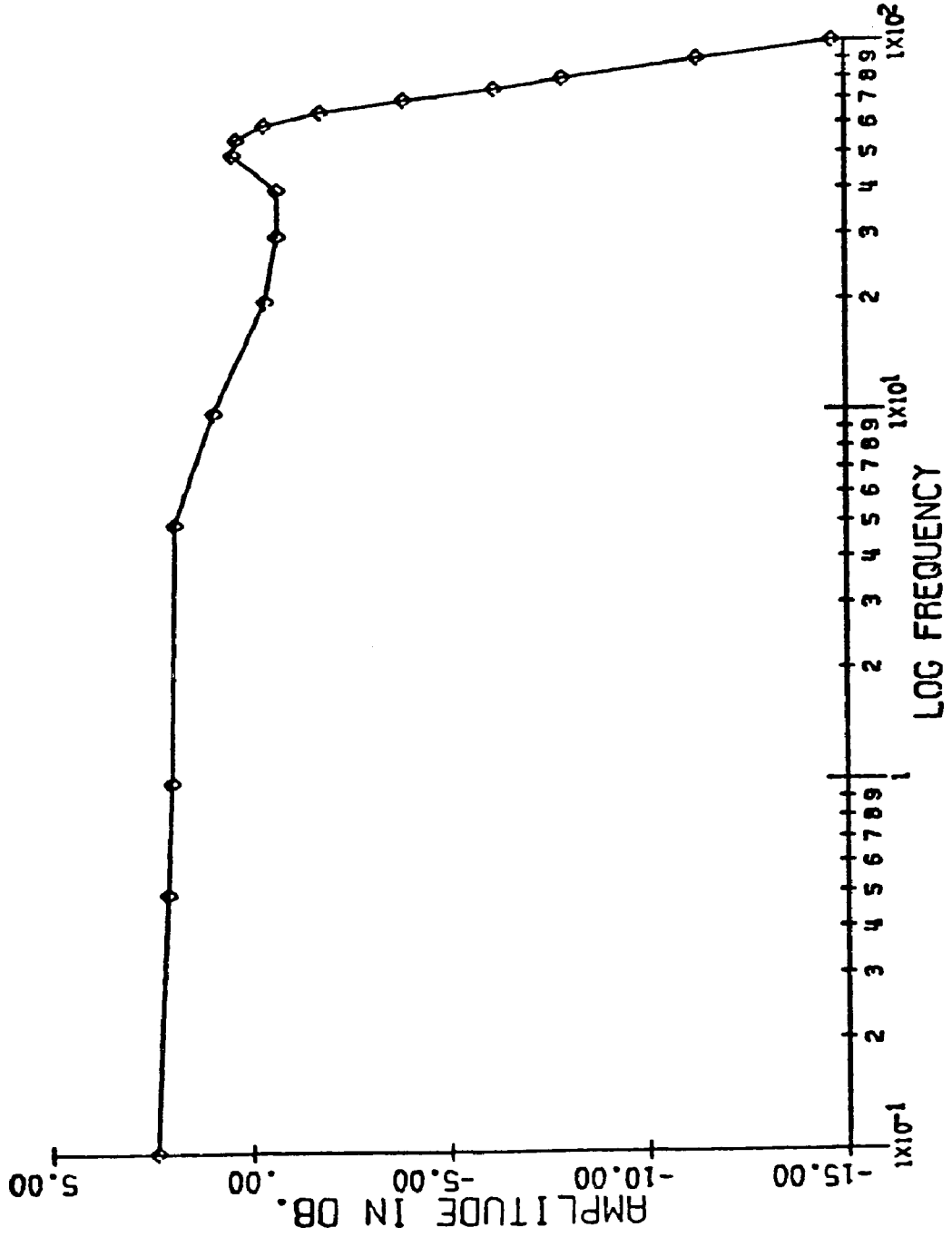

FIGURE 4.4. Bode Plot of Target Projection System.

4.4 Data Recording

All experimental data were recorded on an HP 3960 FM tape recorder at 3-3/4 IPS. The input (stimulus waveform) was recorded on another channel. Calibration was accomplished by using the following procedure:

1) The target projection apparatus was adjusted in gain until the ±1 volt square wave calibration signal caused the target spot to deflect ±5° of arc. Each recorded input waveform used as a stimulus was preceded by this calibration signal.
2) To calibrate the eye monitor amplifier gain, the subject was asked to fixate carefully on the ±1 volt (±5° on the screen) calibration square wave. The square wave was of low frequency (0.2 Hz) giving the subject plenty of time to obtain good fixation.
3) The calibration signal and the subject's response were both recorded on adjacent channels on the HP 3960 FM recorder. If the amplitude of the calibration signal is known, then the amplitude of the subject's response can be determined.
4) To minimize the effect of blink artifact and prevent saturation of the FM input channels, both

channels (stimulus and response) were adjusted for 90% modulation at an input of ±1 volt (equivalent to ±5° of arc) and the input to the response (eye monitor) channel was clipped at the 100% modulation level. Otherwise, blink artifacts would easily saturate (over modulate) the FM channel. Peak amplitude of the stimulus rarely exceeded ±5° of arc.

The input to the target projection apparatus and the output of the eye monitor were continuously monitored by a Sanborn 296 strip chart recorder.

The HP 3960 tape recorder has tape monitor outputs on all channels. These were monitored continuously with a storage oscilloscope to assure that input and output data were being recorded properly.

4.5 Data Analysis

The Bioelectrical Science Laboratory has a HP2115A computer equipped with an analog to digital (A-D) convertor. A set of programs have been developed based on the Fast Fourier Transform (FFT) algorithm for computing discrete Fourier transforms. By sampling analog data with the A-D convertor, these programs allow a wide range of data analysis. Using these programs, one can compute the Fourier transform of a waveform segment and, hence, both the power density spectrum and autocorrelation function. The cross-power

density spectrum of two waveforms can be computed from which the cross correlation function is obtained. Using wide-band input waveforms, a system transfer function can be extracted by computing the input-output cross-power density spectrum (see Appendix B and Figure 4.5).

Figure 4.5 explains diagrammatically how a linear system transfer function can be obtained using one example of a wide-band input time sequence; in this case, a linearly swept sinusoid. Other wide band signals can also be used; for example, the use of a band limited Gaussian process will be discussed in Chapter VIII.

The IBM 360 computer of the Michigan Terminal System (MTS) was used for some data computations and for plotting results using a set of Calcomp programs developed by personnel of the Bio-electrical Science Laboratory.

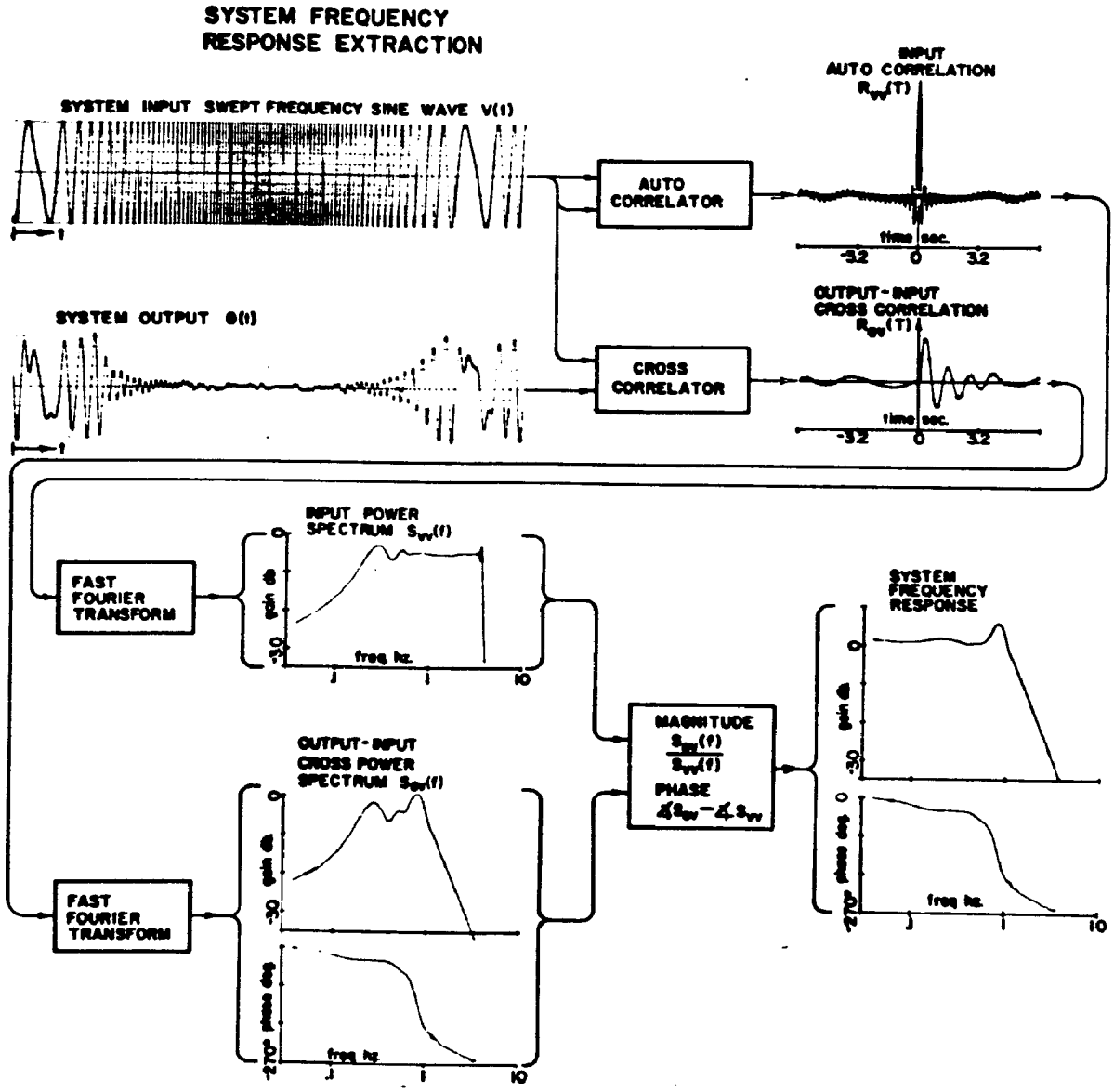

FIGURE 4.5. A System Frequency Response Extraction Technique.
Source: Williams, W. J.; Gesink, J. W.; and Stern, M. M., "Biological Transfer Function Extraction Using Swept Frequency and Correlation Techniques." Medical and Biological Engineering (In Press.)

CHAPTER V

GENERAL EXPERIMENTAL OBJECTIVES

Certain background information has been discussed in the preceding chapters. At this point, after our discussion of experimental methods, it seems worthwhile to discuss the objectives of the experiments to be presented in this study.

In a preliminary experiment (Experiment 1), the oculomotor responses to single sinusoids are analyzed by crosscorrelation techniques to obtain gain and phase information sufficient to determine the frequency response characteristics of the oculomotor control system for single sinusoid inputs. The crosscorrelation technique is a very powerful way of extracting such information when the response is greatly attenuated and corrupted by noise. The mathematical basis for the method will be outlined.

In Experiment 2 the nature of the nonlinearities of the system are explored. The mathematical definition of a linear system is given and experiments to test this definition for the oculomotor control system are discussed. In particular, Experiment 2a was devised to determine if the system is highly sensitive to amplitude scaling of the input stimuli. Experiment 2b was devised

to determine if the superposition principle holds for the oculomotor control system. Experiment 2b also was devised to explore the performance characteristics of the predictive tracking mechanism as a function of input signal-to-noise (S/N) ratios. The results of the experiment shed some light on how the brain implements the predictive tracking mechanism.

In the past, frequency response profiles of the oculomotor control system have been obtained by the use of three methods. One method, mentioned in a preceding paragraph, is to extract the necessary gain and phase information from the oculomotor response to single sinusoids. In another method, a subject tracks the sum of several non-harmonically related sinusoids. The system gain and phase for each frequency component is computed. A third method is based on an important relationship in statistical communication theory; namely, that the system transfer function (graphically represented by the Bode plot) can be obtained by computing the ratio of the cross-power density spectrum to the input power density spectrum (36, 39). For this method to work, the spectrum of the input waveform must extend over the range of frequencies for which the system makes a significant response. In the past, those employing this last method have used some form of band-limited random noise waveform for the input stimulus.

The differences between the frequency response characteristics obtained by the above methods are interesting and important. In particular, it has been found that the gain decreases and the phase lag increases as a function of increasing spectral content of the input waveform. Therefore, Bode plots obtained using single sinusoid inputs have resulted in higher gain and significantly less phase lag than when random noise waveforms are used to identify the system. On the basis of these differences, some investigators have postulated the existence of a "predictor" mechanism which somehow reduces the phase lag and increases the gain when predictable (i.e., periodic) waveforms are being tracked (14, 15). Other investigators have discounted this possibility (54) and claim that the differences between the Bode plots obtained by the different methods are due to the wide differences in spectral content of the input signals used. Therefore, an important question remains: Are the differences in the transfer functions due to the differences in spectral content of the signals or to the signal predictivity differences?

To answer the question, an experiment (Experiment 3) was devised which used two input waveforms having the same time autocorrelation function to obtain Bode plots of the system. From a basic theorem in statistical communication theory (36, 39), the two functions must have the same mean square amplitude and the same power density spectrum. The signals also can

have the same time duration. However, the two waveforms are very different otherwise: one signal is highly predictive (a swept sinusoid) and the other signal is highly random (a Gaussian band limited random noise). These waveforms are described more completely in Chapter VIII.

Using these two waveforms, a highly controlled set of experiments can be performed to determine the effect of signal predictivity on the system transfer characteristics apart from other input waveform statistics. In particular, the mean square amplitude of the two signals and the power density spectrum of the signals are the same. Perhaps of equal importance is the fact that the experimental runs can now be of equal duration. When single sinusoids are used to obtain Bode plots, an experimental run must be made for each discrete frequency whereas, with the swept sinusoid or the random noise, a single run may result in sufficient data to compute the desired Bode plot. This is particularly important if Bode plots obtained by different signals are to be compared and inferences drawn about internal functioning of the oculomotor control system. Bode plots obtained with single sinusoids as inputs take significantly more time and subject effort than the use of wide-band input signals. However, when the swept sinusoid and the random noise waveforms are used, the power spectral density, the mean square amplitude, and the duration of the experimental runs can be the same. These are important controls not used in any previous investigations.

The two types of signals (swept and noise waveforms) allow another important experiment to be performed. Since the two waveforms can be summed together in different proportions by a summing amplifier, it is possible to vary the predictivity of the stimulus waveform while still keeping the spectrum, amplitude, and time duration of the different waveforms the same. Therefore, it is possible to determine how the oculomotor control system changes from the predictive to the nonpredictive mode of operation. This is essentially the purpose of Experiment 4.

Given the system configuration shown in Figure 1.1 and given a transfer function for the oculomotor plant (see Appendix D), it is possible (for a given input waveform) to compute the frequency response data for the oculomotor controller. By using an optimization procedure (computer program) it is possible to see how parameters of a mathematical model of the controller operator change as a function of input signal predictivity. For example, how do the gain and bandwidth of the controller behave as a function of input signal predictivity? What happens to the phase and how is this related to prediction? The questions are considered more closely in Chapter IX.

CHAPTER VI

EXPERIMENT 1

6.1 Purpose of the Experiment

The purpose of Experiment 1 is to obtain oculomotor control system Bode plots based on tracking of single sinusoids. This experiment has been done by several investigators. However, each investigator used a different method of extracting gain and phase information from the oculomotor response to the input sinusoid (14, 25, 61, 66). Consequently, the results from the different investigators are not entirely consistent (54). A new method for extracting gain and phase information from signals heavily obscured by noise is presented here.

6.2 Description of the Experiment

In this experiment, the two subjects tracked 10 sinusoids, each 1 minute in duration. The sinusoids ranged in frequency from 0.2 Hz to 2.5 Hz. The RMS amplitude of the sinusoids was 3.5° of arc. Both the stimulus (input) waveform and the oculomotor response (output) waveform were FM recorded on adjacent channels on magnetic tape. By using a special data analysis technique (explained in the next section), the necessary gain and phase information for the Bode plots was extracted.

6.3 Experimental Methods

The subjects were placed into the darkened booth and the eye position monitor adjusted. Each subject was given instructions to "follow the spot as closely as possible." The length of the rest period after each 60 sec. tracking segment was determined by the subject. Additional details of the experimental methodology are given in Appendix H.

The recorded data were processed on the HP 2115A computer--A to D convertor combination. Extraction of the gain and phase information was based on certain properties of crosscorrelation functions.[1] In particular, if $f_1(t)$ and $f_2(t)$ are different periodic functions (of the same fundamental frequency ω_1 and period T_1), then the crosscorrelation function of $f_1(t)$ and $f_2(t)$ is defined as

$$\phi_{12}(\tau) = \frac{1}{T_1} \int_{-.5T_1}^{.5T_1} f_1(t) f_2(f + \tau) dt \qquad (6.1)$$

and the cross-power spectrum as

$$\Phi_{12}(n) = \bar{F}_1(n) F_2(n) \quad . \qquad (6.2)$$

$F_1(n)$ and $F_2(n)$ are the complex spectra of $f_1(t)$ and $f_2(t)$ respectively. The complex spectrum $F(n)$ of a function $f(t)$ is simply the Fourier transform of the function, i.e.,

$$F(n) = \frac{1}{T_1} \int_{-.5T_1}^{.5T_1} f(t)\, e^{-jn\omega_1 t} dt \quad . \qquad (6.3)$$

$\bar{F}(n)$ is the complex conjugate of $F(n)$.

---

[1] For details see Y. W. Lee (1960) Statistical Theory of Communication, John Wylie and Sons, Inc., New York.

By an important theorem of communication theory, the crosscorrelation function and the cross-power spectrum are Fourier transform pairs. Therefore,

$$\phi_{12}(\tau) = \sum_{n=-\infty}^{\infty} \bar{F}_1(n) F_2(n)\, e^{jn\omega_1\tau} \tag{6.4}$$

Now, for a general formula giving $\phi_{12}(t)$ in terms of the Fourier series coefficients of the given functions $f_1(t)$ and $f_2(t)$, we consider the Fourier series expansions

$$f_1(t) = \frac{a_{10}}{2} + \sum_{n=1}^{\infty} (a_{1n} \cos n\omega_1 t + b_{1n} \sin n\omega_1 t) \tag{6.5}$$

and

$$f_2(t) = \frac{a_{20}}{2} + \sum_{n=1}^{\infty} (a_{2n} \cos n\omega_1 t + b_{2n} \sin n\omega_1 t) \tag{6.6}$$

where

$$F_1(n) = \frac{a_{1n} - jb_{1n}}{2} \tag{6.7}$$

and

$$F_2(n) = \frac{a_{2n} - jb_{2n}}{2} \,. \tag{6.8}$$

If, for $f_1(t)$ and $f_2(t)$, we define

$$C_n = \sqrt{a_n^2 + b_n^2} \tag{6.9}$$

and

$$\theta_n = \tan^{-1}(-\frac{b_n}{a_n}) \tag{6.10}$$

then

$$F(n) = \frac{C_n}{2} e^{j\theta_n} \quad . \tag{6.11}$$

Equation (6.4) can be reduced to the following form

$$\phi_{12}(\tau) = \frac{a_{10}a_{20}}{4} + \frac{1}{2} \sum_{n=1}^{\infty} C_{1n}C_{2n} \cos(n\omega_1\tau + \theta_{2n} - \theta_{1n}) \, . \tag{6.12}$$

Two implications from Equation (6.12) are very important to the following. First, the harmonic coefficients of $\phi_{12}(\tau)$ appear as products of the corresponding quantitites in the given functions $f_1(t)$ and $f_2(t)$. Consequently if any harmonic is absent in either $f_1(t)$ or $f_2(t)$, the corresponding harmonic term will be absent in the crosscorrelation function $\phi_{12}(\tau)$. Second, note that the crosscorrelation function retains the phase differences of the harmonics which are present in both $f_1(f)$ and $f_2(t)$.

With these two results in mind, consider a system having an input $f_i(t)$ and an output $f_0(t)$. If the input function $f_i(t)$ is the sinusoid

$$f_i(t) = A \sin \omega_1 t \tag{6.13}$$

and the output function the sinusoid

$$f_0(t) = B \sin (\omega_1 t + \theta) \tag{6.14}$$

then, from Equation (6.11) the input-output crosscorrelation function is the following

$$\phi_{i0}(\tau) = \frac{A \cdot B}{2} \cos(\omega_1 \tau + \theta) \quad . \tag{6.15}$$

Now, if a number of these functions are computed for different frequencies and with A constant, then, output amplitude B and phase shift θ can be determined, i.e., a Bode plot can be drawn.

This method has several important advantages. For example, if the system contains lumped nonlinearities, then the output $f_0(t)$ may contain significant harmonics of the input fundamental frequency. However, as long as the input $f_i(t)$ is a pure sinusoid of frequency ω_1, $\phi_{i0}(\tau)$ will be a sinusoid of frequency ω_1, i.e., the method selectively computes the gain and phase through the system at only the fundamental frequency. This can be very important in the study of some physiological systems.

Furthermore, if the output response contains even large amounts of noise, then the input-output crosscorrelation function will remain unchanged as long as the output noise and input signal are uncorrelated. Hence, correlation is a powerful technique for detecting signals even in large amounts of noise. This is also quite important in the study of physiological control systems. For example, in the oculomotor control system, responses to sinusoids above about 1.5 Hz are greatly attenuated and often hidden in the noise caused by inappropriate responses,

amplifier noise, and blink artifacts. With the crosscorrelation function technique, the gain and phase information can still be computed and a Bode plot determined.

6.4 Results of Experiment 1

Bode plots for subjects W.W. and M.C. are given in Figure 6.1 and Figure 6.2, respectively. The curves are based on data points taken at ten different single frequencies between 0.2 Hz and 2.5 Hz. Each data point is the average of five separate runs. The vertical bars around the average values indicate standard deviations of the data.

For subject W.W. the gain-frequency curve is practically flat to approximately 1 Hz. For higher frequencies the gain drops rapidly (about 60 decibels per decade). The gain-frequency curve for subject M.C. (Figure 6.2) is similar, with a slightly lower corner frequency. The phase frequency curves for both subjects are virtually identical; each having a monotonic increase in phase lag. The maximum phase shift in both subjects is approximately 100°. This is considerably less than one would expect from a minimum phase system: for a slope of 60 db/decade, the phase lag in a minimum phase system should increase asymptotically toward 270°. It is evident that the data are not representative of a minimum phase system. This is even more evident if the effect of neural transport delays are considered. Such delays would contribute additional phase lag to the lag of a third order system.

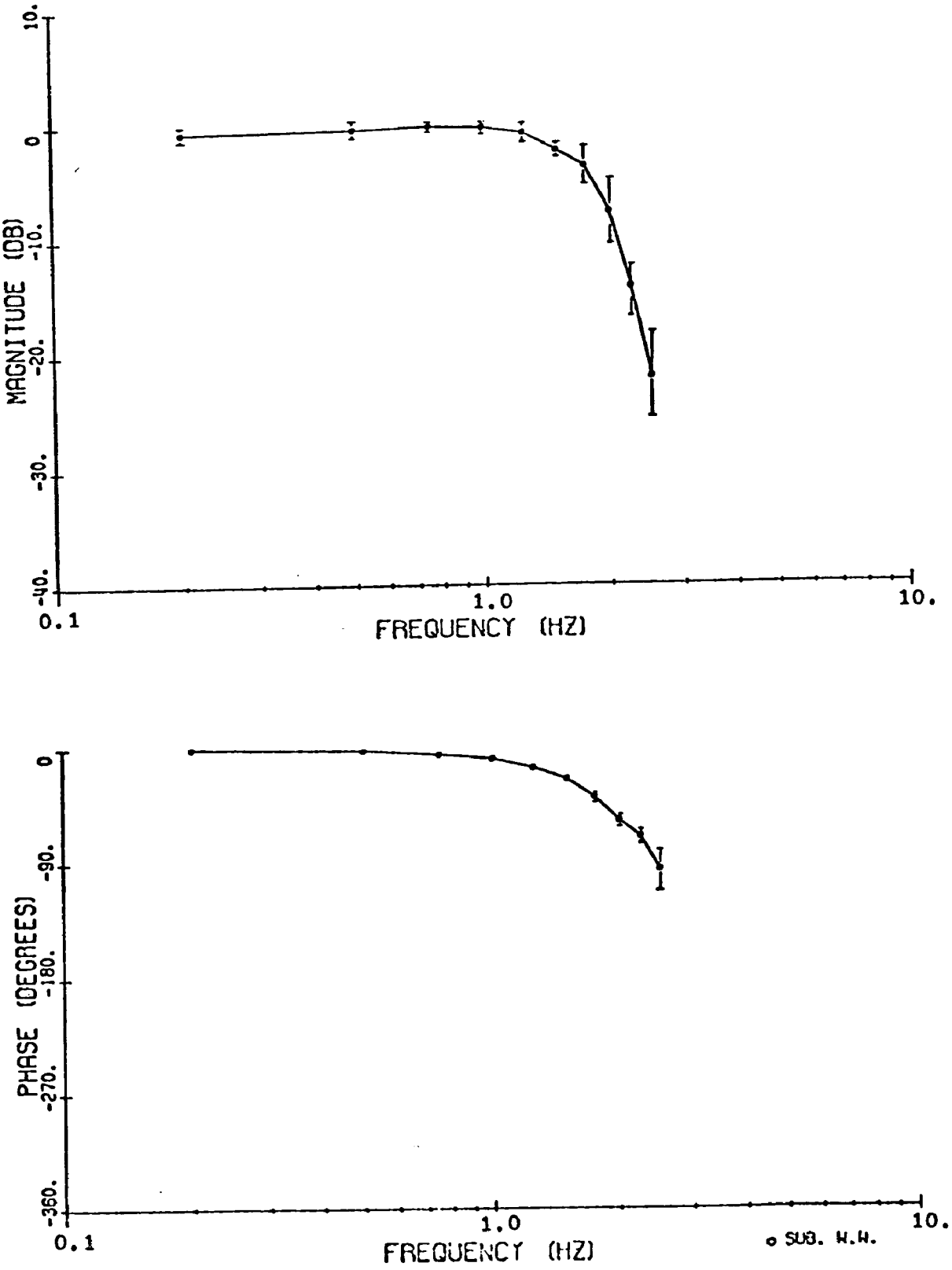

FIGURE 6.1. Bode Plot (Single Sinusoids).

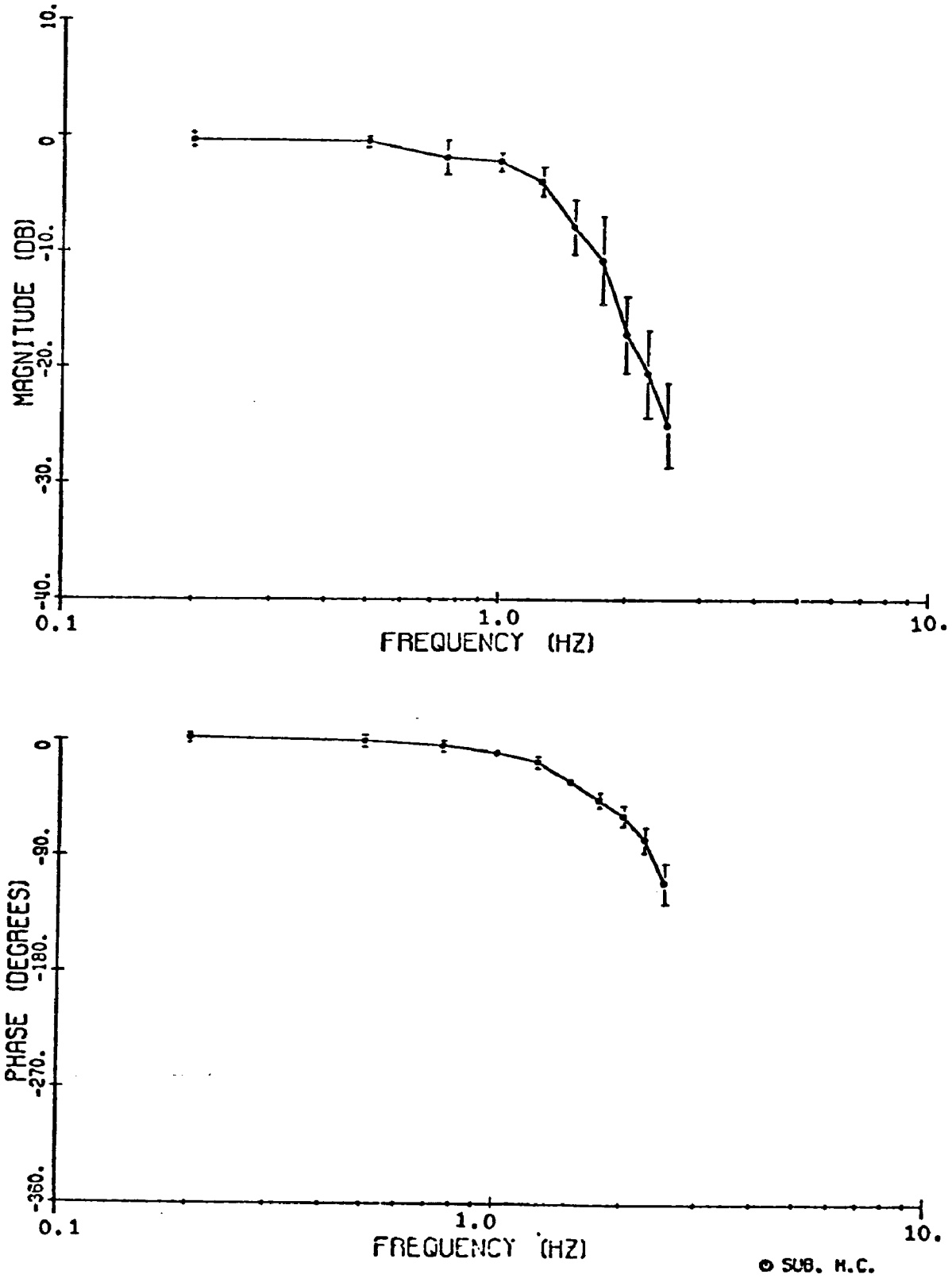

FIGURE 6.2. Bode Plot (Single Sinusoids).

A computer programmed optimization procedure was used to obtain parameters for a third order system for best-fit to the gain-frequency data shown in Figure 6.2 (subject M.C.). The computed closed loop transfer function for best-fit is

$$\frac{225}{(S + 3.9)(S^2 + 5.3S + 60)} \qquad (6.16)$$

Figure 6.3 illustrates how well Equation (6.16) models the gain-frequency data for subject M.C. However, a minimum phase system represented by Equation (6.16) would have the phase shift shown by the solid line on the phase-frequency plot of Figure 6.3. Obviously, the phase shift of the oculomotor control system for sinusoidal inputs is much less that what is predicted by Equation (6.16). This unexpectedly small phase shift has been attributed to "learning" and to the presence of a "prediction mechanism" somewhere in the human brain (14, 15). Experiments discussed in Chapters VIII and IX of this study will explore predictive tracking more closely.

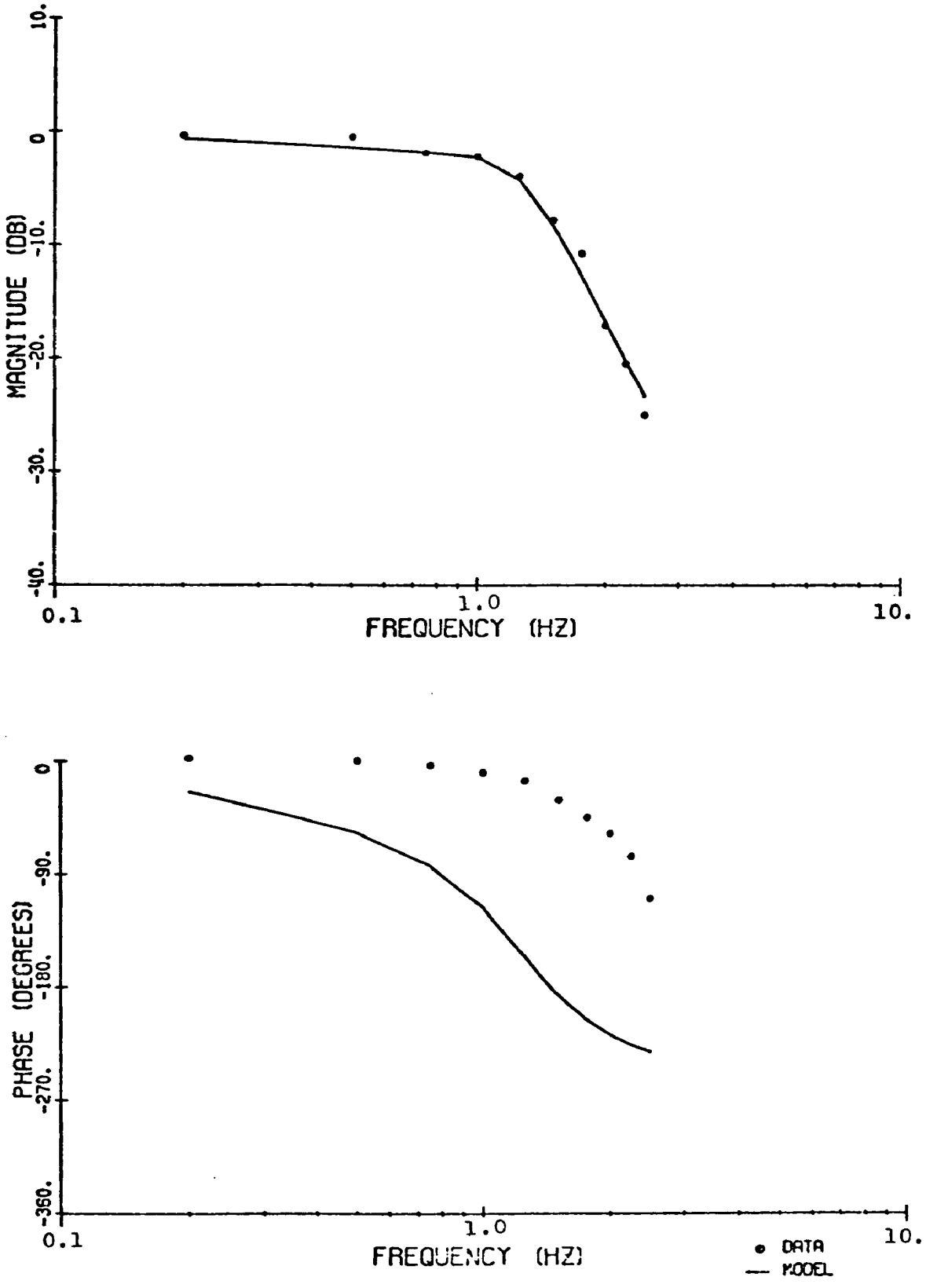

FIGURE 6.3. Bode Plots - Data and Model Subject M.C.

CHAPTER VII

EXPERIMENT 2

7.1 Purpose of the Experiment

One purpose of Experiment 2 is to determine if the oculomotor control system can be represented by a fixed linear system. Although some evidence exists to show that the oculomotor control system is nonlinear, much evidence also exists to show that the system has many qualities of a linear system. For example, when tracking single sinusoids, or sums of non-harmonically related sinusoids, almost no harmonics or subharmonics can be detected in the response; this virtually rules out the existence of lumped nonlinearities in the system (54).

A linear system is any system in which the output function $f_0(t)$ can be related to input function $f_i(t)$ by some linear operator H, i.e.,

$$H[af_1(t) + bf_2(t)] = aHf_1(t) + bHf_2(t) \qquad (7.1)$$

In our case, we let linear operator H be the convolution (or superposition) integral such that

$$Hf_i(t) = f_0(t) = \int_{-\infty}^{\infty} h(\tau) f_i(t - \tau) d\tau \equiv f_i(t) * f_0(t) \qquad (7.2)$$

where h(t) is the response of the system to a unit-impulse function (36, 39).

An overall block diagram for the oculomotor control system has been given in Figure 1.1. As shown, this feedback system consists of the plant and the controller. If it is assumed that the plant does not change its characteristics in response to changing input parameters and, in fact, can be represented by a linear system, then any changes in the overall system input-output characteristics are due to changes in the controller. The primary purpose of Experiment 2 is to determine if the predictive controller can be represented by a fixed linear system. The nature of the experiment, however, is such that the results should provide much insight into the nature of the predictive mechanism.

7.2 Description of Experiment 2a

The purpose of Experiment 2a is to determine the degree to which the system is sensitive to amplitude scaling of the input target motion waveforms. The experiment consists of having the subject track a random noise waveform having an average RMS amplitude of 3.5°. The subject also tracks the same waveform at half amplitude. Additional details of the experimental methodology are given in Appendix H.

Stimulus and response waveforms are recorded on adjacent channels of an FM tape recorder. The recorded data are used to compute frequency response profiles (Bode plots) of the system (see Figure 4.5). These can be compared to determine the degree to which amplitude scaling effects system response. The input waveforms used in this experiment will be described fully in Chapter VIII.

7.3 Results of Experiment 2a

Figure 7.1 shows two Bode plots for subject M. C.: one for an RMS amplitude of 3.5°; the other for 1.75°. Except for amplitude, the input waveforms are identical band-limited random noise sequences. From Figure 7.1 it is obvious that, at least for small amplitudes, scaling of the input has little effect on the system response. The shape of both the magnitude and phase curves shown in Figure 7.1 are nearly identical. Hence, we conclude that the system is relatively insensitive to input waveform scaling, at least for "small signal" inputs.

This result is in agreement with Fender and Nye (25) who computed two Bode plots from single sinusoids of different amplitude. However, Wheeless (61), for much larger amplitude signals (greater than 10°), found the system

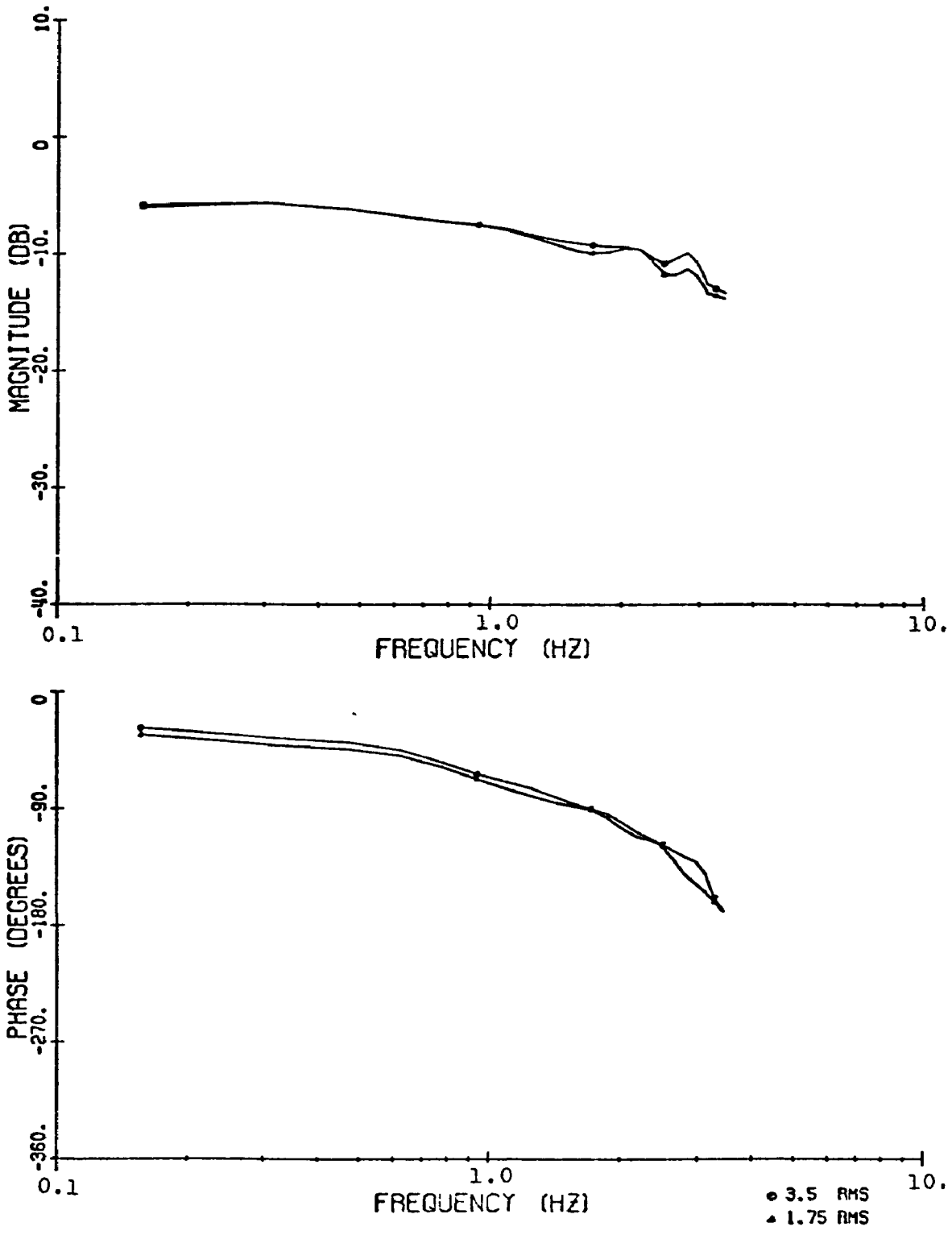

FIGURE 7.1 Amplitude Effects - Subject M.C.

to be somewhat dependent on amplitude differences. Perhaps this is to be expected for large signal inputs. For small signals, however, the system appears to be insensitive to changes in amplitude.

7.4 Description of Experiment 2b

The purpose of Experiment 2b is to determine the degree to which the principle of superposition holds for the oculomotor control system. This experiment examines the signal-to-noise (S/N) characteristics of the predictive tracking of sinusoidal target motion waveforms. A predictive signal (a sinusoid) and band-limited random "noise" are mixed (added together) in different propositions. The resulting waveform is used as the stimulus input to the oculomotor tracking system. The response (output eye position), the complete input waveform and the predictive component (sinusoid) of the input waveform are FM recorded on three channels of a magnetic tape.

If the system is linear, then superposition must hold. Therefore, the addition of noise to the input should have no effect on the amplitude (A) and phase (θ) of the sinusoidal (signal) component of the eye movement response waveform. In Experiment 2b, the degree to which A and θ are dependent on the S/N ratio is investigated.

One experimental run consists of having the subject track 7 waveforms, each 90 sec. in duration. The amplitude of the sinusoidal part of each input waveform remains unchanged at 2° of arc (RMS). Only the amplitude of the "noise" component of the waveform changes. The S/N ratio (ratio of mean square amplitudes, or "power" ratio) ranges from infinity (pure sinusoid) to 1.21 db over the 7 waveforms. These values (see Figure 7.2) were determined by using autocorrelation techniques.

A complete experiment consists of five runs, each with a different frequency of the sinusoidal signal. Hence, in a complete experiment, the subject tracks thirty-five different waveforms of 90 sec. duration. A complete experiment was repeated five times to obtain data for averaging.

Figure 7.2 shows the power density spectrum of the band-limited Gaussian random process used for the noise. Figure 7.3 shows seven different S/N ratio input waveforms which a subject follows to make one experimental run. The signal amplitude remains constant; only the amount of noise added to the signal changes.

7.5 Experimental Methods (Experiment 2b)

Subjects were placed in the darkened booth with the eye position monitor adjusted. Each subject

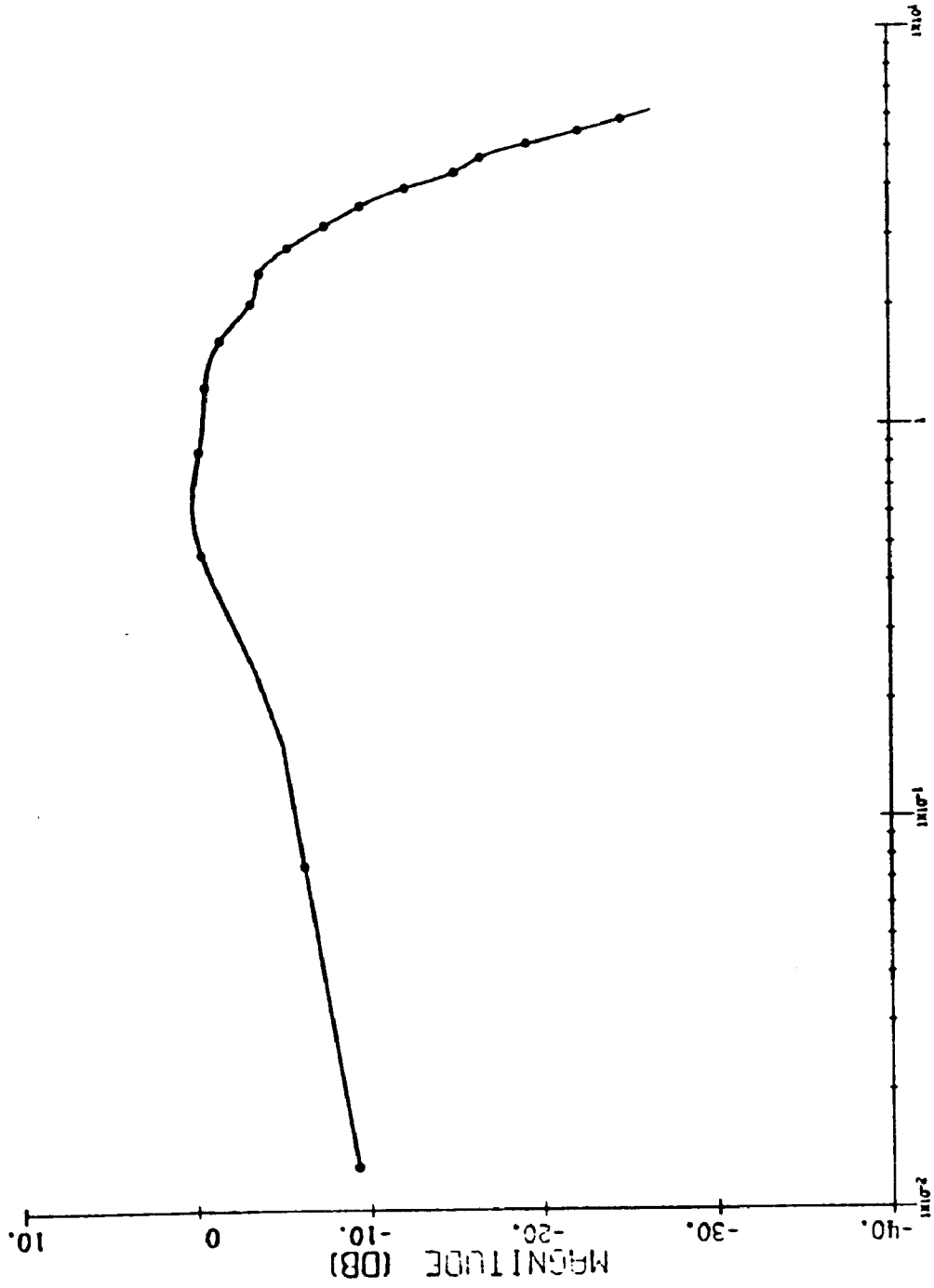

FIGURE 7.2. Power Density Spectrum of Noise.

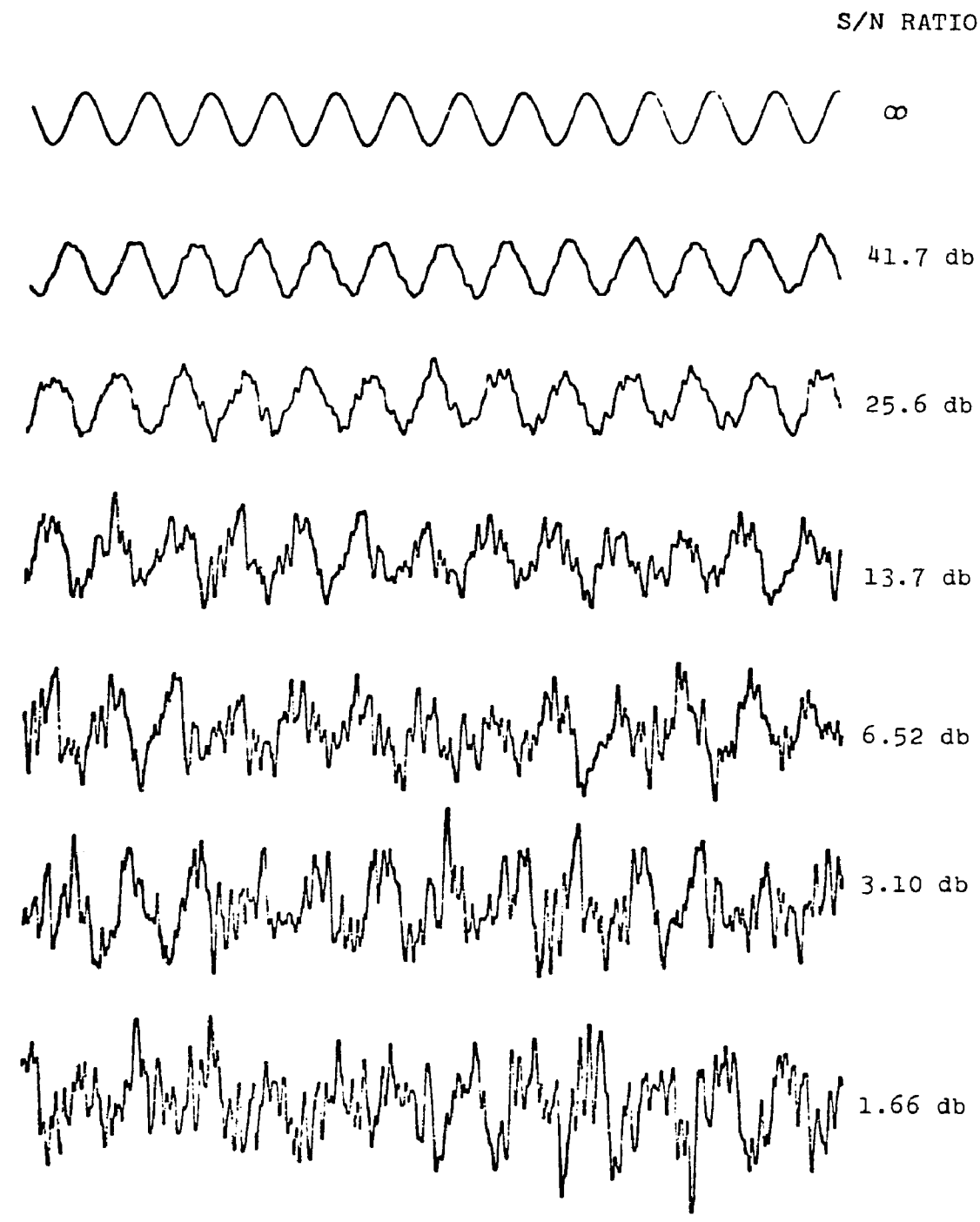

FIGURE 7.3. Constant Amplitude Signal Corrupted with Increasing Amounts of Noise (S/N Ratios are ratios of Mean Square Amplitude).

was given instructions to "follow the spot as closely as possible." The length of the rest period after each 90 sec. tracking interval was determined by the subject. Three subjects were used for this task. Additional details of the experimental methodology are given in Appendix H.

The recorded data were processed on the HP 2115A computer--A-D converter combination. The crosscorrelation function between the input sinusoid (without noise) and the eye's response to the signal-plus-noise input was computed. Since the input sinusoid and the "noise" are uncorrelated, the resulting crosscorrelation function, $\phi_{i0}(\tau)$, is a sinusoid the same frequency as the input sinusoid but, in general, with a different amplitude and phase angle (see Section 6.3). The amplitude and phase of $\phi_{i0}(\tau)$ is a measure of the attenuation and phase change through the system at the particular frequency of the input sinusoid. The mathematical basis for the data processing scheme is given in Appendix A.

7.6 Expected Results for Experiment 2b

From the above considerations, if the principle of superposition holds, addition of noise to the input should not effect the amplitude and phase of the output

signal component as long as the input signal remains unchanged. We have shown that the computation of $\phi_{i0}(\tau)$ provides a key to the gain and phase of the system at a given frequency. Therefore, a plot of the amplitude (A) of $\phi_{i0}(\tau)$ and the phase (θ) of $\phi_{i0}(\tau)$ as a function of the input signal-to-noise (S/N) ratio should be straight lines parallel to the S/N axis if the principle of superposition holds.

If the system is not linear, but somehow adapts in response to the addition of noise to the signal, then a plot of the amplitude and phase of $\phi_{i0}(\tau)$[A and θ, respectively] as a function of the input S/N ratio will be curves dependent on the S/N ratio. In any case, the nature of these curves should give clues as to how the input-output characteristics of the oculomotor control system adapt to changing input waveform parameters. It should be remembered that A and θ are the gain and phase, respectively, of the system transfer function at some input signal frequency ω.

7.7 Results of Experiment 2b

Figures 7.4, 7.5 and 7.6 are plots of the phase angle of $\phi_{i0}(\tau)$ at five different input signal frequencies as a function of the input S/N ratio for three subjects. As noted in Section 6.3, this phase angle is a measure of the system phase lag for a sinusoid at the indicated

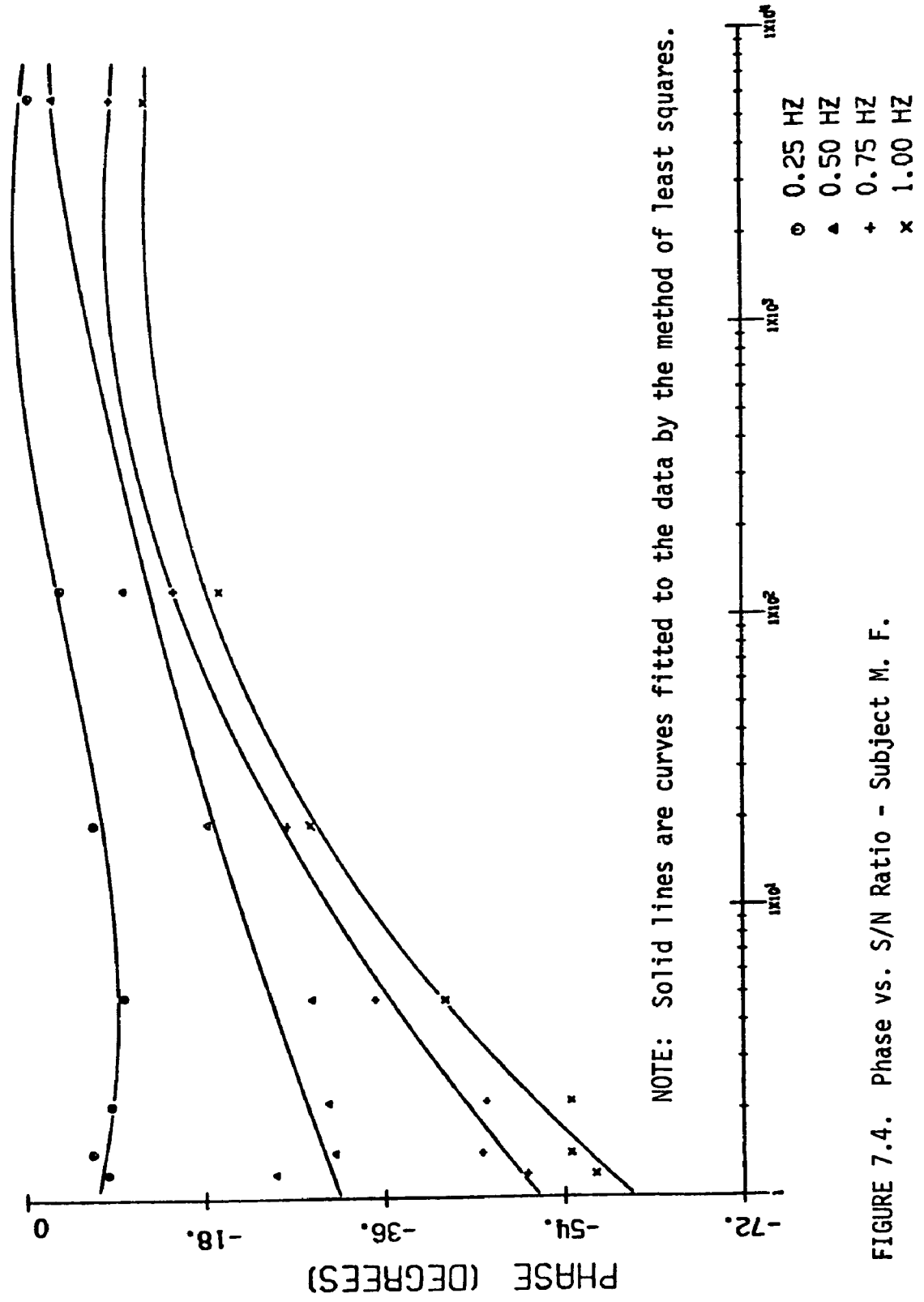

FIGURE 7.4. Phase vs. S/N Ratio - Subject M. F.

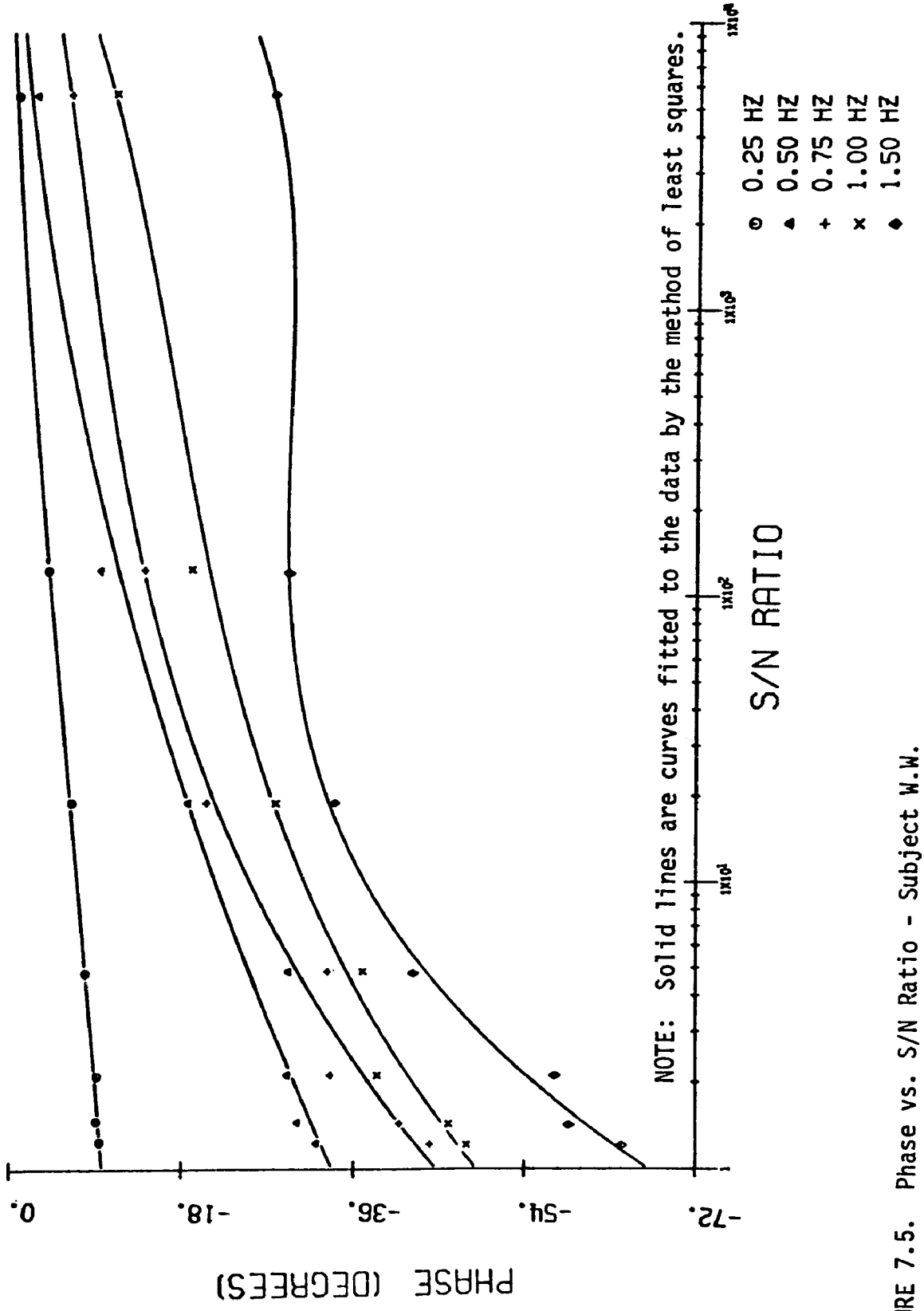

FIGURE 7.5. Phase vs. S/N Ratio - Subject W.W.

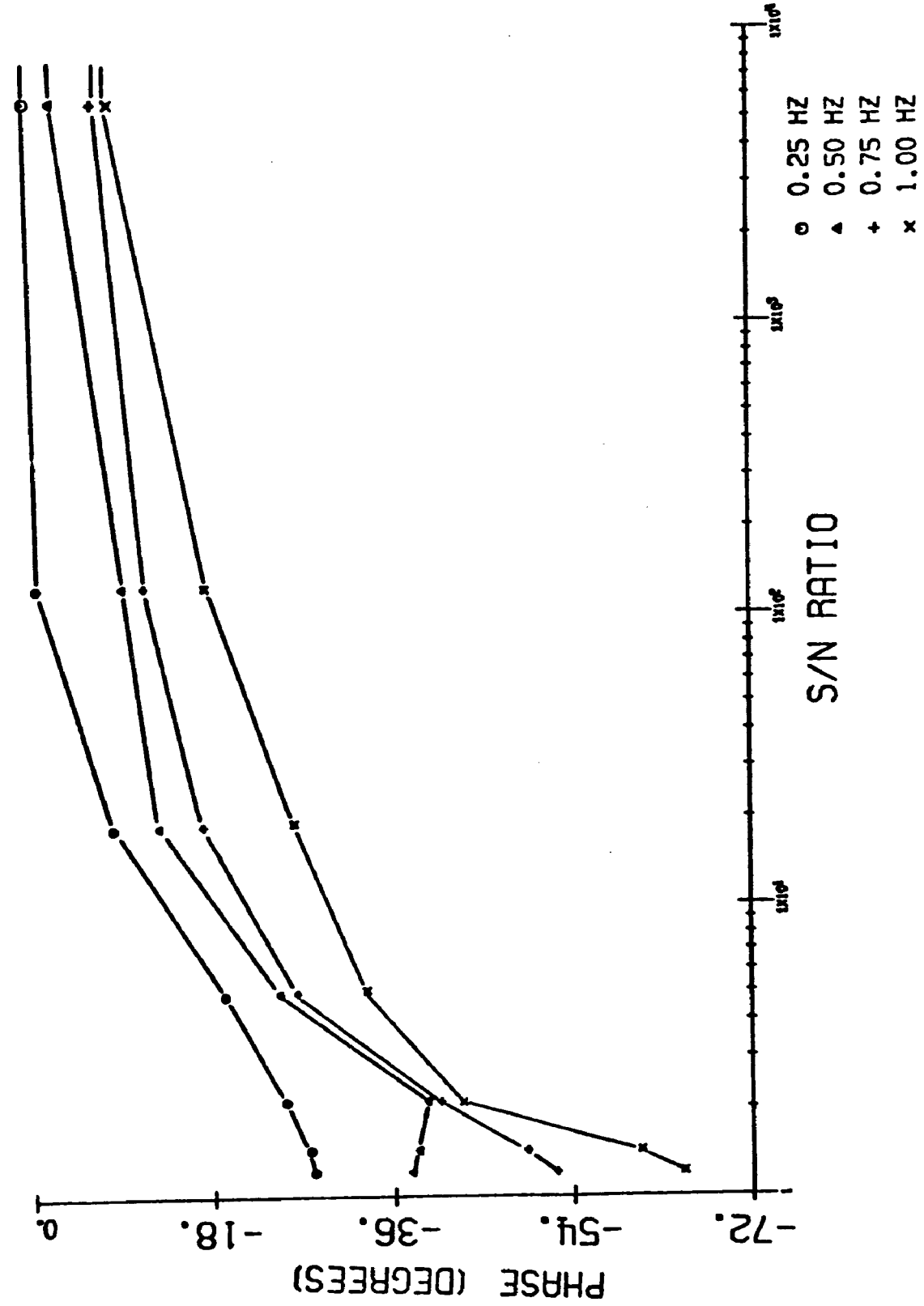

FIGURE 7.6. Phase vs. S/N Ratio - Subject T. Y.

frequency. A complete list of these data along with standard deviations is given in Appendix E.

The general trend of the curves is the same for all subjects. As was expected, the phase lag for the pure sinusoidal inputs (S/N = ∞) increases with increasing frequency. This behavior was expected since the phase angle is the same as that computed for the Bode plots for Experiment 1.

The behavior of θ as a function of the S/N ratio is most interesting. With the exception of a few data points, an increase in the noise content of the input waveform (decrease in the S/N ratio) results in more phase lag, i.e., θ becomes increasingly negative as the S/N ratio decreases. This holds true for all five signal frequencies for each subject.

Figures 7.7, 7.8 and 7.9 are plots of the normalized amplitude of $\phi_{i0}(\tau)$ at five different frequencies as a function of the input S/N ratio for the same three subjects. These data points are listed along with the appropriate standard deviations in Appendix F.

No attempt was made to obtain relative amplitude information for these frequencies, since the nature of amplitude changes as a function of frequency was explored in Experiment 1. Here, we are interested only in how the

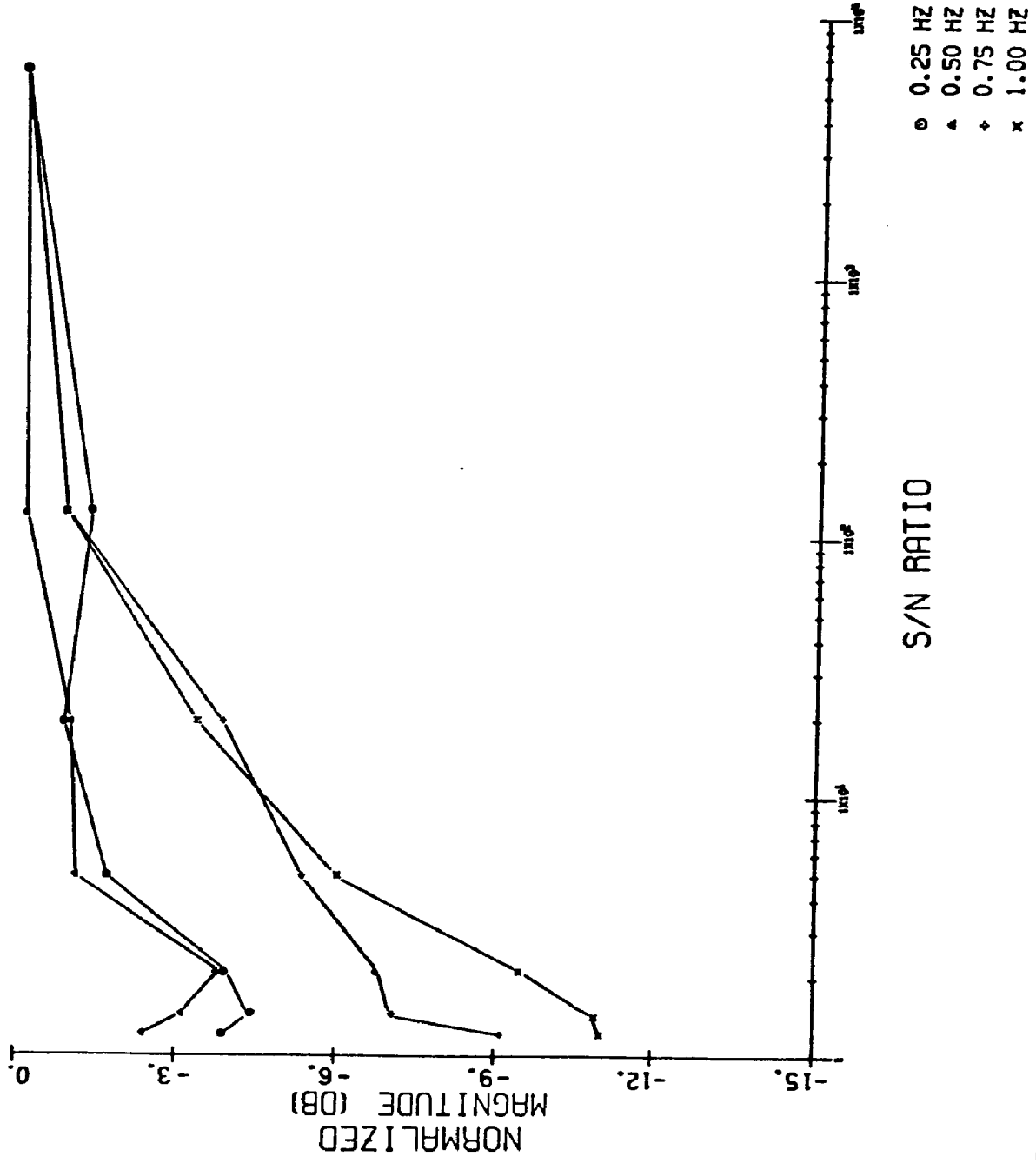

FIGURE 7.7. Magnitude vs. S/N Ratio - Subject M. F.

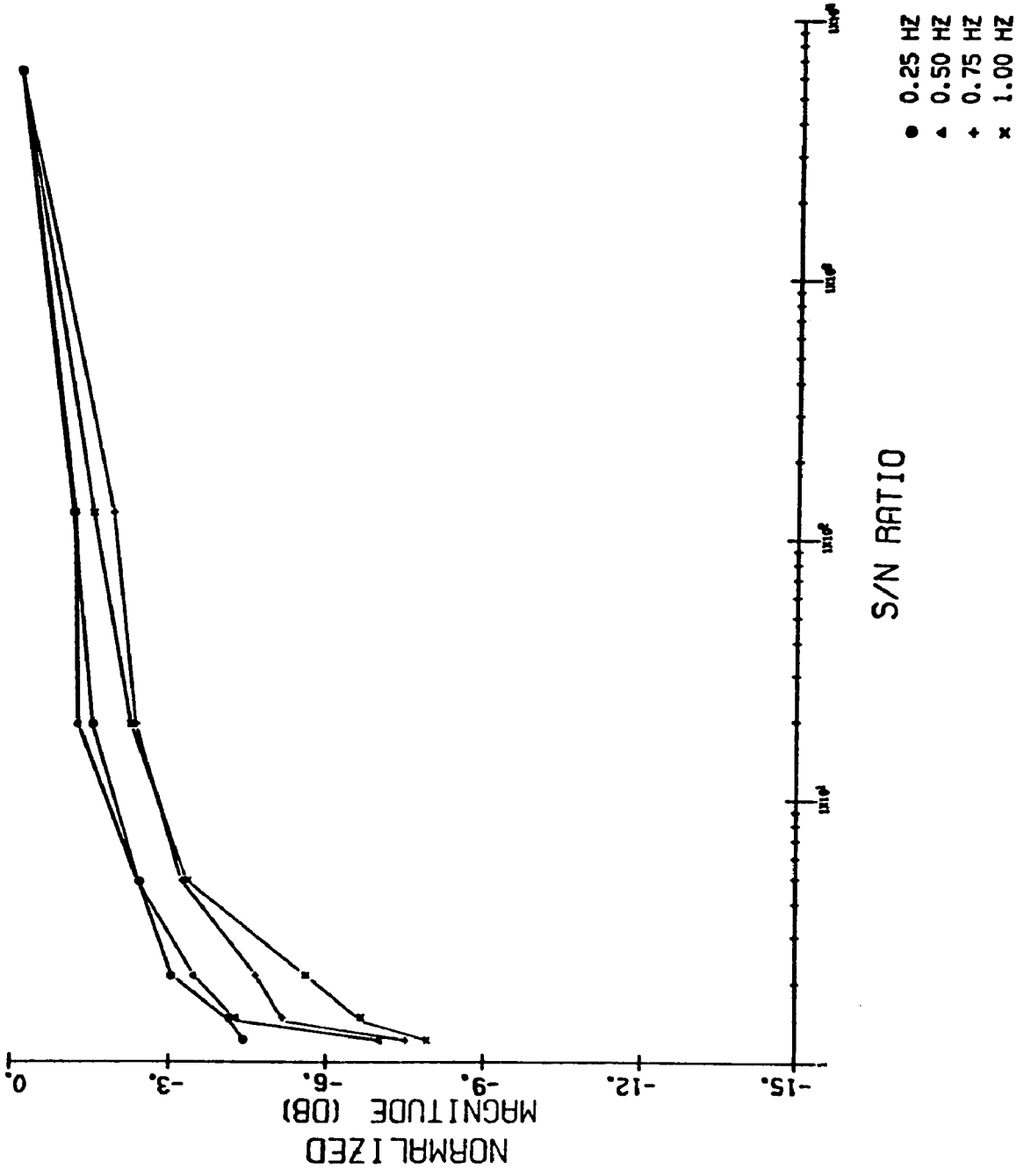

FIGURE 7.8. Magnitude vs. S/N Ratio - Subject W. W.

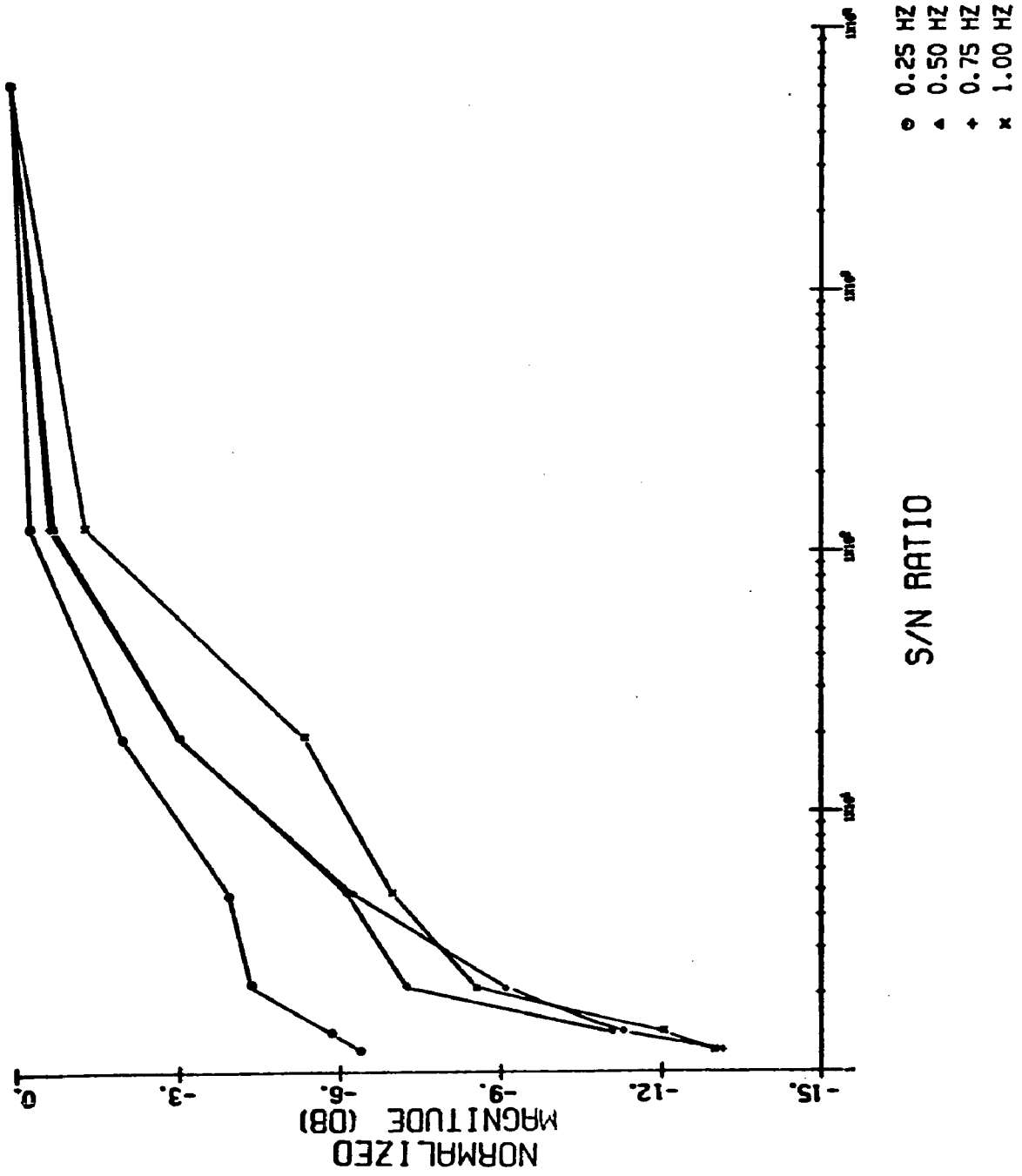

FIGURE 7.9. Magnitude vs. S/N Ratio - Subject T. Y.

amplitude changes as a function of the S/N ratio. It is obvious from these data that the amplitude of the oculomotor response to the sinusoidal signal is most definitely a function of the S/N ratio. In general, the lower the S/N ratio (increasing noise) the greater the attenuation of the response amplitude.

7.8 Discussion of Results

If the oculomotor control system were strictly linear, then the amplitude (A) and the phase angle (θ) of the signal component of the oculomotor response should be independent of the input S/N ratio. In fact, if the system were linear, plots of the amplitude and phase angle of the output signal component should be straight lines parallel to the S/N axis at a given frequency of input signal. Examination of the data shows that both A and θ are functions of the S/N ratio. Therefore, it must be concluded that the principle of superposition does not hold, i.e., the system is not strictly linear.

There is much evidence, however, which suggests that the system behaves in many ways like a linear system. For example, the results of Experiment 2a suggest that the system transfer function is independent of the input amplitude if the input signals are kept small. Furthermore, St. Cyr

and Fender (54), using a signal composed of a sum of non-harmonically related sinusoids, found in the output virtually no detectable harmonics or sub-harmonics of the fundamental frequencies of the component sinusoids. This rules out the existence of significant "lumped-nonlinearities" in the system. Therefore, the nonlinearity arises from the adaptive nature of the system, i.e., the mathematical function relating the input stimulus waveform to the output response waveform changes with alterations in the input waveform parameters and statistics. Later we will determine how the system adapts to certain controlled changes in the waveform parameters.

Before Experiment 2 was conducted, several hypotheses were considered. The basic hypothesis, that the system is fixed and linear, was disproved by the results of Experiment 2. Another hypothesis was that the system contains an adaptive linear filter that keys on the frequency of the signal, i.e., for each frequency of input sinusoid, the system would have a fixed input-output transfer function which would change only when the input signal frequency changed. An adaptable notch filter is an example of such a system. However, the changes in A and θ as a function of the S/N ratio at a give signal frequency disproves this hypothesis.

What more can be said about the properties of human predictive tracking based on the results of the S/N experiments? Another interesting aspect to note is that the changes in A and θ begin to occur at very low levels of noise input (high S/N ratios). From Figure 7.3, when the S/N ratio is 41.7 db, one can see that the sinusoid is corrupted very little and can be very easily detected through the noise. However, from the plots of A and θ, it is obvious that even this small noise component has an effect on the predictive mechanism. Therefore, we can conclude that the predictor is highly sensitive to noise, even at such low levels of noise that the signal is still very clearly discernable.

One possibility that the results of Experiment 2b tend to support is that predictive mechanism determines the future trajectory of a target by computing the derivatives of the motion waveform. Now, a knowledge of even the first derivative (slope) of a simple function (such as a sinusoid) gives enough information to predict with some accuracy the future trajectory of a moving target for suitably small values of future time. The more derivatives that are computed, the more accurately the function can be estimated by something similar to a Taylor's series or power series expansion. Obviously, even a little random noise would be sufficient to make the derivatives of the S + N waveform different from

the derivatives of the S waveform only. Hence, a predicted trajectory based on the values of the derivatives of a function would be erroneous and the predictor quite dependent on the S/N ratio of the input waveform. The results of Experiment 2b show that prediction is highly dependent on the S/N ratio.

CHAPTER VIII

EXPERIMENT 3

8.1 Purpose of the Experiment

The purpose of this experiment is to test the hypothesis that the transfer function of the oculomotor control system remains unchanged for all signals having the same RMS amplitude and power density spectrum, i.e., for all input waveforms having the same autocorrelation function.

The necessity for testing this hypothesis arises from the differences one notes between transfer functions obtained using the "traditional" methods of computing transfer functions: the use of single sinusoids to obtain the gain-phase data as a function of frequency and the use of more "complex" input waveforms.

Several methods have been used to determine a transfer function with complex waveform inputs. One method uses a sum of non-harmonically related sinusoids to move a target spot. A transfer function is determined by computing the system gain and phase for each input frequency component (66). Another method uses band-limited random noise as the input (14); a transfer function is computed from knowledge of the input

power density spectrum and the input-output cross power density spectrum (see Appendix B). In either case, one finds that an increase in the spectral content of the input waveform decreases the gain and increases the phase lag of the oculomotor control system.

It is well known (54) that the transfer function obtained by using certain predictive signals (sinusoids) is different from that obtained by using the more complex non-predictive inputs. In general, transfer functions obtained using non-predictive inputs have resulted in decreases in gain and increases in phase lag of the oculomotor control system. However, the complex non-predictive inputs used in these past studies have considerably wider power spectral densities than those of the single sinusoids used as the predictive inputs. Therefore, it is debatable (54) whether the differences in the transfer functions are due to the differences in spectral content of the signals or to the signal predictivity differences. Hence, this is the reason for testing the hypothesis proposed in this section. It is important to note that two waveforms can share the same autocorrelation function and still be very different in appearance: one signal can be "predictive" and the other "random."

Experiment 3, along with Experiment 4, provides some insight as to how the oculomotor control system adapts to changes in input signal predictivity when all the other important parameters

known to affect the transfer function are held constant, i.e., the predictivity of the signal changes, but not the RMS amplitude, the power density spectrum, the intensity of target spot illumination, or the time duration of the tracking task. These are important controls that have not been considered adequately in previous experiments concerning the tracking of predictive target movements.

8.2 Description of the Experiment

In this experiment, the subjects track two different waveforms having the same autocorrelation function. Each waveform is two minutes in duration. The predictive waveform is a band pass filtered linearly swept sinusoid (See Figure 8.1) having a sweep period of two minutes. The non-predictive waveform is a band-limited Gaussian random process (see Figure 8.2). Both waveforms have the same power density spectrum (see Figure 8.3) and RMS amplitude (3.5°).

The swept sinusoid is generated by driving a voltage controlled oscillator with a triangular waveform from a function generator. The Gaussian pseudo-random noise sequence is generated on the HP 2115A digital computer via a digital to analog converter, following a method suggested by Korn.[1]

---

[1]See G. A. Korn (1966). Random-Process Simulation and Measurements, New York: McGraw Hill Book Company.

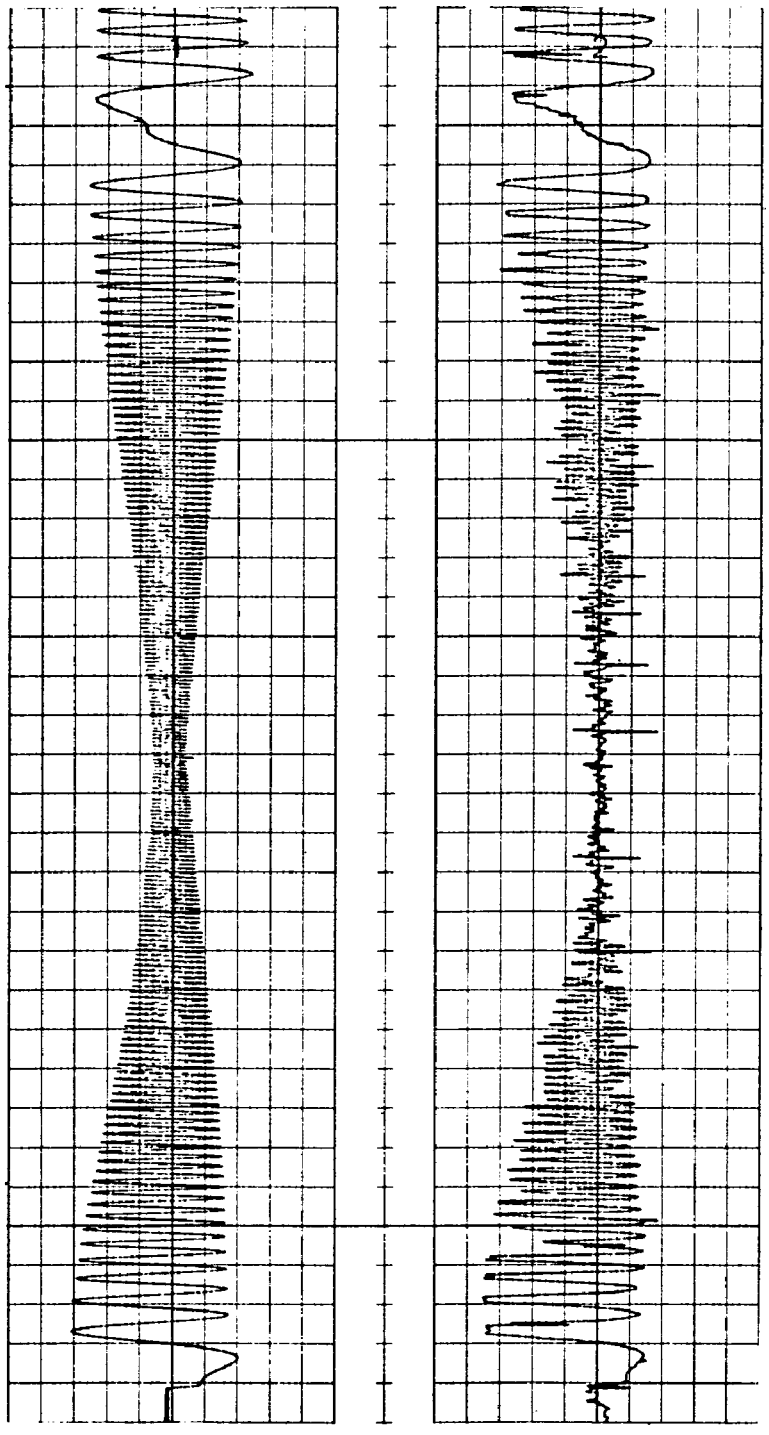

TOP TRACE: Swept Sinusoid
BOTTOM TRACE: Oculomotor Response

FIGURE 8.1. Swept sinusoid input waveform and the eye tracking response.

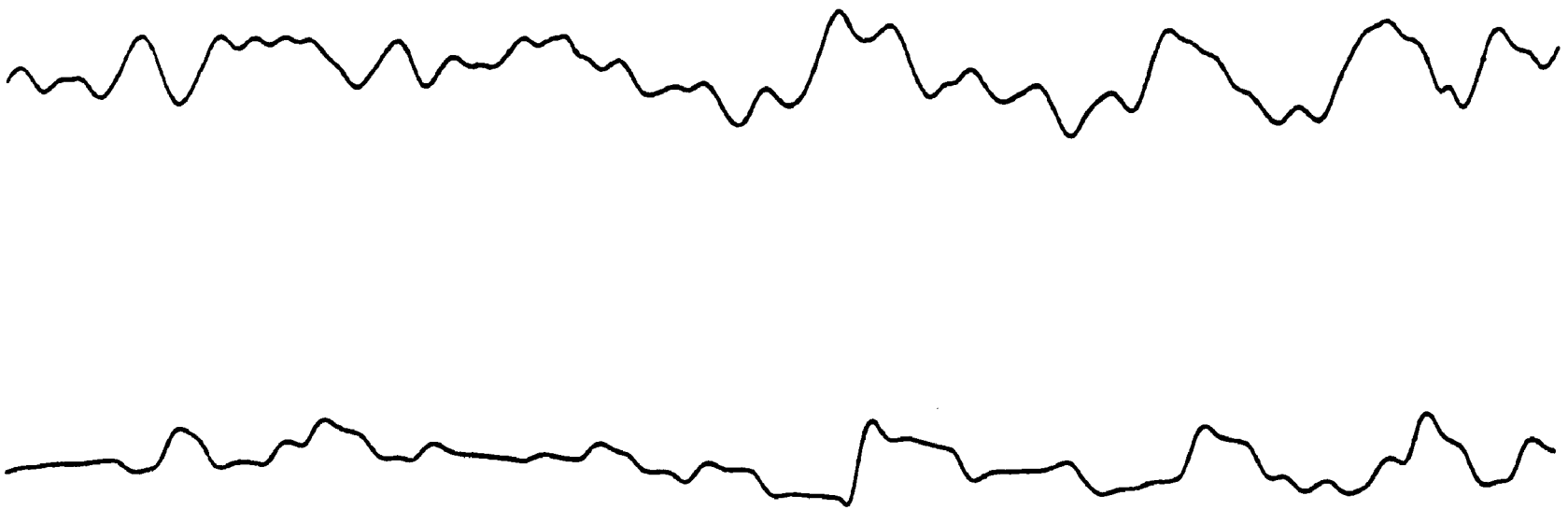

TOP TRACE: BAND-LIMITED RANDOM PROCESS INPUT WAVEFORM
BOTTOM TRACE: OCULOMOTOR RESPONSE

FIGURE 8.2. Band-limited Random Input Waveform and the Eye Tracking Response.

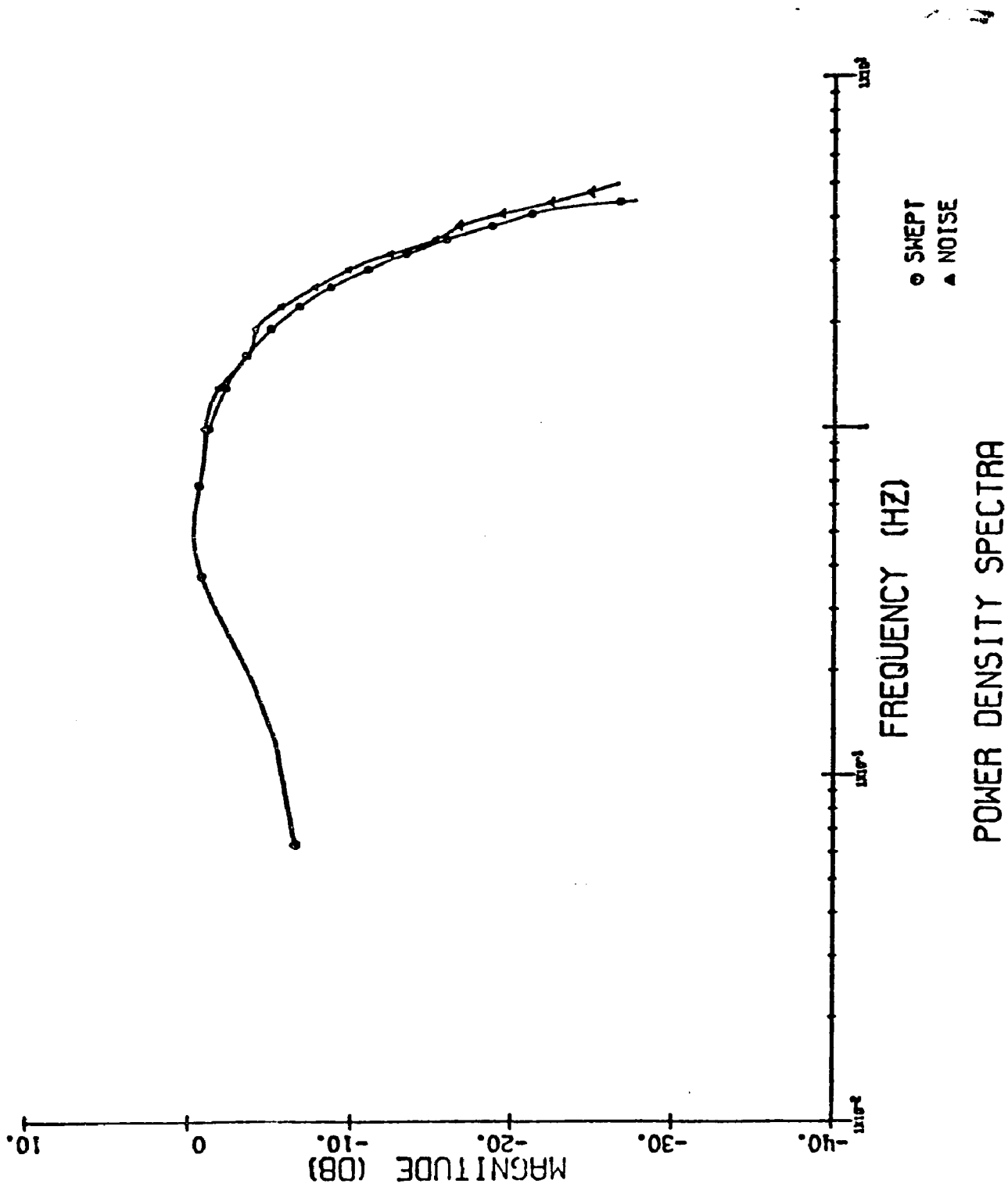

FIGURE 8.3. Matched Power Density Spectra for the Swept Sinusoid and the Random Noise Input Waveforms.

Both sequences were passed through a Krohn-Hite band-pass filter. The autocorrelation function $\phi^{N}_{ii}(\tau)$ of the desired band-limited Gaussian pseudo-random noise waveform was computed. Then the swept frequency sinusoid was band-pass filtered in such a way that its autocorrelation function, $\phi^{S}_{ii}(\tau)$, matched the autocorrelation function of the random noise sequence, i.e., $\phi^{S}_{ii}(\tau) \simeq \phi^{N}_{ii}(\tau)$. Matching was judged by superimposing autocorrelation displays on a storage oscilloscope. The two autocorrelation functions are shown in Figure 8.4. From statistical communication theory we know that the autocorrelation function is the key to the frequency spectrum of any time sequence (36, 39). Thus, two time sequences with the same autocorrelation function also have the same power density spectrum. Furthermore, since $\phi_{ii}(0) = \int_{-\infty}^{\infty} f^2(t)dt$, the two functions have the same mean square (or RMS) amplitude. Therefore, the "swept" waveform and the "noise" waveform have the same power density spectrum and the same RMS amplitude. Figure 8.3 shows how closely the power density spectra of the two waveforms are matched.

The input waveform and the subject's oculomotor response were both FM recorded on magnetic tape. These data tapes were used to compute input-output transfer functions by a method described in the next section.

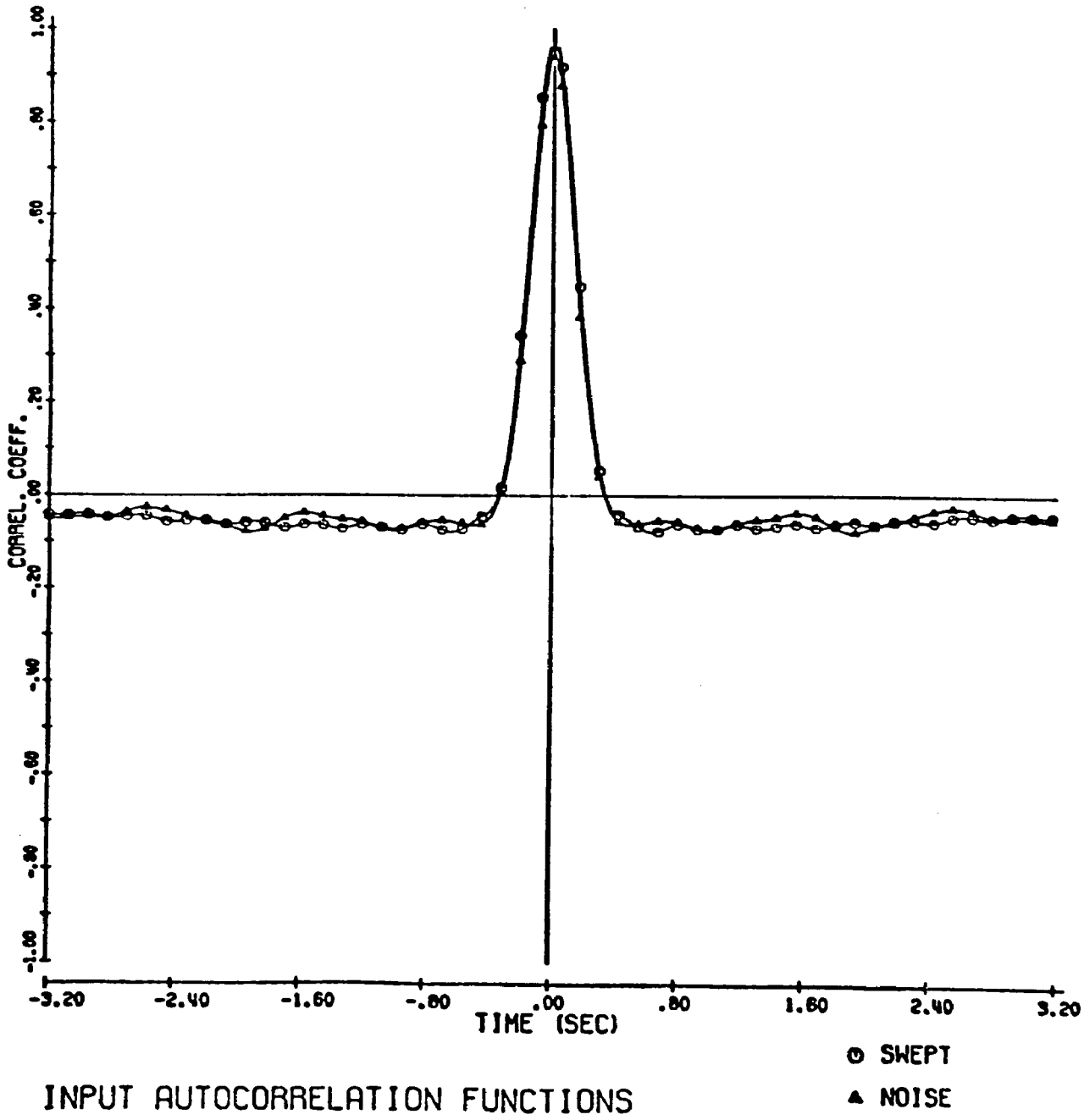

FIGURE 8.4. Matched Autocorrelation Functions for the Swept Sinusoid and the Random Noise Input Waveforms.

8.3 Experimental Methods

The subjects were placed in the darkened booth and the eye position monitor adjusted. Each subject was given instructions to "follow the spot as closely as possible." The length of the rest period after each two minute tracking segment was determined by the subject. Additional details of the experimental methodology are given in Appendix H.

The recorded data were processed on the HP 2115 A computer--A to D convertor combination. The system transfer functons were computed by first obtaining the input waveform power density spectrum (Fourier transform of the input autocorrelation function) and the input-output cross power density spectrum (Fourier transform of the input-output crosscorrelation function). The system transfer function is obtained by dividing the input-output cross power density spectrum by the input power density spectrum. This process is described graphically in Figure 4.5. A mathematical justification of this process is given in Appendix B.

It is often instructive to characterize systems by functions in the time domain as opposed to the more usual "transfer function" in the frequency domain. With this in mind, a comparison of the input-output crosscorrelation functions for a given subject is a good test of the hypothesis stated at the beginning of this chapter. In particular, if the system remains fixed for all inputs having the same autocorrelation function, $\phi_{ii}(\tau)$, then the input-output crosscorrelation function, $\phi_{io}(\tau)$, will be the same for both swept sinusoid and random noise inputs. This is

true because $\phi_{i0}(\tau)$ can be expressed mathematically as the convolution of $\phi_{ii}(\tau)$ and the impulse response $h(\tau)$ of the system (see Appendix B). If the system is fixed then $h(\tau)$ does not change and all inputs having the same autocorrelation function will produce the same input-output crosscorrelation function.

8.4 Expected Results

If the original hypothesis is true, i.e., if the system remains unchanged for all input waveforms having the same autocorrelation function, then the transfer function obtained with the swept sinusoid input will be identical to the transfer function obtained with the band-limited random noise waveform. If the transfer functions (graphically represented by Bode plots) are significantly different, then the difference must be attributed to some input waveform parameter other than power density spectrum, RMS amplitude, intensity of target spot illumination, or time duration of the input waveforms. In the time domain, if the system is fixed for the class of input waveforms having the same autocorrelation function, then the crosscorrelation functions between input and output will remain the same for all input waveforms of this class.

If the Bode plots for the swept sinusoid are different from the Bode plots for the random noise, then some statistic other than the controls mentioned above must be responsible for the difference. If the predictivity of the input

waveforms is the difference that causes the system to change in some way, then examination of the phase-frequency plots should provide evidence to this effect. In particular, if the system is using the inherent pattern of the swept sinusoid to predict future trajectories of the target spot, then the phase lag at given frequencies should be significantly less for the swept sinusoid input as compared to the phase lag for the random noise input. Likewise, in the time domain the input-output crosscorrelation functions will be different if the system employs a predictive mechanism. In particular, the cross-correlation function for the predictive input should be significantly shifted in the direction of time "lead" as compared to the function obtained with the random noise input waveform.

8.5 Results

Figures 8.5 and 8.6 show Bode plots obtained from two subjects for both the swept sinusoid input and the random noise input. It is obvious from these figures that the Bode plots obtained with predictive input are very different from Bode plots computed for the random input. In fact, for both subjects the gain is greater and the phase lag considerably less for the Bode plots obtained using the predictive (swept sinusoid) input waveform. This implies that the system is not fixed for the

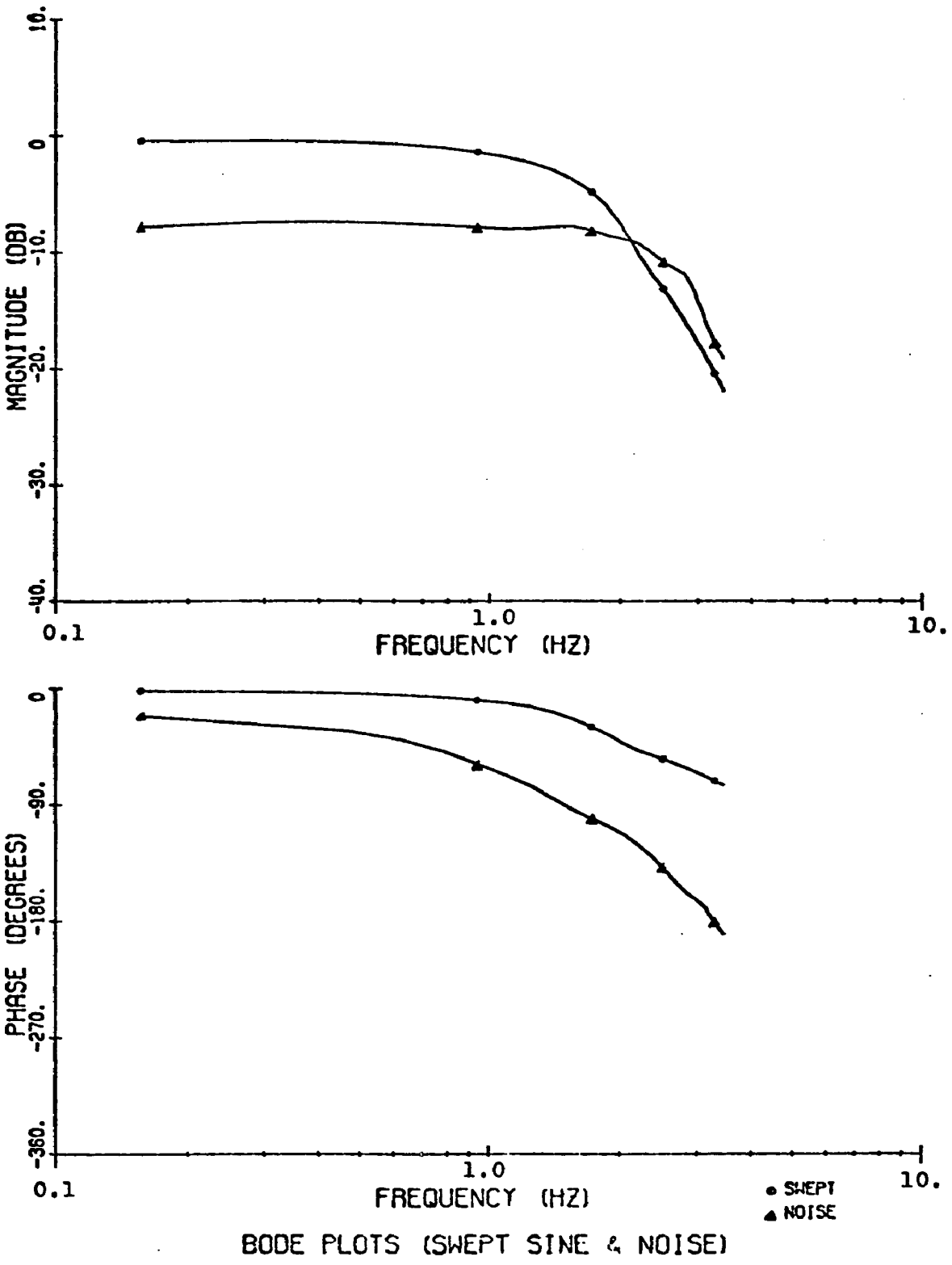

FIGURE 8.5. Bode Plots - Subject W. W.

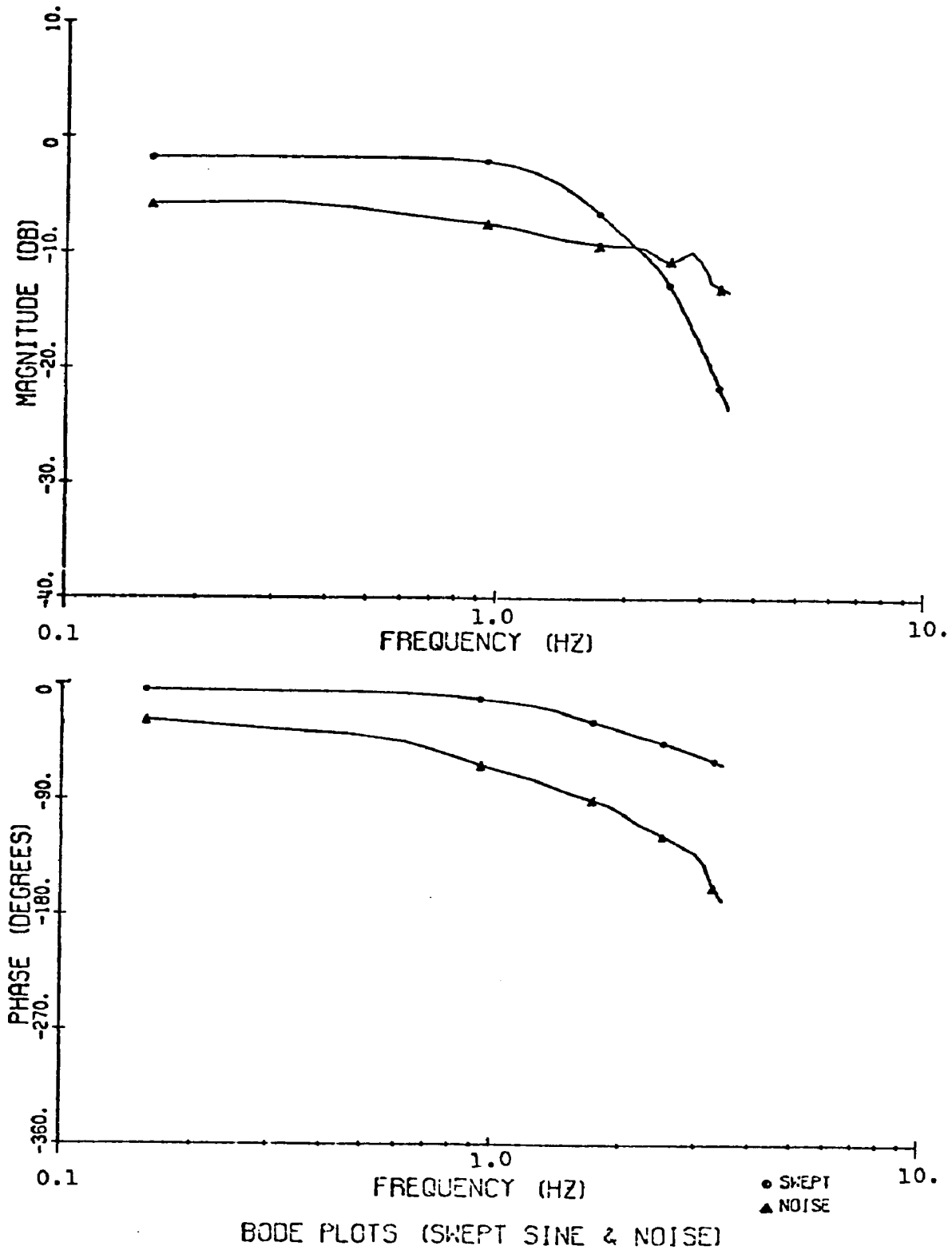

FIGURE 8.6. Bode Plots - Subject M.C.

set of input waveforms having the same power density spectrum, RMS amplitude, and time duration. Also, the increased gain and significantly decreased phase lag obtained for the predictive case imply the system is using the information inherent in a predictive waveform to improve tracking performance significantly.

Further evidence to support the above conclusion can be given in the time domain. Figure 8.7 shows the crosscorrelation functions for Subject M.E. for both the predictive and the random inputs. Since the autocorrelation functions for both inputs are the same, the differences in the crosscorrelation functions imply that the system is not fixed but has changed in some way. The crosscorrelation response for the random input is seen to have a lower amplitude and is shifted to the "right" in the plot, implying a greater time delay or phase lag for non-predictive inputs. This is the same result as obtained from the frequency domain Bode plots of Figures 8.5 and 8.6.

In conclusion, the decreased phase lag and increased gain observed for predictive inputs cannot be explained away by the differences in power density spectrum, RMS amplitude, and time duration of the input waveforms involved. Therefore, the system must be using a pattern inherent in the predictive waveform to increase gain and decrease phase lags and time delays, i.e., the brain implements some sort of predictive mechanism to improve

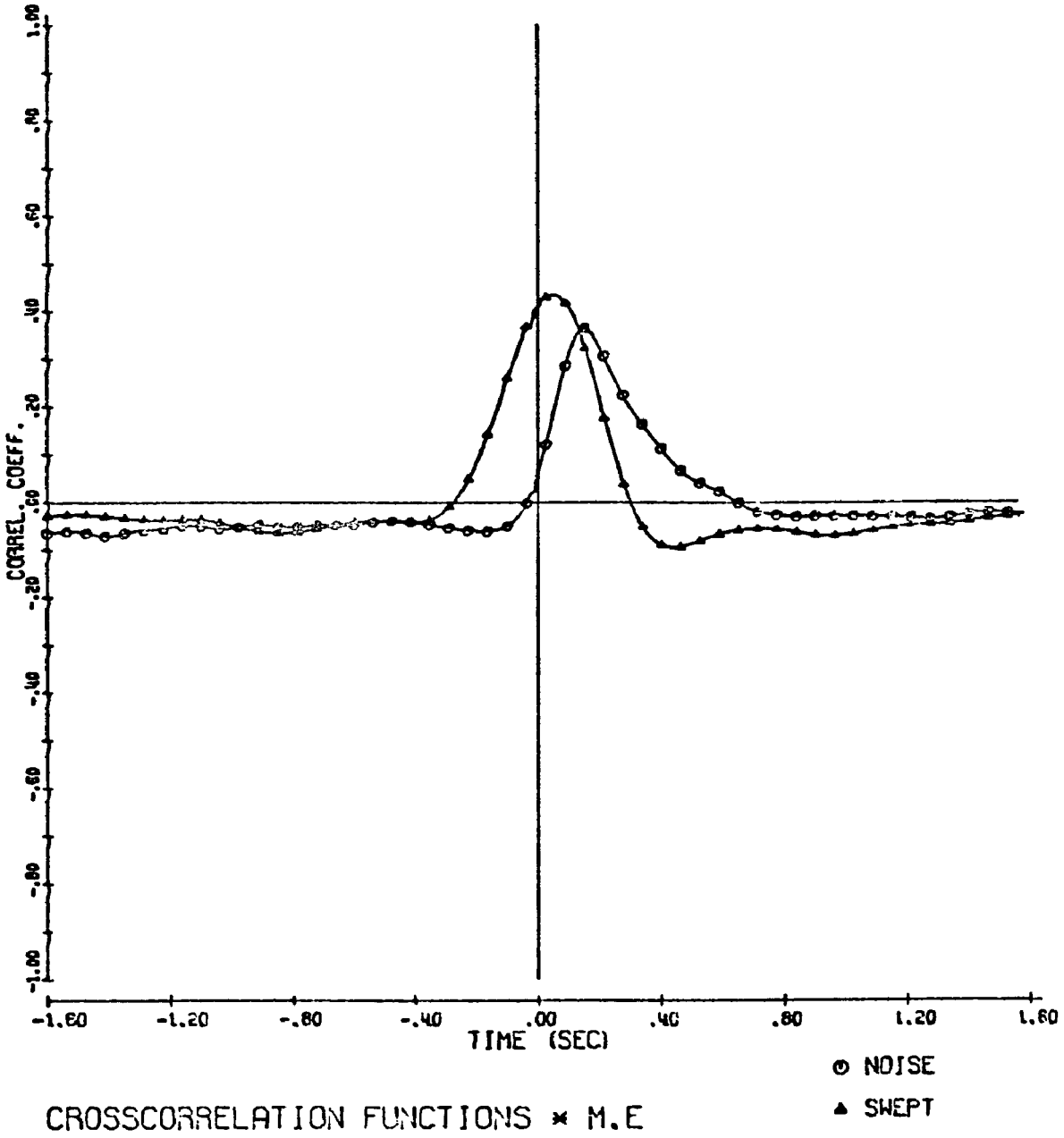

FIGURE 8.7. Input-output Crosscorrelation Functions for Subject M.E.

tracking performance. Chapter IX will explore quantitatively the way in which the system changes from the non-predictive to the predictive mode of tracking.

CHAPTER IX

EXPERIMENT 4

9.1 Purpose of the Experiment

The purpose of Experiment 4 is to determine quantitatively how the system changes from the non-predictive to the predictive mode of operation. The only quantitative control system studies of prediction tracking have been based on a comparison of transfer functions obtained from the responses of the system to single sinusoids in one case and to random noise sequences in the other case (14). As pointed out in Chapter VIII, there are certain problems involved when comparing results obtained from these two very different methods. For example, the input waveforms for the two methods have very different frequency spectra and the gain and phase of the systems are known to be a function of the spectral content of the input waveforms. Also, the amount of subject effort and time required per data point is very different in the two methods. Furthermore, the experimental paradigms of the two methods are so different that it is not possible to design an experiment to determine how the system changes from the predictive to the non-predictive mode of operation. Therefore, only the two extremes can be studied and compared.

The experiment described in this chapter is based on the use of two basic input waveforms: the swept sinusoid and the random noise waveform. These waveforms were described fully in Chapter VIII. For details of the methodology for Experiment 4, see Appendix H.

9.2 Description of the Experiment

By adding the swept sinusoid and the random noise sequence together in different proportions with a summing amplifier, a set of waveforms which vary in the degree to which they are predictive can be generated. However, each member of the set can be made to have the same time duration and autocorrelation function. This means that each member of the set has the same RMS amplitude (3.5°) and power density spectrum.

In Experiment 4, the subjects were asked to track a set of five different waveforms. Each member of the set had a different ratio of random noise amplitude to swept sinusoid amplitude. Two members of the set were the pure swept sinusoid and the pure random noise sequence. The other three members of the set had ratios of random noise amplitude to swept sinusoid amplitude plus random noise amplitude of 25%. 50% and 75%, respectively.

Each subject was asked to track the five input waveforms. The input waveform and the oculomotor response were recorded on adjacent channels of an FM tape recorder. These records were then processed on a digital computer to

extract the closed loop frequency response data (Bode plot information) using the method described in Appendix B and shown diagrammatically in Figure 4.5.

It should be emphasized the P(S), the oculomotor plant, is the only part of the system shown in Figure 9.1 that is considered to be fixed and linear. Hence, P(S) can be considered a true transfer function. Since the parameters of the oculomotor controller, $C_\alpha(S)$, are dependent on the input waveform statistics, it cannot be called a transfer function. Instead, the term "mathematical operator" or "operator" will be used to refer to $C_\alpha(S)$, $G_\alpha(S)$ and $g_\alpha(S)$.

Assuming the unity feedback configuration of Figure 9.1 and given a fixed transfer function P(S) for the oculomotor plant (see Appendix D), an operator describing the open loop system can be computed from the experimentally derived closed loop data. The operator describing the closed loop system is

$$G_\alpha(S) = \frac{\theta_0(S)}{\theta_i(S)} = \frac{C_\alpha(S)P(S)}{1 + C_\alpha(S)P(S)} \tag{9.1}$$

where $C_\alpha(S)$ is the controller operator and where the subscript α denotes the input waveform for which the operator corresponds (α = 1, 2, 3, 4, and 5 correspond to input waveforms with ratios of random noise amplitude to swept sinusoid amplitude plus random noise amplitude of 0%, 25%, 50%, 75%, and 100%, respectively).

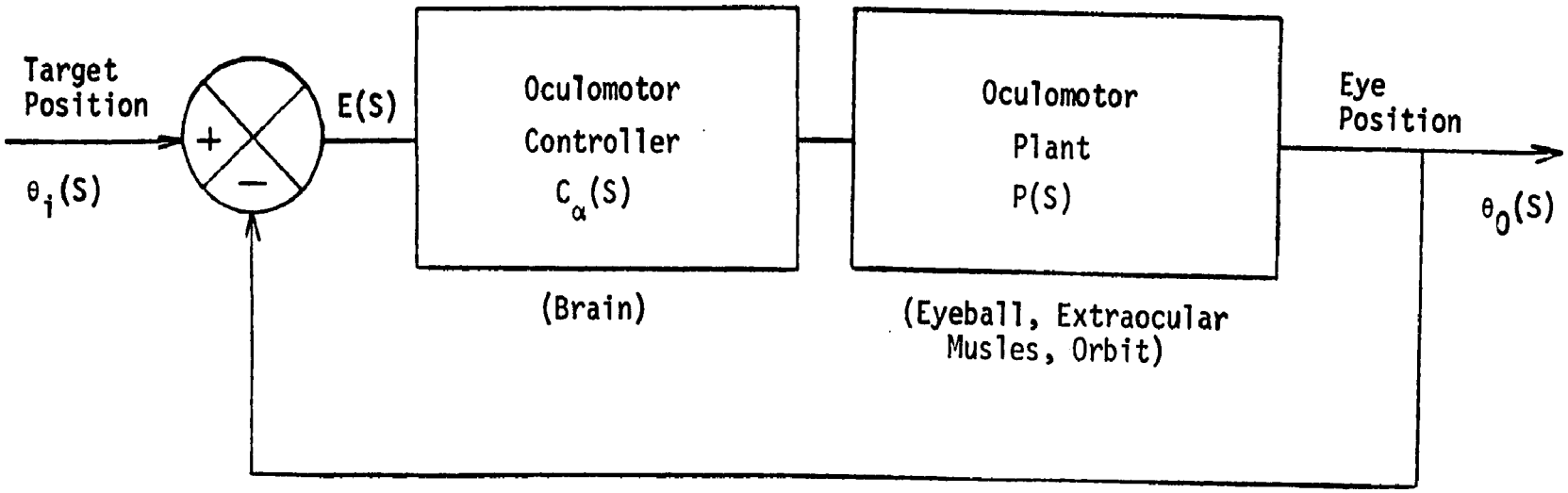

$$P(S) = \frac{68(S + 3.78)}{(S + 1.69)(S + 15.2)}$$

FIGURE 9.1. Basic System Configuration.

By mathematically opening the loop, it is possible to compute the data points for the operator $g_\alpha(S)$ describing the open loop system. These points are computed from the closed loop data with the formula (see Appendix C):

$$g_\alpha(S) = C_\alpha(S)P(S) = \frac{G_\alpha(S)}{1 - G_\alpha(S)} \quad . \tag{9.2}$$

Since the data points for $g_\alpha(S)$ can be computed and $P(S)$ is a known function (see Equation 3.4), then the data points for $C_\alpha(S)$ be computed from the formula

$$C_\alpha(S) = \frac{g_\alpha(S)}{P(S)} \quad . \tag{9.3}$$

With the computed data points for $C_\alpha(S)$ in hand, it is possible to use a program to optimize parameters of an assumed mathematical model for best fit to the data. It is of obvious interest to determine how these parameters change as the predictability of the input waveform changes. This is the primary purpose of Experiment 4.

9.3 Results

The closed loop Bode plots for five input waveforms of different percent noise are shown for subject W.W. in Figures 9.2 to 9.6. These plots represent the mean values of six runs for each input waveform. The mean values and standard

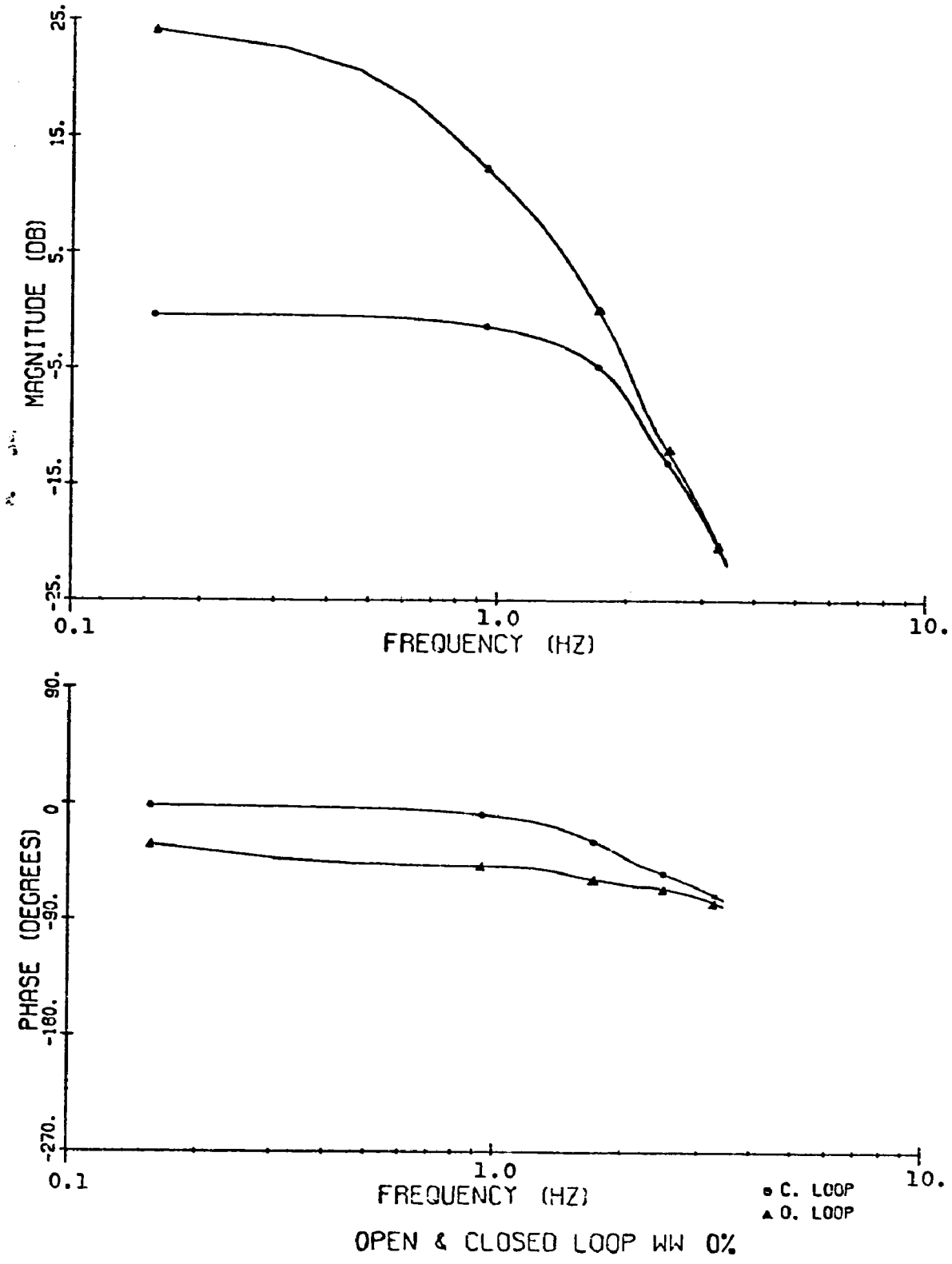

FIGURE 9.2. Open and closed loop Bode plots (0% Noise).

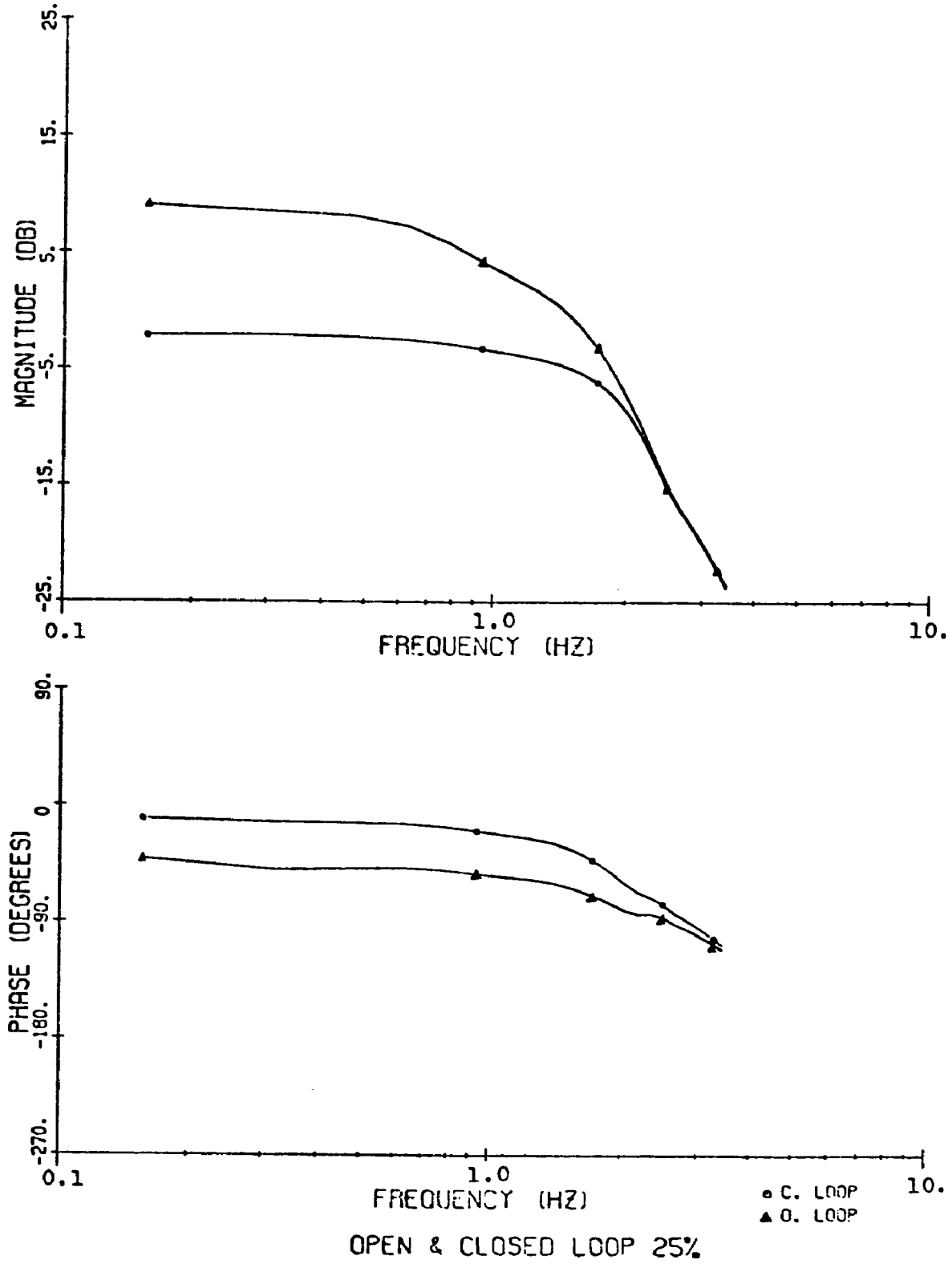

FIGURE 9.3. Open and closed loop Bode plots (25% Noise).

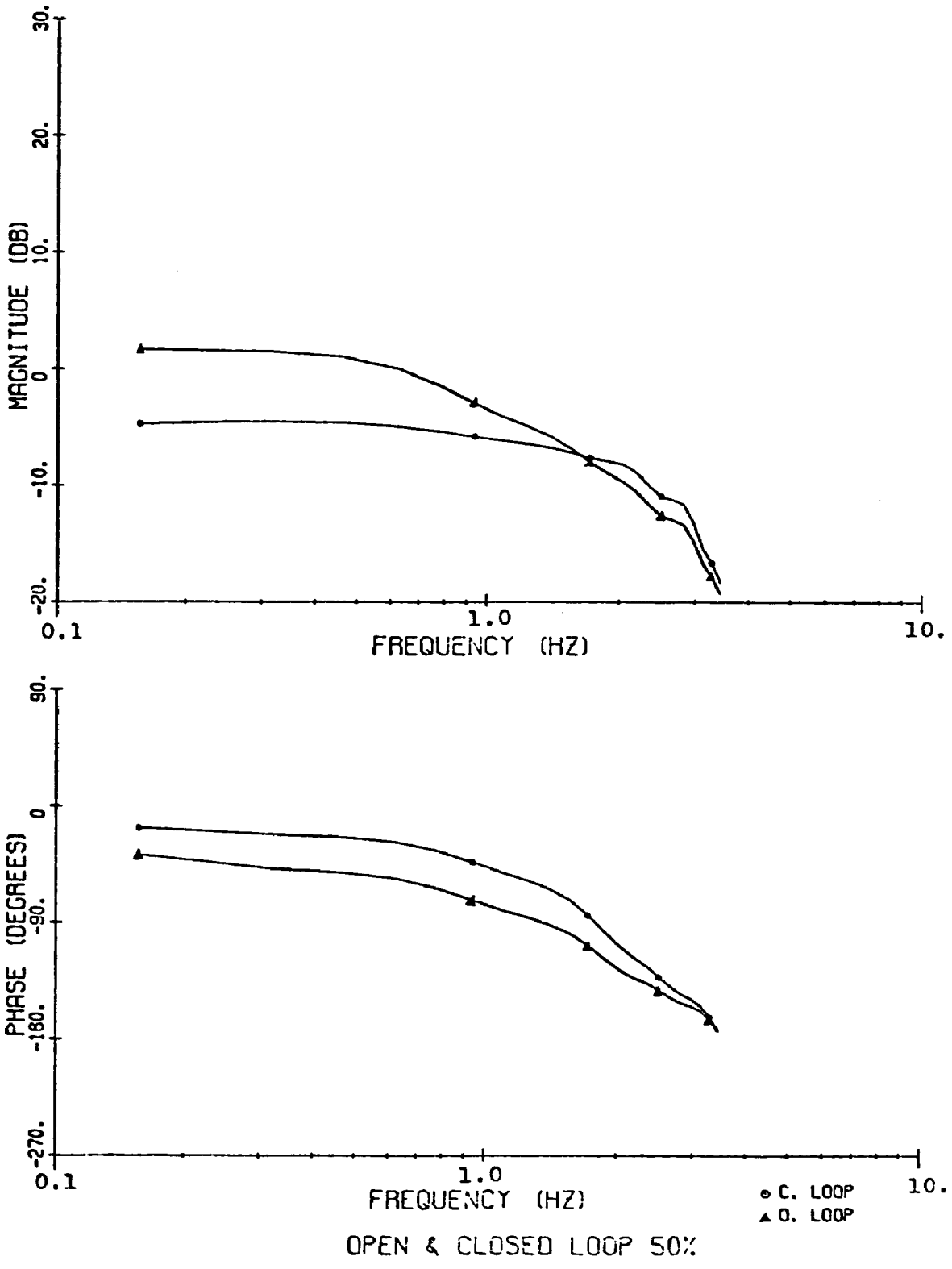

FIGURE 9.4. Open and closed loop Bode plots (50% Noise).

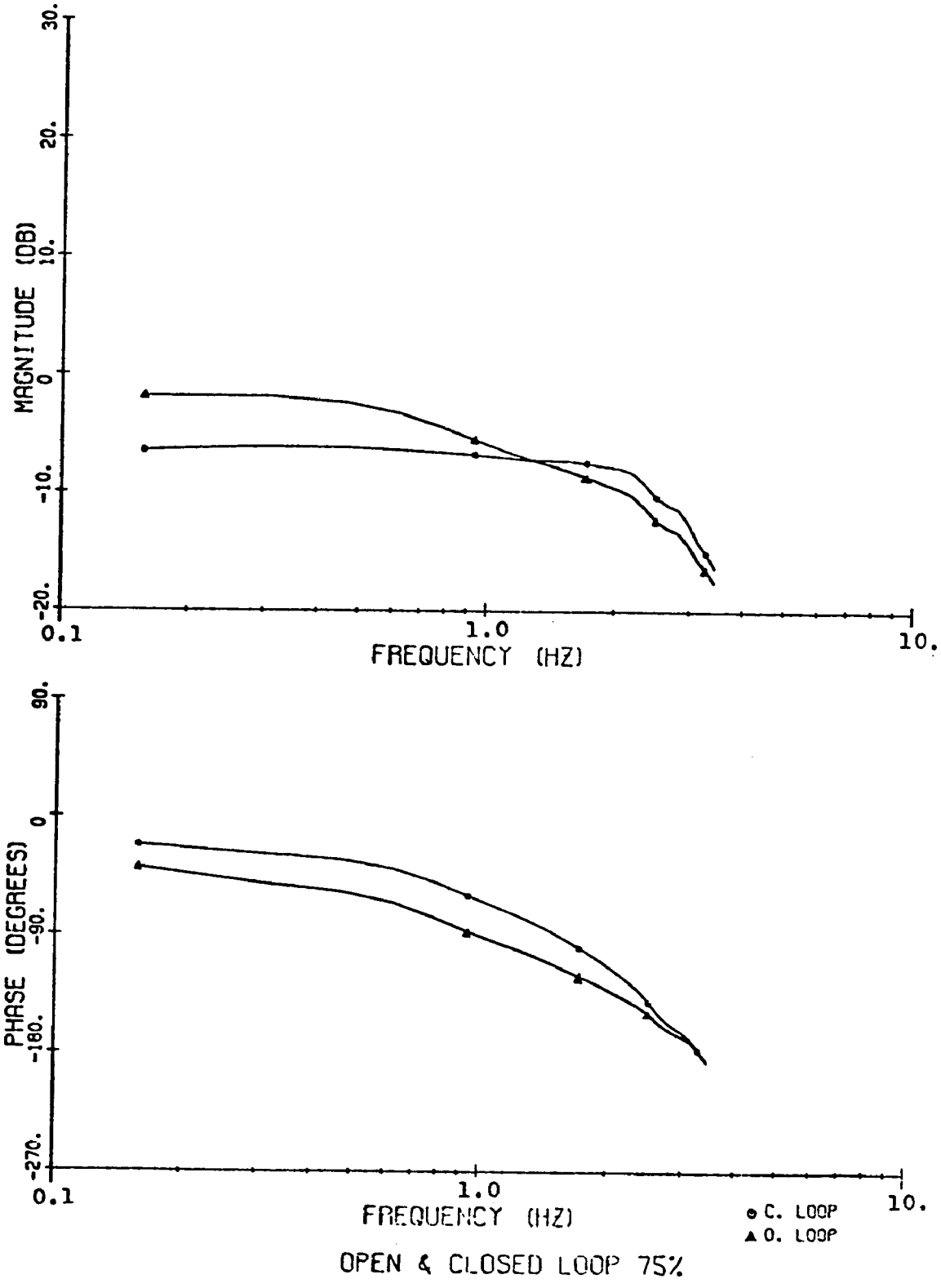

FIGURE 9.5. Open and closed loop Bode plots (75% Noise).

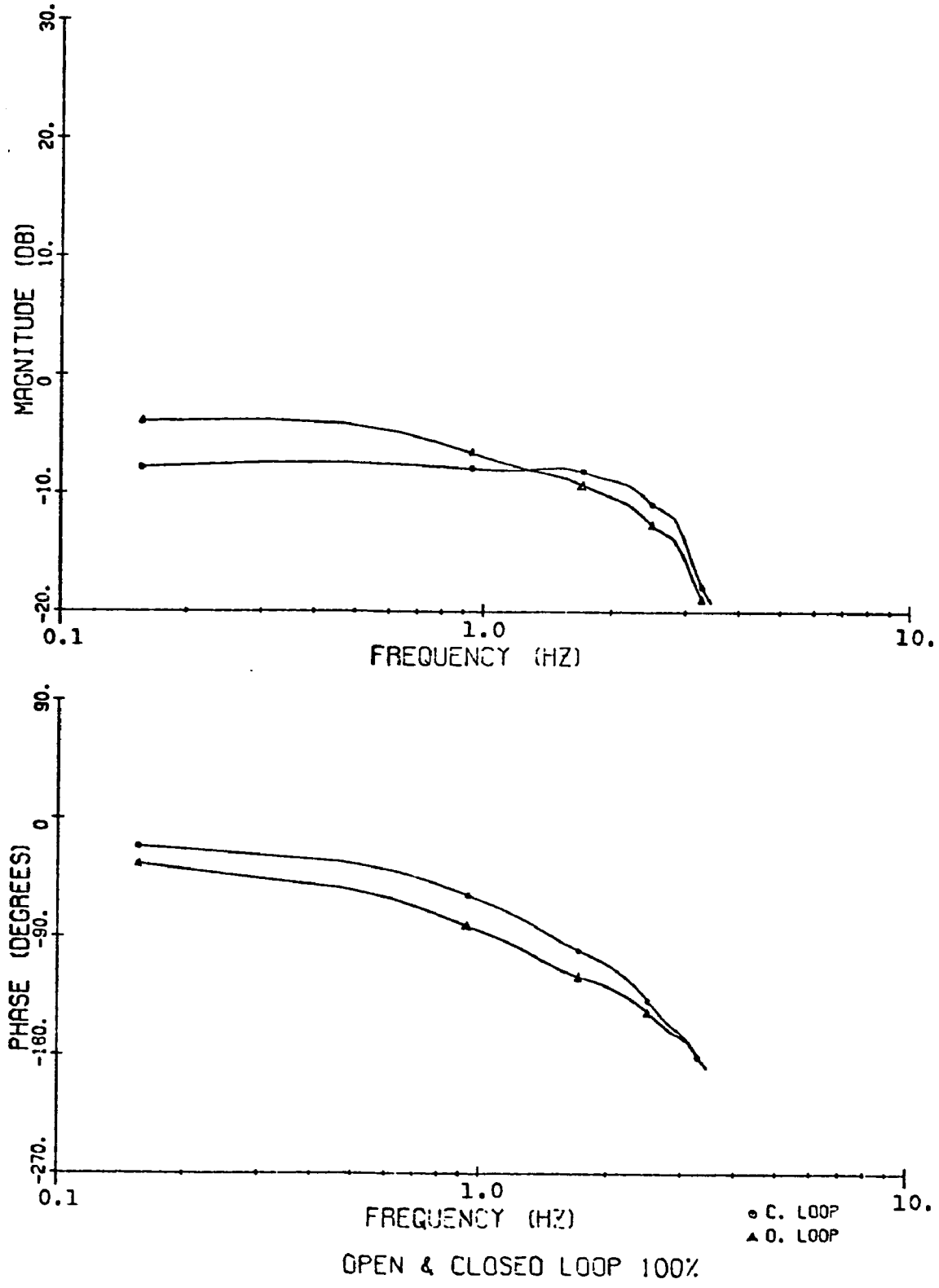

FIGURE 9.6. Open and closed loop Bode plots (100% Noise).

deviations are given in Appendix G. The open loop data computed from Equation (9.2) are also shown on each of these figures.

Qualitatively, one can see a gradual change in the closed loop Bode plots as the predictability of the input waveform changes; as the predictability decreases the gain decreases and the phase lag increases at the higher frequencies.

The open loop data in Figures 9.2 to 9.6 indicate that the open loop zero frequency gain increases rapidly and the phase-lag decreases as the predictivity of the input increases. This is exactly what would be expected if the system were using the information inherent in the more preditive inputs to improve tracking performance. The data show that tracking performance is improved by increasing the amplitude of the eye response and by reducing the phase lag between the target motion and the resulting eye movements.

These Figures show another interesting and somewhat surprising result. From examination of both the closed and open loop Bode plots, it is obvious that the bandwidth of the system decreases as the predictability of the input increases. This is particularly true for the open loop Bode plots.

All the gain-frequency plots for both the open and closed loop cases have an attenuation rate at higher frequencies of approximately 60 db per decade. This suggests that perhaps the

data can be fit with a mathematic operator having three poles in the complex frequency domain. This is in general agreement with results obtained with single sinusoid inputs in Experiment 1 and also agrees with the single sinusoid data from Young and Stark (68), Wheeless (61), and Fender and Nye (25). Dallos (15), however, reports a system with a 40 db per decade roll-off at higher frequencies that implies a second order instead of a third order system.

Equation (9.3) was used to compute the data for the open loop controller; the corresponding Bode plots are shown in Figures 9.7 to 9.11. The gain-frequency part of these plots have an attenuation rate of approximately 40 db per decade which implies that the controller magnitude function behaves like that of a second order system. Later in this chapter, a computer programmed optimization routine is used to see how the parameters of a best fit second order system behave as a predictability of the input changes.

One very important aspect of the open loop controller Bode plots should be stressed: namely, that the phase lag and attenuation due to the mechanics of the oculomotor plant (eyeball, muscles, etc.) have been removed from these plots. Therefore, the resulting data must account for neural time delays, for whatever prediction occurs, and for other information processing occurring within the CNS. This is

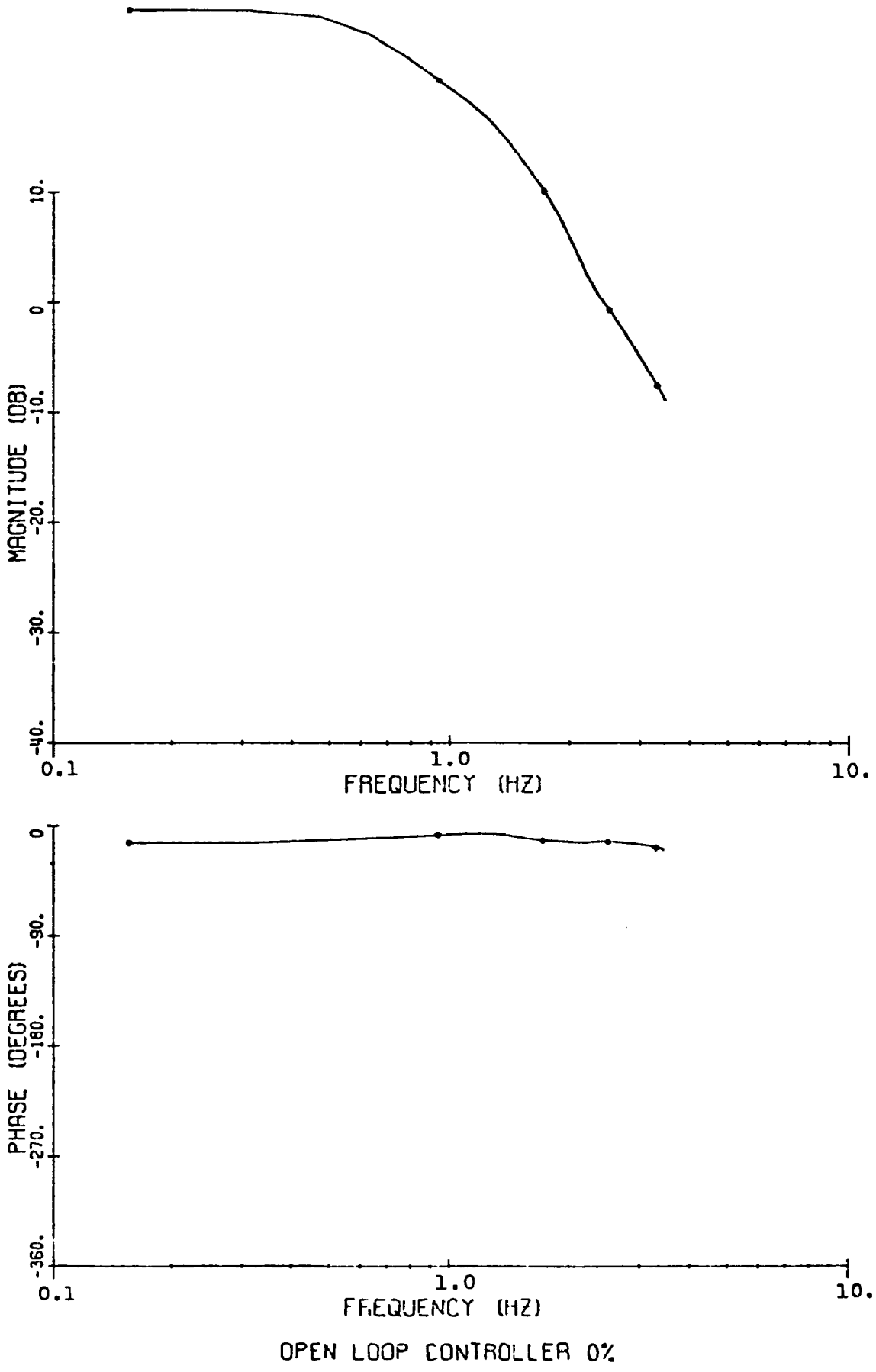

FIGURE 9.7. Open loop controller Bode plot (0% Noise); $C_1(S)$.

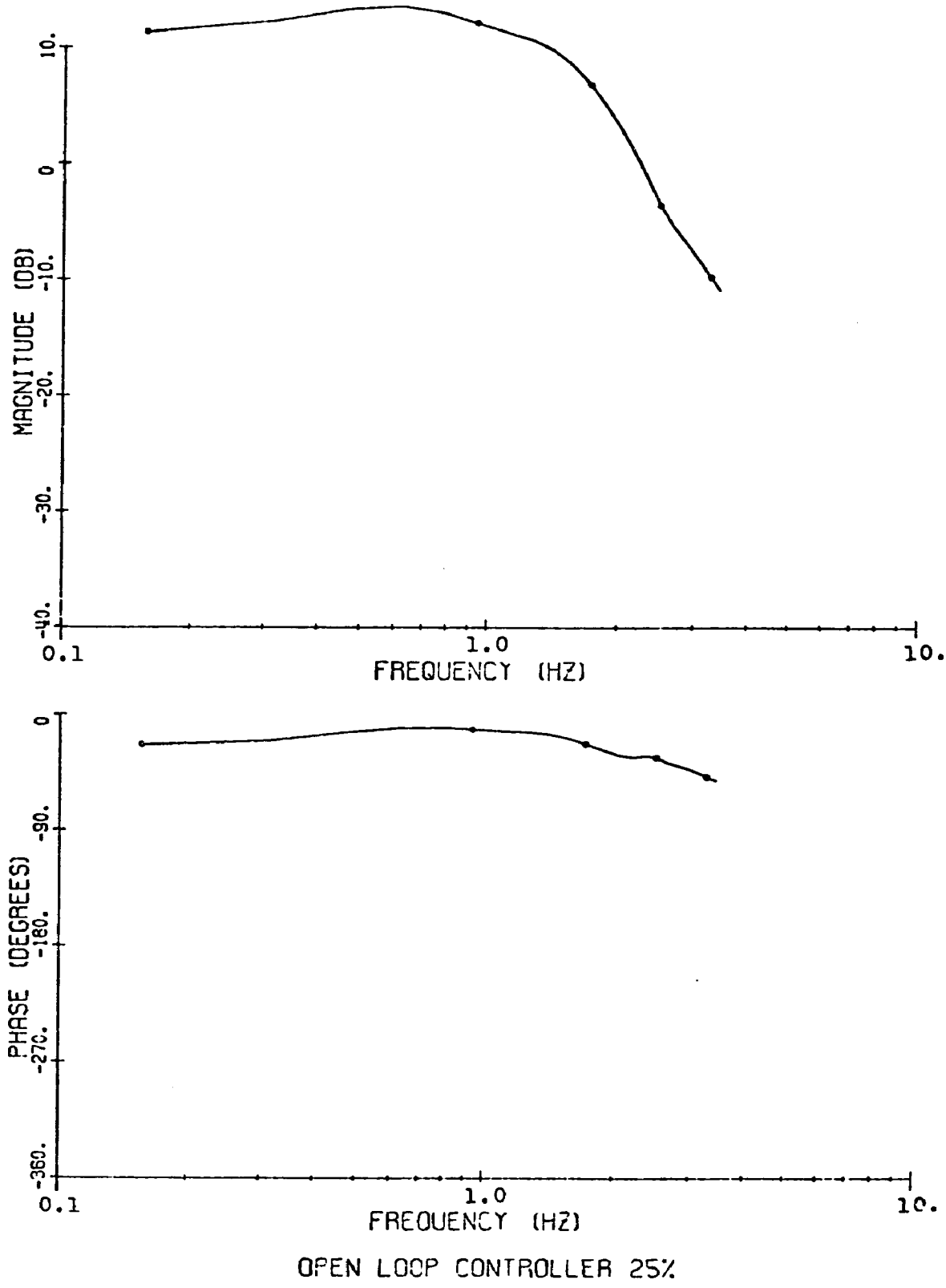

FIGURE 9.8. Open loop controller Bode plot (25% Noise); $C_2(S)$.

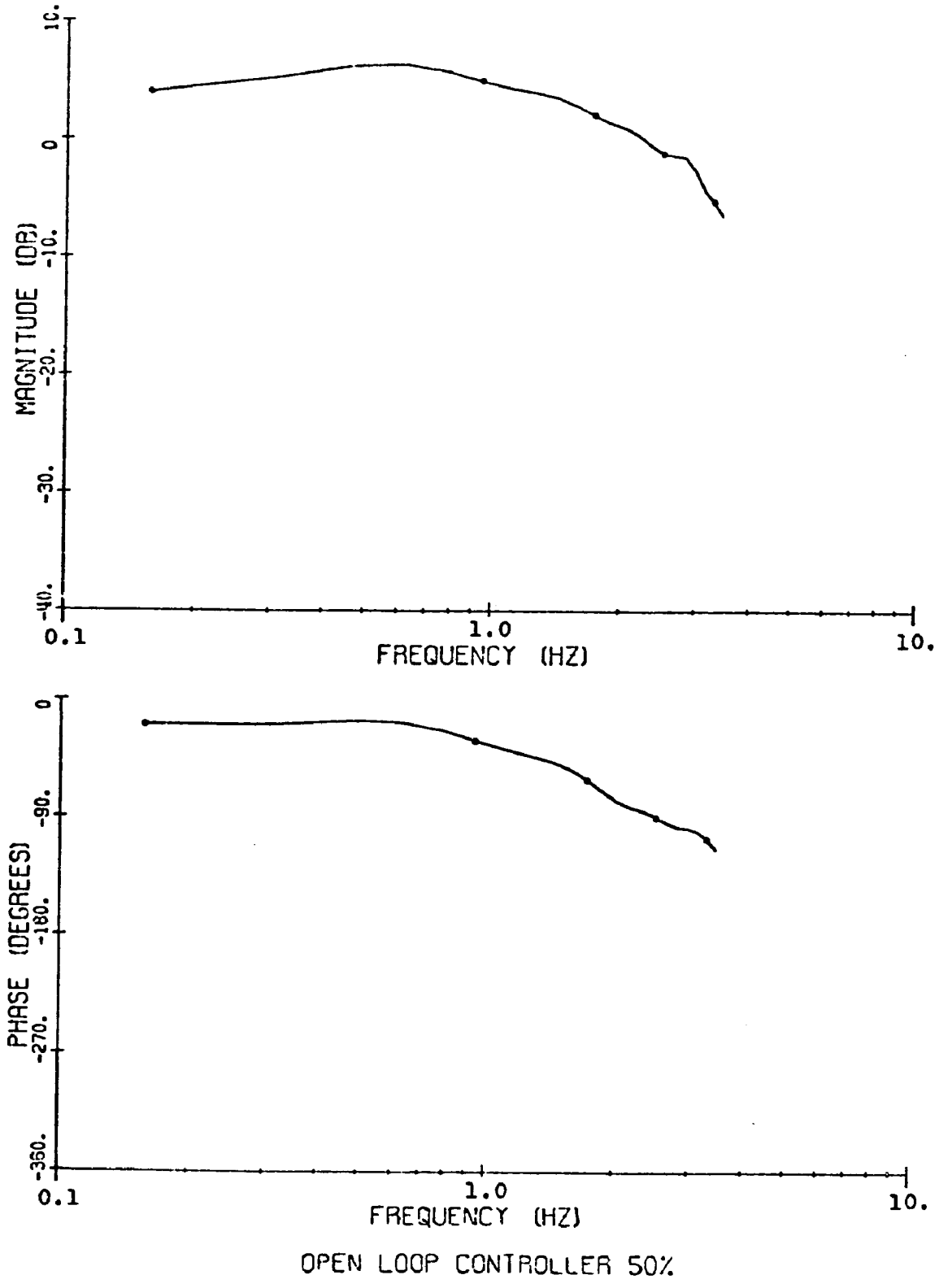

FIGURE 9.9. Open loop controller Bode plot (50% Noise); $C_3(S)$.

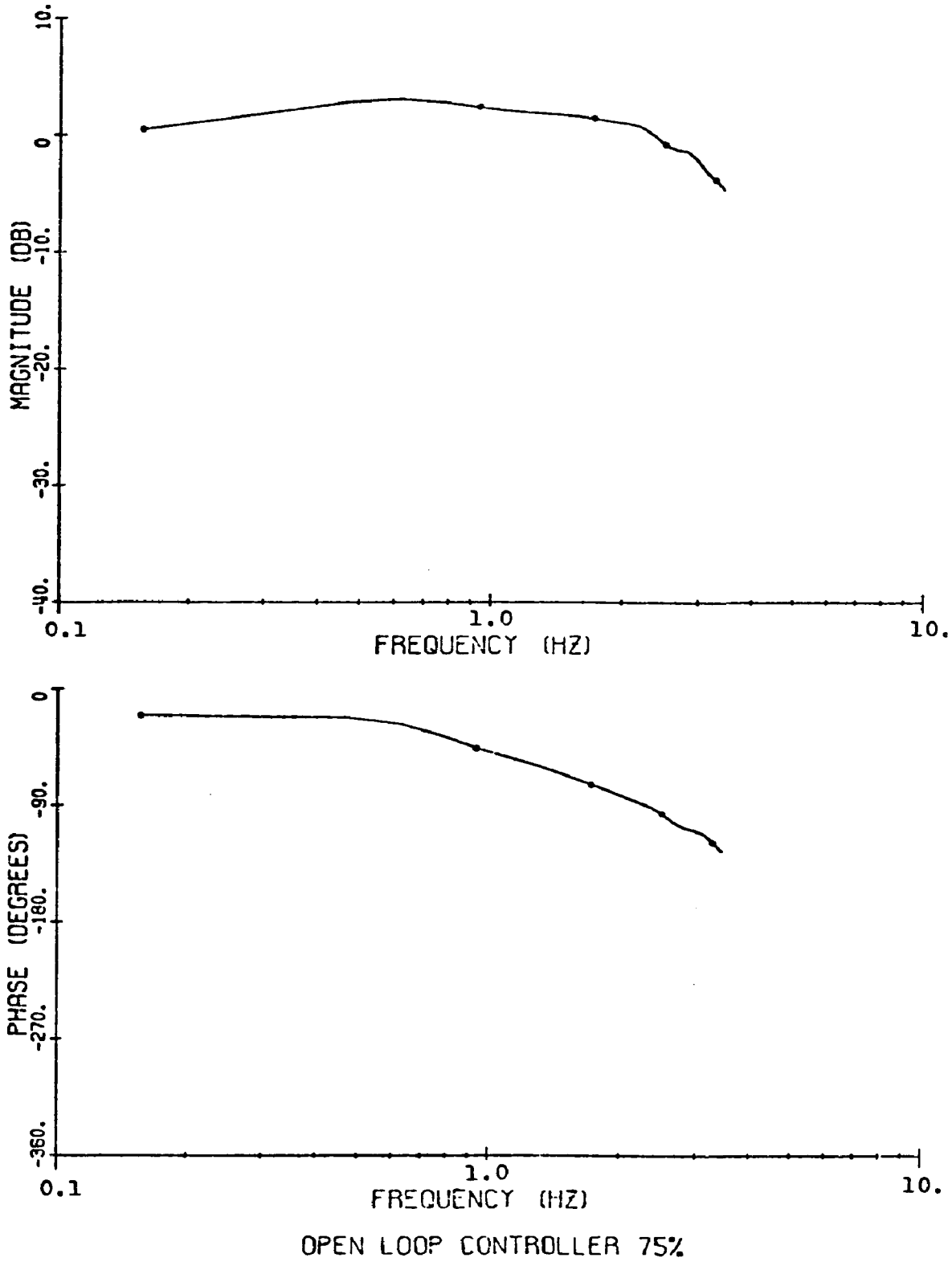

FIGURE 9.10. Open loop controller Bode plot (75% Noise); $C_4(S)$.

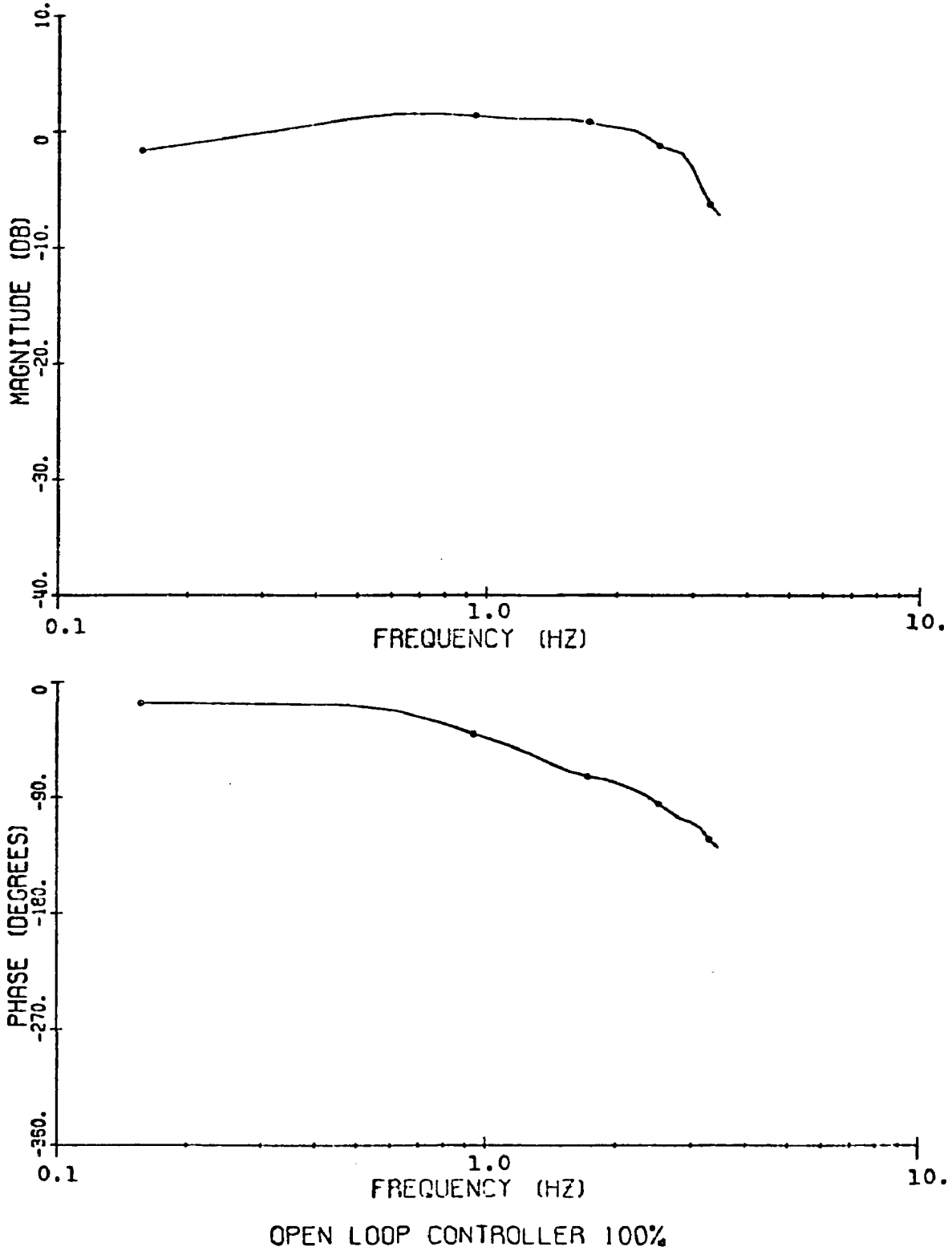

FIGURE 9.11. Open loop controller Bode plot (100% Noise); $C_5(S)$.

especially important when the whole question of prediction is considered. For example, St. Cyr and Fender (52) suggest that all the phase lag in the phase-frequency plots obtained by different investigators is due to simple neural time delays. They completely disregard the mechanics and dynamics of the extra-ocular muscles as well as the eyeball with its supporting tissue. As can be seen in Figure D.2 (Appendix D), the plant introduces a considerable amount of attenuation and phase lag into the system that must be considered.

Figure 9.7 shows the controller frequency response characteristics for the pure swept sinusoid input. In this graph it is interesting that the phase lag actually decreases somewhat over part of the frequency range. This certainly would not be expected from the behavior of the magnitude plot as a function of frequency. If a second order system is to provide a reasonable fit to all the magnitude-frequency data, one would expect a phase lag that approaches 180° at higher frequencies. The actual phase lag is obviously much less and does not increase appreciably with frequency. This would imply that something unconventional is taking place, particularly when the data for the predictive controller (Figure 9.7) are compared to the most non-predictive case (Figure 9.11). In Figure 9.11, the phase lag increases and is not inconsistent with a minimum phase system. The

implication, of course, is that the system uses the pattern in the predictive input to increase the gain of the system and to decrease the phase lag.

It is possible to study these results in a quantitative way with a computer programmed technique that optimizes parameters of an assumed mathematical model to fit experimental data. By examination of the data for the open loop controllers (Figures 9.7 to 9.11), and by the results of "trial and error" runs, the following mathematical form was found to provide a reasonable fit for most of these data (The exceptions will be discussed later.).

$$C_\alpha(S) = \frac{K\, e^{S\tau}}{(S + S_a)(S + S_b)} \tag{9.4}$$

where K, τ, S_a, and S_b are "free parameters" with values computed by the optimization routine. K is a gain constant and τ is a time lag (or lead). S_a and S_b are either complex conjugate numbers or real numbers.

Using Equation (9.4) as the mathematical form for the open loop controller, $C_\alpha(S)$, and Equation (D.4) for the oculomotor plant, P(S), of obvious interest is how well the open loop data for all five input waveforms can be fit by

$$g_\alpha(S) = C_\alpha(S)P(S) \tag{9.5}$$

where P(S) remains fixed and $C_\alpha(S)$ is an operator whose four parameters depend on the statistics of the input waveform. For each of the five input waveforms with the various noise percentages, Figures 9.12 to 9.16 show both the open loop data and the mathematical models obtained after optimization of the $C_\alpha(S)$ parameters.

These figures show that the mathematical model given in Equation (9.5) can fit the open loop gain-frequency data with appropriate optimization of the four free parameters associated with $C_\alpha(S)$. The mathematical model also fits the phase-frequency data for the three most non-predictive waveforms (α = 3, 4, 5). However, for the two most predictive waveforms (α = 1, 2), a simple time lead (τ positive) is not sufficient to provide a good fit to the phase-frequency data (see Figures 9.15 and 9.16). This is contrary to a model of the predictive controller proposed by Sugie (56) who suggests that the whole predictive controller can be mathematically represented by a simple time lead. Actually, it would be surprising if the brain were to implement so complex a process as predicting future target trajectories by use of a constant time lead irrespective of the frequency of target motion.

If the phase lag which corresponds to the gain function is subtracted, a residual phase lead results which cannot be described by minimum phase elements nor, as we have seen, by a simple time lead of the form $e^{S\tau}$. A mathematical expression for this residual phase can be readily obtained by fitting it

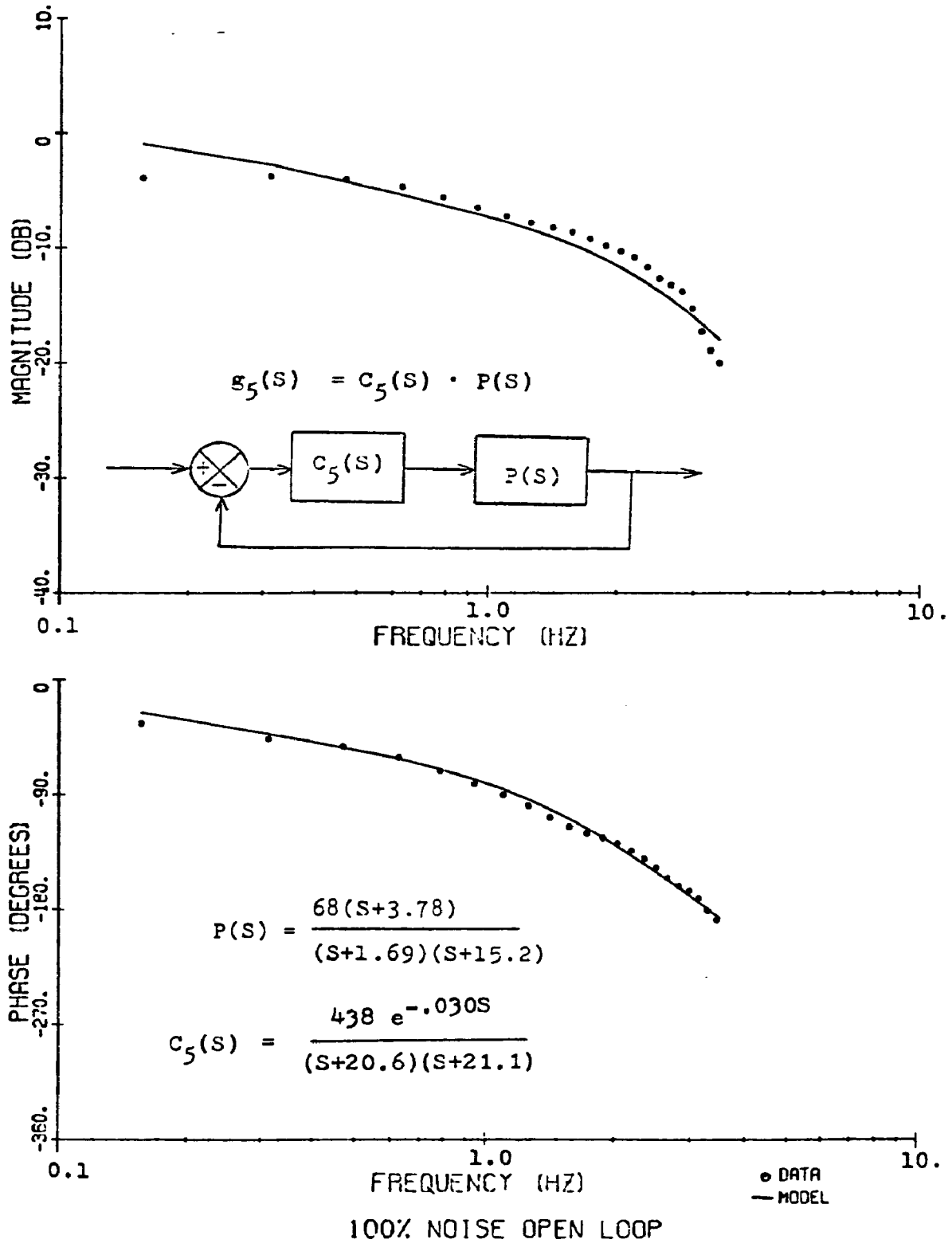

FIGURE 9.12. Open loop data and Model (100% Noise).

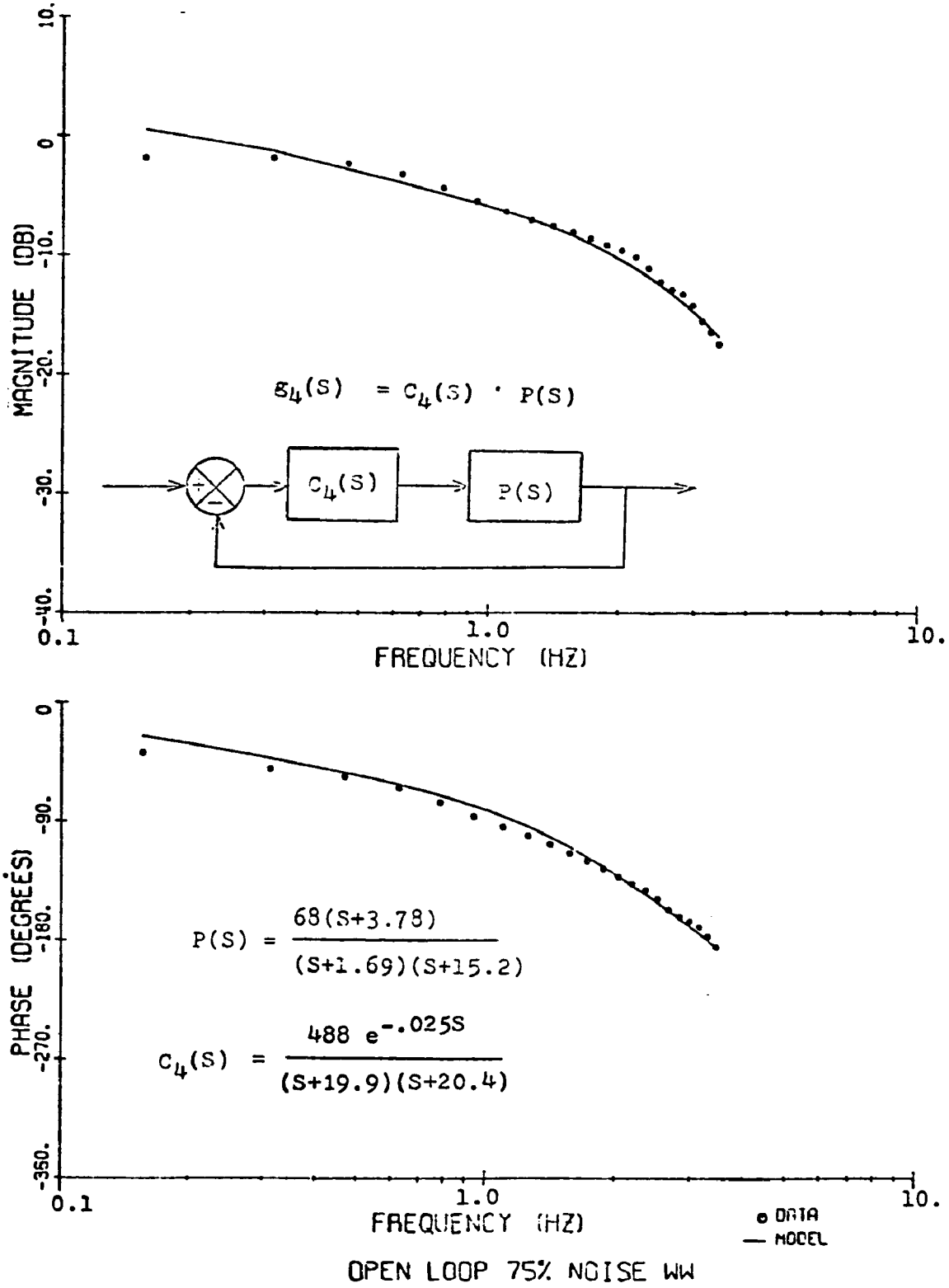

FIGURE 9.13. Open loop data and Model (75% Noise).

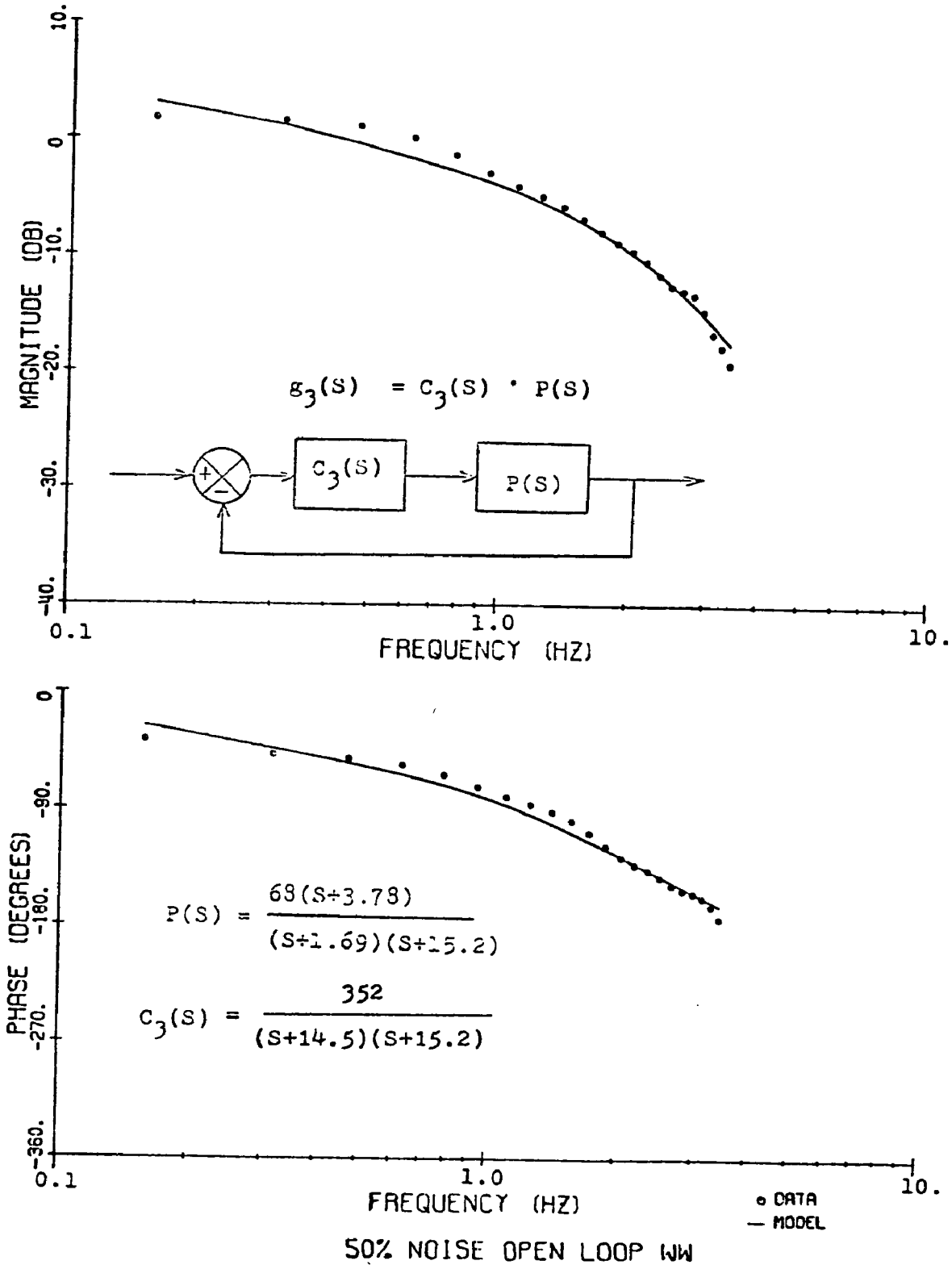

FIGURE 9.14. Open loop data and Model (50% Noise).

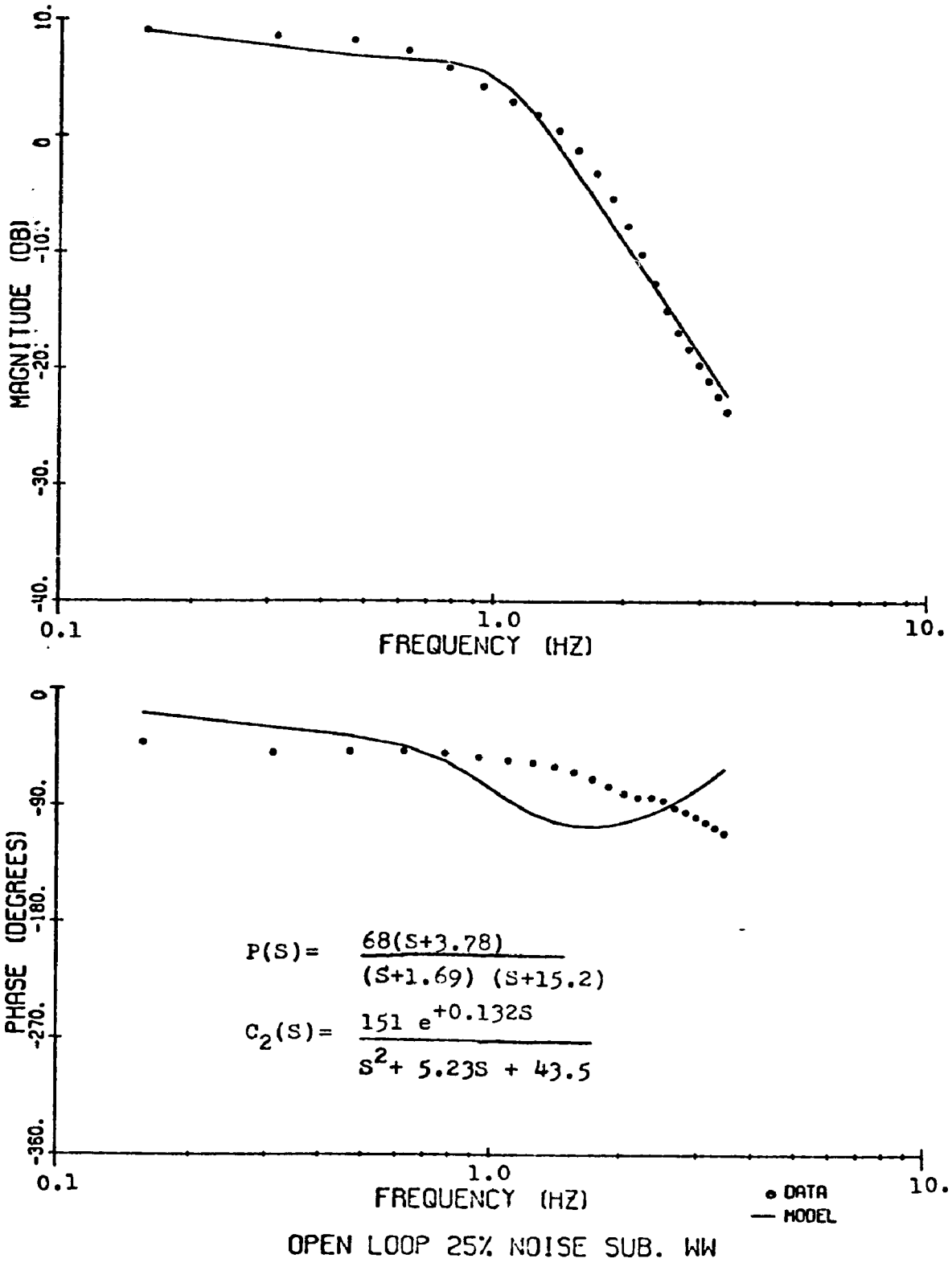

FIGURE 9.15. Open loop data and Model (25% Noise).

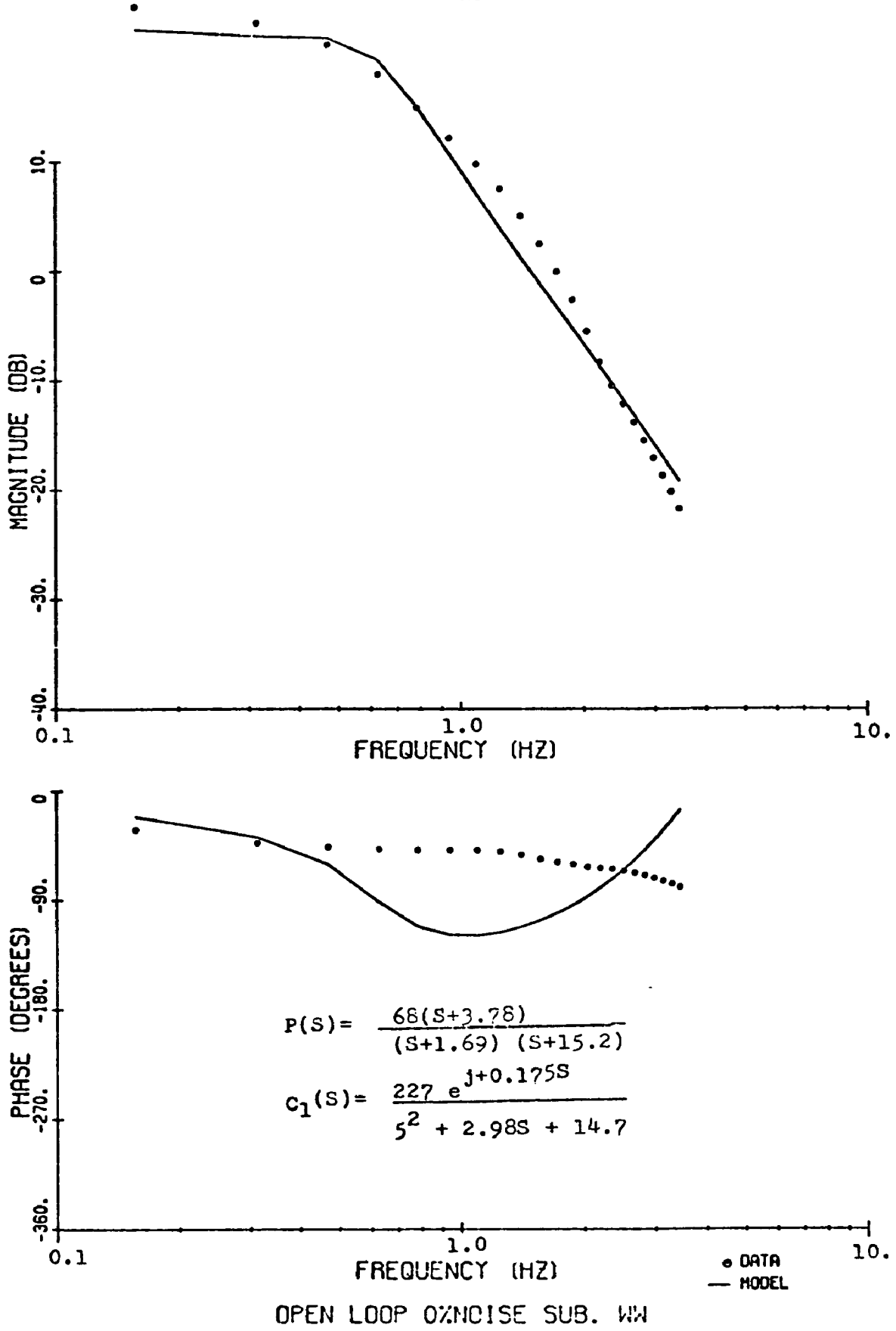

FIGURE 9.16. Open loop data and Model (0% Noise).

with a simple polynomial:

$$\rho_\alpha(\omega) = a + b\omega + c\omega^2 + d\omega^3 + \ldots . \tag{9.6}$$

The controller would then have the form

$$C_\alpha(j\omega) = \frac{K\, e^{j\rho_\alpha(\omega)}}{(j\omega + S_a)(j\omega + S_b)} \tag{9.7}$$

where all the parameters are the same as in Equation (9.4) except $\rho_\alpha(\omega)$ which is given in Equation (9.6).

Clearly the element which is described by Equation (9.6) is a mathematical abstraction and not physically realizable (with conventional components). However, it should be remembered that prediction is an unconventional process and that the brain, capable of memory and learning, is an unconventional component.

Figure 9.17 shows the phase plots for $C_\alpha(j\omega)$ when $\alpha = 1, 2$. In these plots, the polynomials represented by $\rho_\alpha(\omega)$ are of fourth order and are fitted to the residual phase lead by the method of least squares. Perhaps the curve fitting is not of primary importance here but it does indicate that prediction and residual phase lead cannot be adequately explained by a constant extrapolation time. The extrapolation time is a function of target motion frequency. In any case, a constant time lead is not as intuitively acceptable as a simple

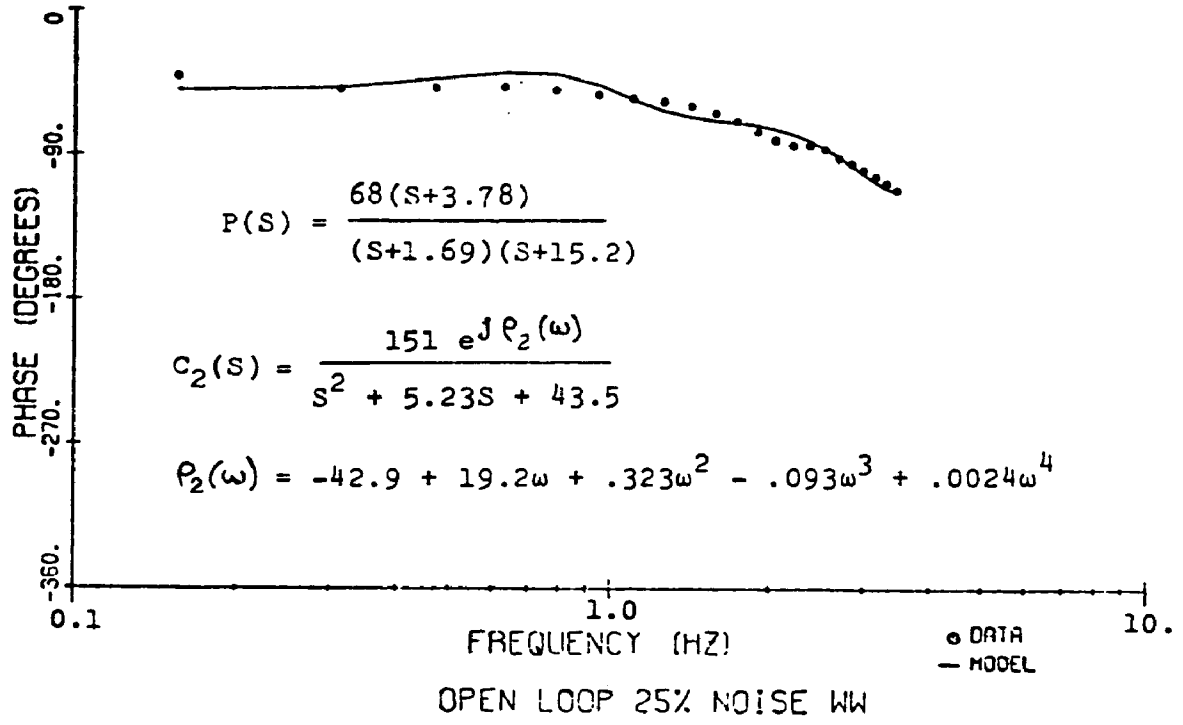

a) $\alpha = 2$

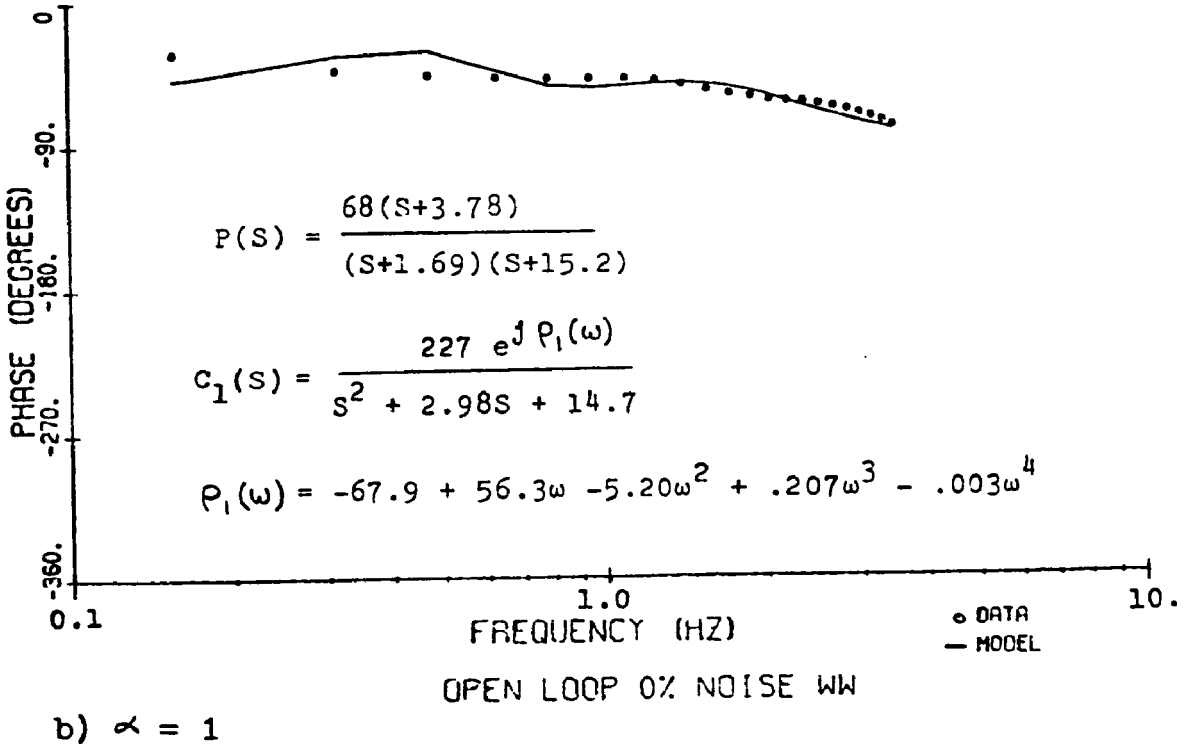

b) $\alpha = 1$

FIGURE 9.17. Phase Plots for $C_\alpha(S)$ when $\alpha = 1, 2$.

time lag (transport delay) which can be physiologically attributed to the finite velocity of neural impulses. Hence, it is not surprising to find that a time lags fits a residual phase lag quite well but that a time lead does not fit the data with a residual phase lead.

As mentioned earlier, most of the open loop controller data can be fit by a mathematical operator with four parameters [see Equation (9.4)]. Table 9.1 is a list of these four parameters for each of the five input waveforms. These parameters show how $C_\alpha(\omega)$, one mathematical operator representing the oculomotor controller, changes as the predictability of of the input waveforms change.

Of special interest is the behavior of parameter τ as the predictivity of the input waveforms change. For the most non-predictive input, the 100% random noise sequence, the optimal value of τ for best fit to the experimental data is - 30 ms, i.e., a 30 ms time delay. As the ratio of non-predictive signal to predictive signal decreases, then τ approaches zero from the negative side and very rapidly goes positive (corresponding to a time lead) for the two most predictive waveforms of the input set. For the pure swept sinusoid input, τ for the "best fit" was computed to be a 175 ms time lead. It should be mentioned again that the "best fit" τ for the two most predictive input waveforms does not fit the data nearly as well as for the more non-predictive cases. However, the computed parameter τ (from minimizing the mean square

TABLE 9.1

CONTROLLER PARAMETERS FOR SUBJECT W.W.

α	Input Waveform	K	τ (ms)	S_a (rad/sec)	S_b (rad/sec)	$\frac{K}{S_a S_b}$
5	100% Noise 0% Swept	438	- 30.	20.6	21.1	1.01
4	75% Noise 25% Swept	488	- 25.	19.9	20.4	1.20
3	50% Noise 50% Swept	352	0.	14.5	15.2	1.60
2	25% Noise 75% Swept	151	+ 132.	2.61+j6.05	2.61-j6.05	3.48
1	0% Noise 100% Swept	227	+ 175.	1.49+j3.53	1.49-j3.53	15.3

error) gives a better feeling for what is happening to the controller phase than polynomials of the type given in Equations (9.6) and (9.7).

Figure 9.18 is a plot of τ vs. the amplitude ratio of random noise to swept sinusoid plus random noise in the input waveform. The shape of this curve is particularly noteworthy. The value of τ rapidly decreases as the amount of random noise in the input waveform increases. This is in agreement with the results of Experiment 2b where predictive tracking is seen to be highly sensitive to the addition of small amounts of random noise to the input waveform.

Figure 9.19 is a diagram in the complex frequency domain showing how the system poles (computed for best fit to the data) behave for all five waveforms in the input set. It can be seen from this diagram that the bandwidth of the system decreases as the predictability of the input increases. Also for the two most predictive waveforms of the input set, the poles S_a and S_b are complex conjugates instead of real numbers. The damping ratio in both cases is approximately 0.4. This diagram again points out that addition of a random component to the predictive input waveform causes the bandwidth of the controller to increase quite rapidly.

Figure 9.20 is a plot of the controller zero frequency gain, defined as K/S_aS_b, vs. the amplitude ratio of random noise to

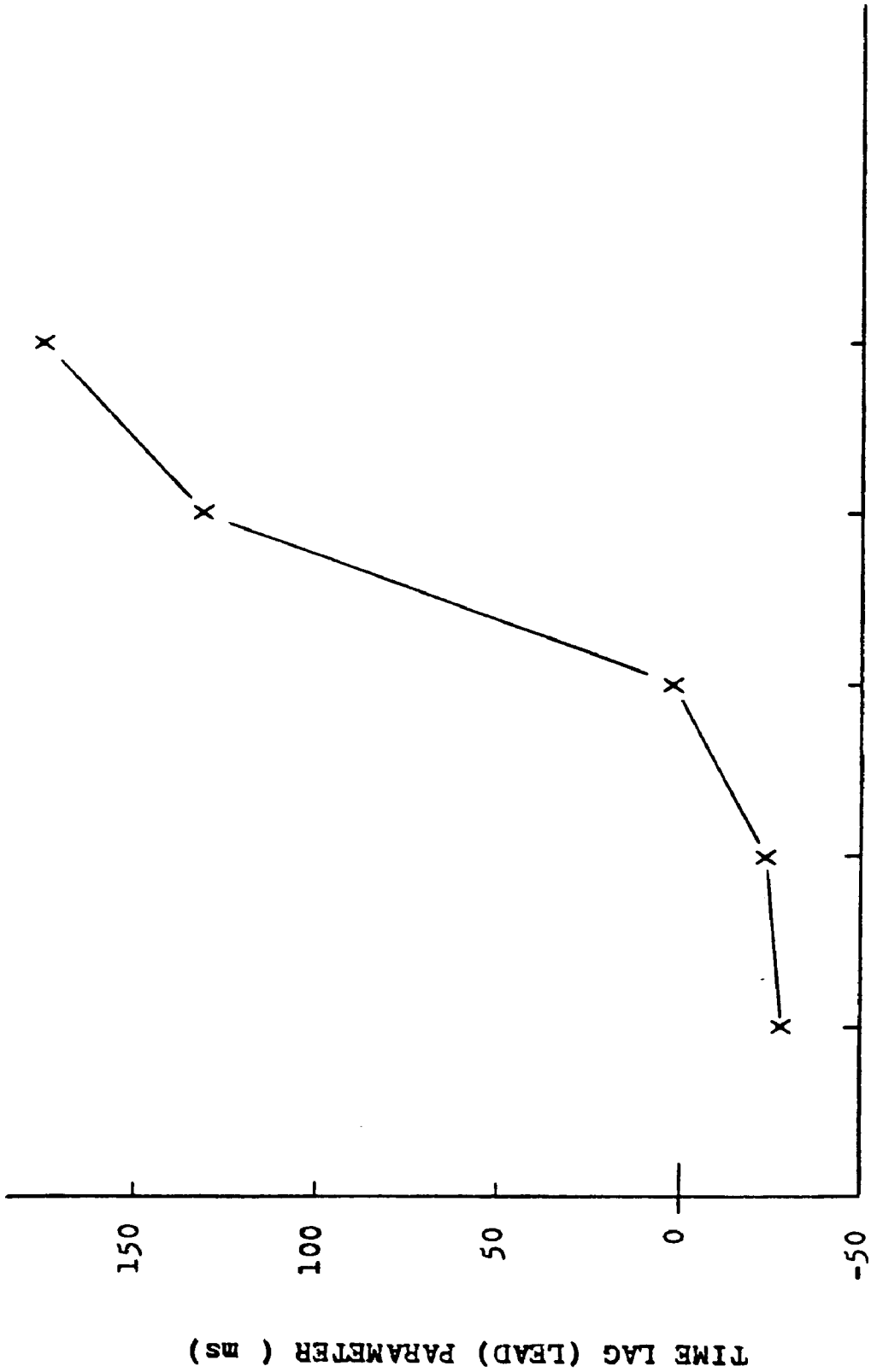

FIGURE 9.18. Plot of Changes in the Parameter τ for Various Random Noise Content.

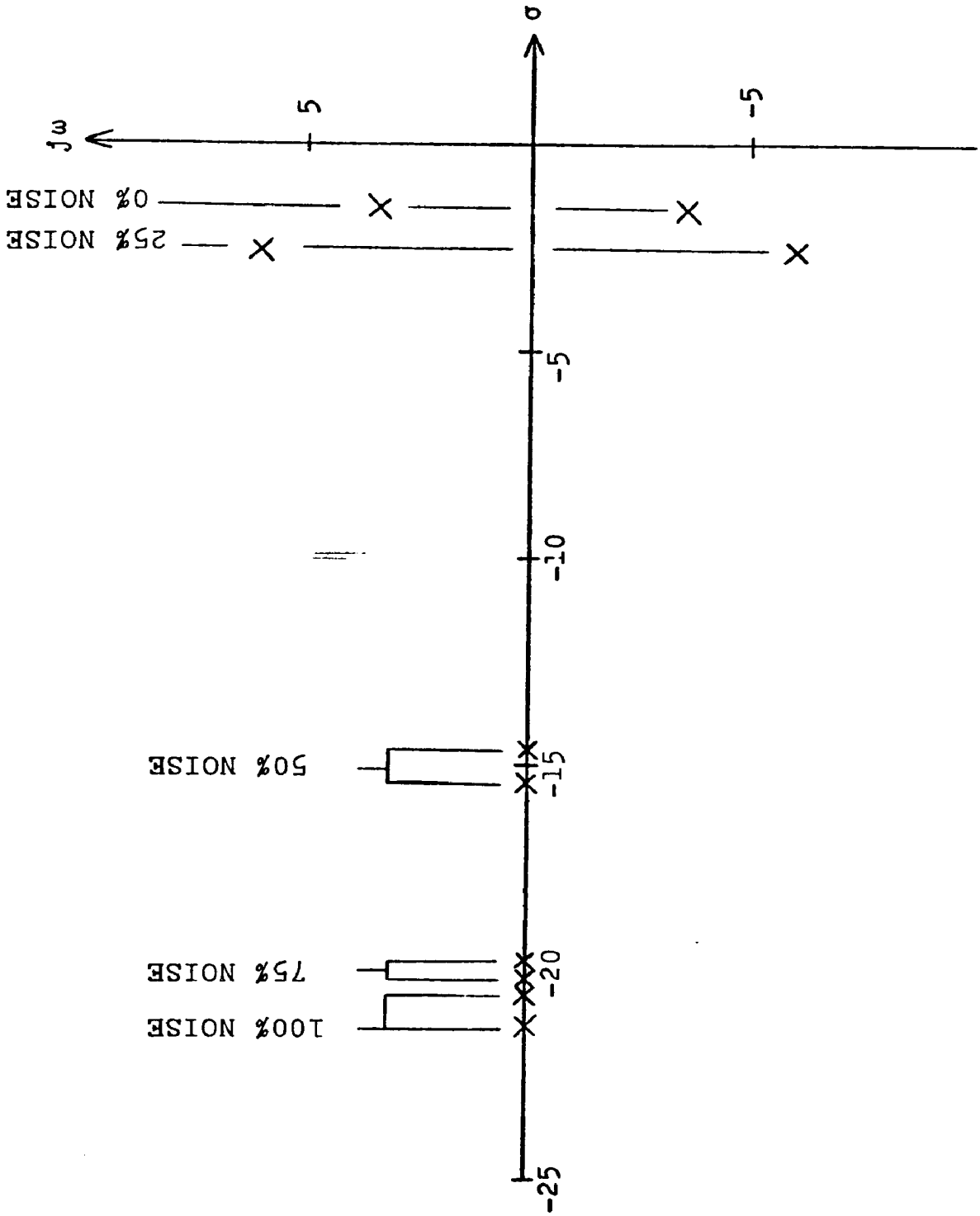

FIGURE 9.19. Root Position Diagram for the Oculomotor Controller given by Equation (9.4).

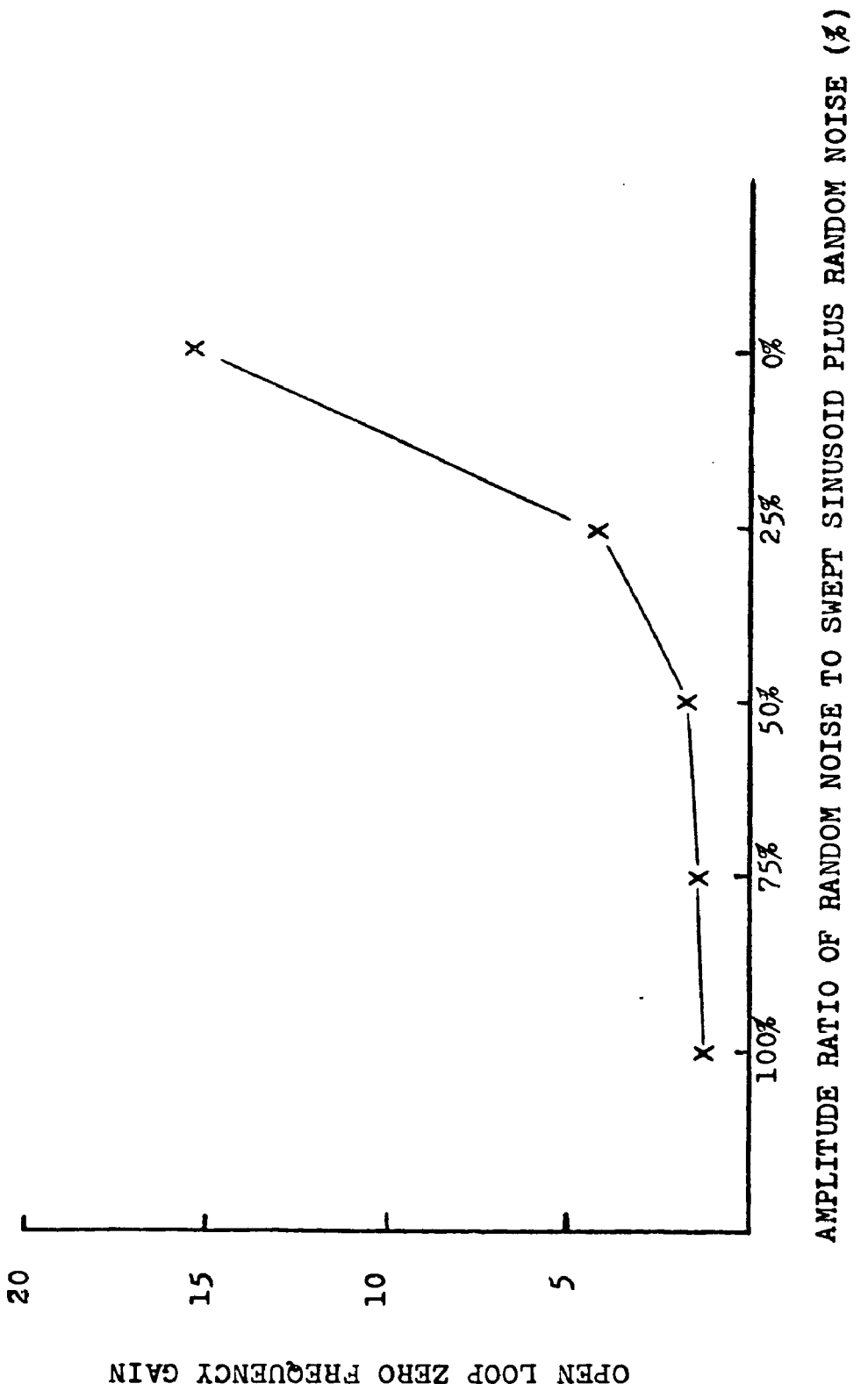

FIGURE 9.20. Plot of Changes in the Open Loop Zero Frequency Gain with Varying Amounts of Noise.

swept sinusoid plus random noise in the input waveform. This curve again shows very rapid changes in zero frequency gain that occur when "noise" is added to the predictive input. In particular, the addition of a random component causes the gain to decrease rapidly.

Different systems are often evaluated by comparing "Figures of Merit" based on parameters indicative of system performance. One widely used Figure of Merit is the gain-bandwidth product because often one cannot increase gain in many systems (or devices) without sacrificing bandwidth or vice versa. In Figure 9.13 we see that the system poles move closer to the $j\omega$ axis as the predictability of the input waveform increases, indicating a steady decrease in bandwidth. Also Figure 9.14 shows that the gain of the controller increases rapidly when the input waveform predictability increases. Therefore, what happens to the gain-bandwidth product as a function of the predictability of the input waveform is of interest. Such a plot is given in Figure 9.21. Here we see that, even though the bandwidth decreases as the predictability increases, the gain-bandwidth product increases as the amount of random noise in the input waveform decreases. This is again in agreement with the results of Experiment 2b. Looking at the gain-bandwidth product as a Figure of Merit, it makes sense that such a parameter would increase for predictive inputs if the system were using prediction to improve system performance.

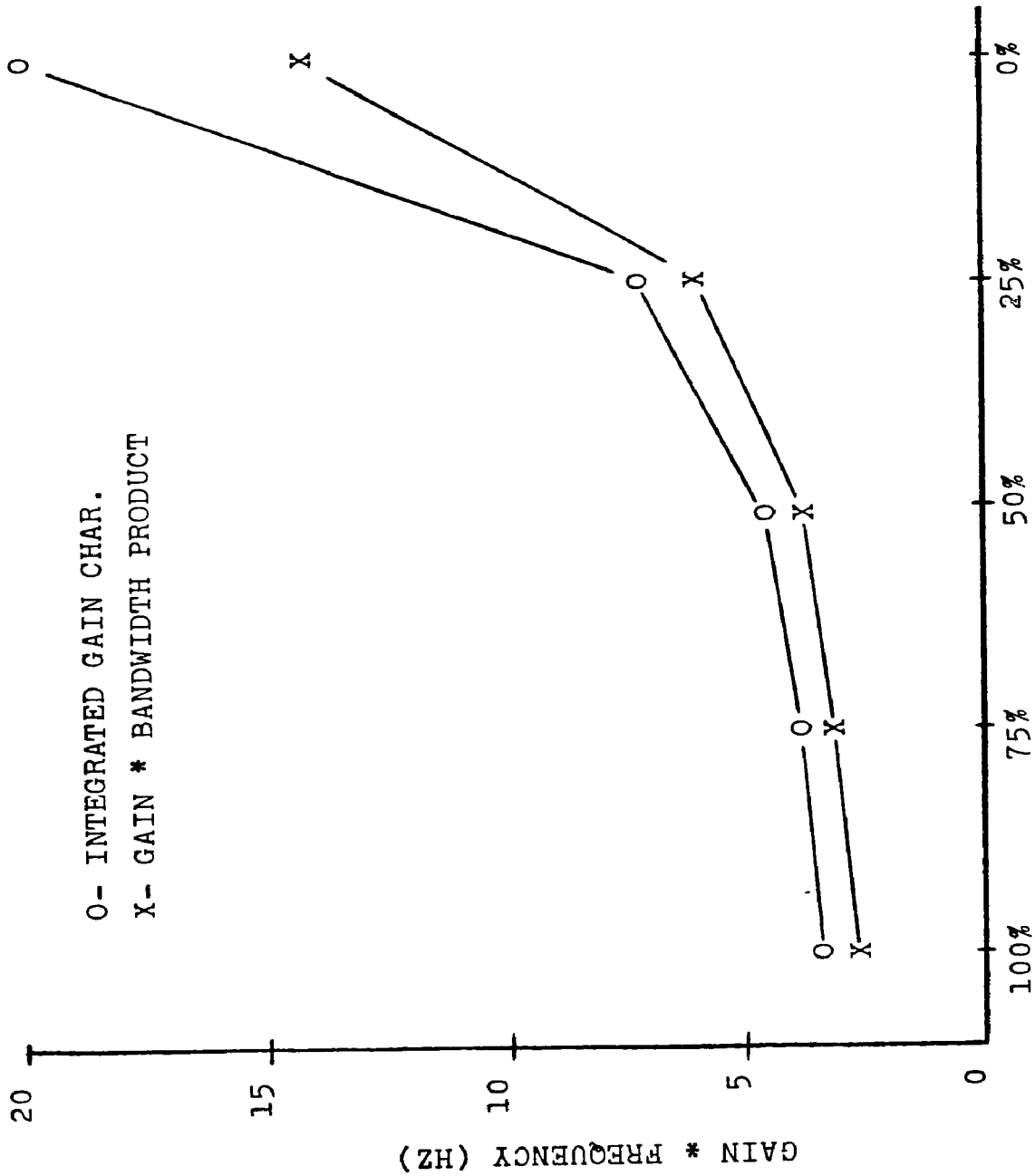

FIGURE 9.21. Two Measures of the Controller Gain Bandwidth Product.

Figure 9.21 gives two curves as different measures of the gain-bandwidth product. The lower curve shows the zero frequency gain times the frequency where the attenuation is - 3 db. The upper curve shows the total area under the gain-frequency curve. Both curves are plotted as a function of the amplitude ratio of random noise to swept sinusoid plus random noise in the input waveform.

Up to this point, the experimental results obtained with one individual have been given (subject W.W.). However, experiments with three other subjects show that the results obtained are generally applicable. A tabulation of the parameters comprising $C_{\alpha}(S)$ for the five input waveforms are given for another individual (subject M.C.) in Table 9.2. Qualitatively, the data for subject W. W. and subject M. C. are very similar. The open loop gain and parameter τ both increase for each subject and the open loop bandwidth decreases for each subject as the predictivity of the input waveform increases. Quantitatively, there are some minor differences. The open loop gain is higher for subject W. W. than for subject M. C. for all input waveforms. However, subject M. C. has a higher bandwidth for all input waveforms. Surprisingly, parameter τ, computed for best fit, was essentially the same for both subjects.

TABLE 9.2

CONTROLLER PARAMETERS FOR SUBJECT M.C.

α	Input Waveform	K	τ (ms)	S_a (rad/sec)	S_b (rad/sec)	$\frac{K}{S_a S_b}$
5	100% Noise 0% Swept	701	- 30.2	26.9	27.2	.959
4	75% Noise 25% Swept	902	- 27.3	29.2	30.9	.998
3	50% Noise 50% Swept	589	- 6.0	20.0	20.5	1.43
2	25% Noise 75% Noise	203	+ 120	5.25+j5.75	5.25-j5.75	3.34
1	0% Noise 100% Swept	159	+ 175	2.06+j5.60	2.06-j5.60	4.50

9.4 Discussion of Results

At this point, it would seem advantageous to discuss some of the assumptions upon which the foregoing results depend. One major assumption is that the system can be represented by a closed loop unity feedback control system. If the image of a small object of interest falls upon the retina such that the image is eccentric with respect to the center of the fovea, then the brain sends neural signals to the oculomotor muscles which cause an appropriate eye motion to return the image to the foveal region. This suggests a closed loop control system that is capable of sensing the difference (error) between the positions of the target and the eye and capable of diminishing that error within some time interval. Moreover, either the motion of the target in front of the stationary eye or the rotation of the eye while the object is stationary, will result in retinal image displacement. Consequently, it is the difference of target and eye positions which determine the whereabouts of the retinal image. This is an important consideration because it establishes a "summing point" in the assumed closed loop control system. Furthermore, the actuating error signal must be the difference between angular target and eye positions, where eye position is the controlled variable. Also, for normal subjects, the positional error is always reduced to very nearly zero as the eye is caused to fixate on the target. These facts suggest that the closed loop control system possesses unity feedback.

Additional evidence (experimental in nature) exists to support the assumption of a unity feedback closed loop control system. Examination of Figure 9.2 shows that the magnitude function of the open loop Bode plot has a much higher zero frequency gain than the closed loop magnitude function. Moreover, at higher frequencies the open loop gain function asymptotically approaches the closed loop gain function. Now, it is possible to vary the retinal image feedback electronically or even to eliminate it altogether, i.e., to open the loop experimentally. This has been done by several investigators (25, 59) with qualitative results very similar to those mentioned above.

Another assumption that should be mentioned is the use of Robinson's oculomotor plant dynamics. Robinson's mechanical schema is based on a large quantity of experimental data (48, 50) and has been corroborated by the results of other investigators (7, 8, 47). A more complete discussion of Robinson's mathematical model of the oculomotor plant is given in Appendix D.

The following is a summary of the assumptions upon which the quantitative results of this chapter depend.

1. The oculomotor control system can be represented by a unity feedback closed loop control system. Justifications for this assumption are given in the above paragraphs.
2. The oculomotor plant can be represented by a <u>fixed</u> linear transfer function. The mechanical schema of Robinson (48, 50) was used to determine P(S) [see Appendix D].

If the oculomotor control system can be represented by a unity feedback closed loop control system, then the open loop data can be

computed from the experimentally determined closed loop data. If the plant can be represented by P(S), a fixed transfer function, then the fixed gain and phase due to the plant can be removed from the open loop data. The data that remain after removing the fixed gain and phase due to P(S) must represent what is happening in that part of the brain which controls the plant, i.e., the oculomotor controller $C_{\alpha}(S)$.

The results of Experiment 4 show for the first time how the oculomotor control system changes from the predictive to the non-predictive mode of operation. In agreement with the results of Experiment 2b, Experiment 4 shows that the predictive mechanism is very sensitive to the addition of non-predictive (or random) components to the target motion waveform. The results also show the gain increases and the phase lag and bandwidth decrease with increasing input waveform predictivity.

We have seen that the oculomotor control system is not fixed but adapts itself according to changes in the input waveforms. The results of Experiment 2a suggest that the system Bode plot is not sensitive to amplitude scaling for small signal inputs. Furthermore, other investigators have shown that very few harmonics of the input frequencies can be detected at the output which implies that the system possesses no lumped nonlinearities. Therefore, the only salient nonlinearity appears to be the adaptive quality of the system, i.e., the mathematical operator relating input to output is not a fixed transfer function but depends on statistics of the input target motion waveform. This suggests that, at any given instant in time, the input-output characteristics may be approximated by a particular linear operator.

In Chapter VI, the system Bode plot was determined from single sinusoids as the input waveforms. In this chapter, and in Chapter VIII,

a swept sinusoidal waveform was used as the predictive input. At this point, a comparison of the results from these two predictive inputs would seem worthwhile.

Figure 9.22 shows the Bode plots obtained by the two different methods for subject W. W. This figure shows that, at low frequencies, both methods give essentially identical magnitude and phase curves. However, at higher frequencies the phase lag and attentuation for the swept sinusoid case is significantly less than the single sinusoid case. These differences verify an essential point made earlier in this study; namely, that results obtained using single sinusoidal inputs cannot be compared blindly with results obtained by other methods. The oculomotor control system is highly adaptive and dependent on the nature of the input used to identify the system. The system cannot be represented by a single fixed linear transfer function.

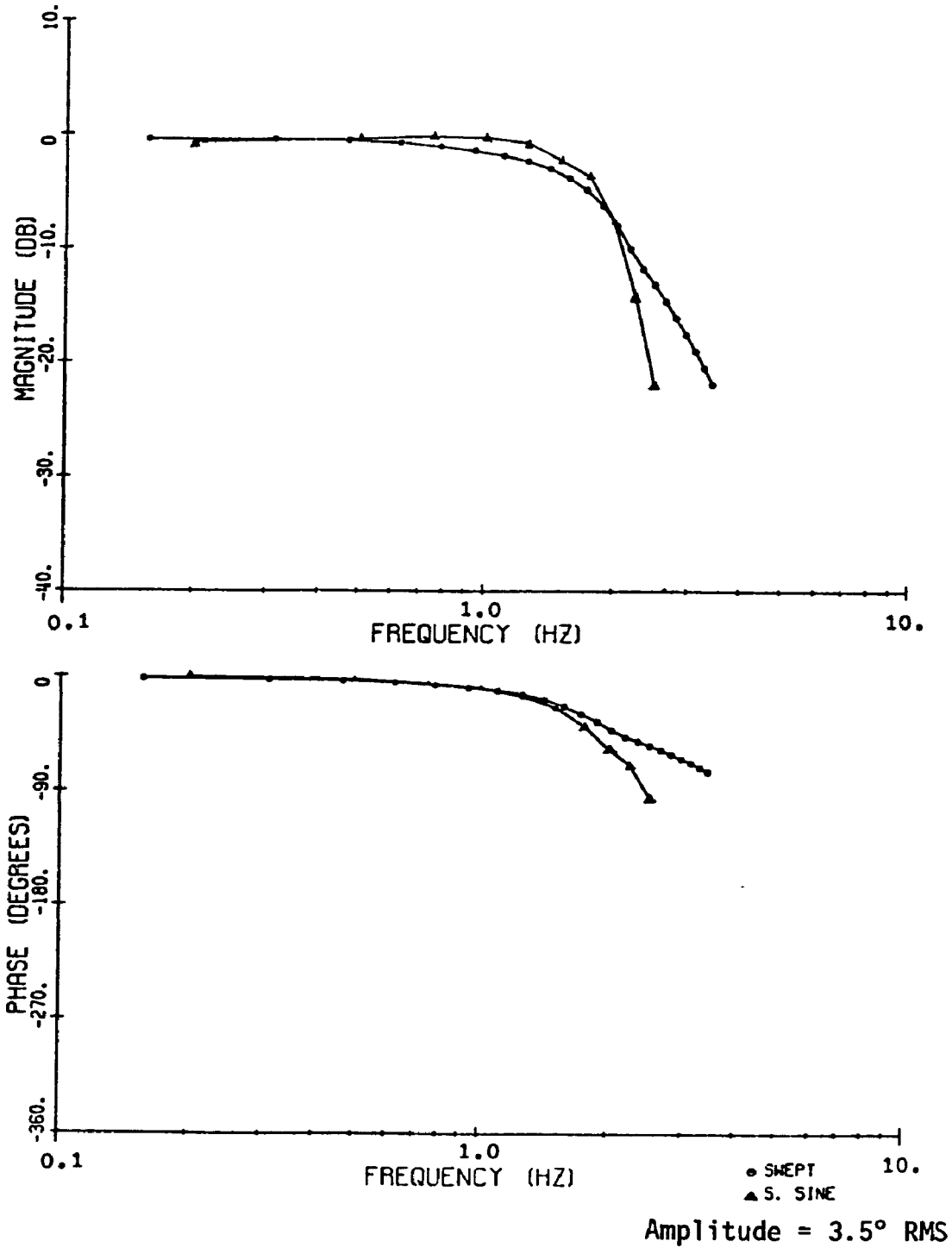

FIGURE 9.22. Single Sine and Swept Bode Plots.

CHAPTER X

CONCLUSIONS

10.1 Summary of Results

The following is a summary of the results presented in this thesis.

1. The oculomotor control system is highly adaptive and cannot be represented by a fixed linear transfer function. The mathematical operator relating input to output continuously varies as the nature of the input varies. This was true for the class of input signals considered in this study.
2. The oculomotor control system is highly dependent on the degree to which the input waveform is predictive.
3. The addition of even a small random component to a predictive input waveform causes the oculomotor control system to change quite rapidly.
4. If the RMS amplitude and power density spectrum of a set of input waveforms are kept constant, the system still changes with alterations in input waveform predictability. In particular, as the predictability of the input waveform increases then:
   a. The gain of the oculomotor controller increases rapidly.
   b. The phase lag of the system decreases rapidly.
   c. The bandwidth of the controller decreases.
   d. The gain-bandwidth product of the controller increases.

e. The residual phase lag for the more non-predictive inputs can be fit adequately by a simple transport delay of the form $e^{S\tau}$ for negative τ.

f. The residual phase lead for the highly predictive inputs cannot be adequately fit by a transport lead of the form $e^{S\tau}$ for positive τ. This implies that the extrapolation time of the predictor is a function of the frequency of the input waveform.

g. The poles of the oculomotor controller are real for non-predictive inputs but become complex for highly predictive inputs. As the predictivity increases, the poles move inwards toward the $j\omega$ axis in the complex frequency domain.

5. For small signals, the system is not amplitude dependent, in agreement with the results of other investigators.

10.2 Suggestions for Further Research

Changes in the oculomotor control system that result from changes in the degree of predictability of the input waveform are considered in this study. Other parameters of the input waveform are known to have some effect on the system transfer characteristics. Experiments analogous to Experiments 3 and 4 should be performed in order to determine the effects of the input frequency spectrum on the system. At some input amplitude level, the system becomes amplitude dependent. Further research is necessary to determine the effects on the system of these larger amplitude inputs.

The oculomotor control system was shown to be highly adaptive. However, very little is known about the dynamics of the adaptive mechanism. It would be interesting to measure the system response to an

instantaneous change in some input waveform statistic. It would also be desirable to determine a Bode plot of the adaptive mechanism for changes in some specific input waveform parameter. This could be done by varying the selected parameter sinusoidally at different frequencies. Variation of the parameter with a swept sinusoid or a random noise sequence might also be productive.

Several investigators have used electronic methods to "open the loop" thereby removing all retinal image feedback. These methods could be used to test the validity of the unity feedback system configuration assumed in Chapter IX. However, some caution should be exercised when interpreting the results of electronic feedback experiments. For example, when all retinal image feedback is removed, very large eye movements result in response to relatively small input waveforms. This raises the possibility of amplitude dependent nonlinearities for large amplitude eye movements. Since the system is plastic and adaptive, the system may also compensate in some way in response to the entirely different sensation one experiences when tracking waveforms "open loop."

Discussions with several people interested in modern control system theory have helped to define several other possibilities for extension of this work. For example, recent developments in analog computer circuitry and theory make it possible to estimate system parameters in real time. This would be an extremely interesting experiment to conduct and would provide the investigator with much information not available otherwise. In particular, it would be interesting to know how fast the system parameters track changes in the input waveform statistics. Also, one could determine rather complete

information on how system parameters are affected by different input waveform statistics.

A real time display of system parameters would be very useful to people interested in human performance. For example, is it possible to develop an index of performance similar to the Intelligence Quotient (IQ) for such tasks as manual tracking? Such an index for different tasks could be useful for testing drivers, pilots, etc., where a person's performance is a matter of public safety and concern. Such an index might also be useful in detecting certain pathological conditions.

Furthermore, it would be interesting to determine the effects of instant feedback (via a performance index) to the subject concerning how well he is performing a task. Could such feedback facilitate learning how to improve performance in a certain task?

The oculomotor control system can be useful for studies of the effects of certain agents on a physiolgoical control system. Unlike some physiological systems, both the input and output of the oculomotor control system are readily available and easily specified by non-invasive techniques. Also, psychophysical data are not necessary for studying the system. For example, preliminary experiments by this investigator have shown that relatively large dosages of carbon monoxide do not cause gross changes in the oculomotor control function. Extension of this kind of research to include other possibly harmful environmental pollutants might be useful. Moreover, the system could be used to determine the effects of certain pharmacological agents (alcohol, barbiturates, and other "drugs") on a physiological control system. Real time display of system parameter variations would be quite useful in this type of study.

Although a lot can be accomplished by input-output studies of a system, it is obvious that neurophysiological studies are necessary to answer many of the questions that arise concerning the oculomotor control system. Unfortunately, according to some investigators, predictive tracking is unique to man (at least in primates). If this is true, then the study of input-output relationships is perhaps the only way of "getting at" the predictive mechanism in man.

APPENDIX A

Mathematically, the data processing schema discussed in Section 7.5 can be explained in the following manner. Assume we are given a linear system (as shown in Figure A.1) having an

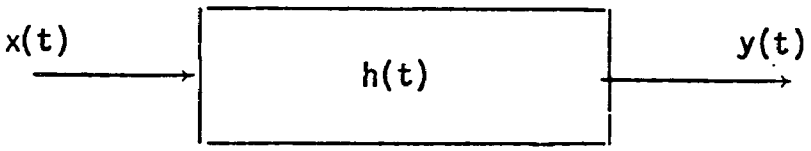

FIGURE A.1

impulse response h(t). If the input signal $S_i(t)$ is a sinusoid with constant amplitude, then the output signal $S_0(t)$ will also be a sinusoid with a different amplitude (A) and phase angle (θ), i.e.,

$$S_i(t) = \sin \omega t \qquad \text{(A-1)}$$

and

$$S_0(t) = A \sin (\omega t + \theta) \qquad \text{(A-2)}$$

Now, if the system is linear, superposition holds and the relationship between $S_i(t)$ and $S_0(t)$ will not be changed by

addition of the noise $n_i(t)$ to the input of the system, i.e., the constants A and θ will remain unchanged if $S_i(t)$ remains unchanged but the noise $n_i(t)$ is added to it.

To show this mathematically, we relate the output $y(t)$ to the input $x(t)$ by the superposition integral [see Equation (7.2)],

$$y(t) = \int_{-\infty}^{\infty} x(\tau)h(t - \tau)d\tau \tag{A-3}$$

or substituting $S_i(t) + n_i(t)$ for $x(t)$

$$y(t) = \int_{-\infty}^{\infty} [S_i(\tau) + n_i(\tau)]h(t - \tau)d\tau \tag{A-4}$$

$$= \int_{-\infty}^{\infty} S_i(\tau)h(t - \tau)d\tau + \int_{-\infty}^{\infty} n_i(\tau)h(t - \tau)d\tau \tag{A-5}$$

$$= S_0(t) + n_0(t) \quad . \tag{A-6}$$

Therefore $S_0(t)$ is independent of the input noise if the system is linear.

To determine the constants A and θ, i.e., the gain and phase lag of the system at frequency ω, the crosscorrelation function between input signal and output signal-plus-noise is computed.

$$\phi_{i0}(\tau) = \int_{-\infty}^{\infty} S_i(t)y(t + \tau)dt \tag{A-7}$$

$$= \int_{-\infty}^{\infty} S_i(t)[S_0(t + \tau) + n_0(t + \tau)]dt \tag{A-8}$$

$$= \int_{-\infty}^{\infty} S_i(t) S_0(t + \tau) dt + \int_{-\infty}^{\infty} S_i(t) n_0(t + \tau) dt \qquad \text{(A-9)}$$

$$= {}^{\phi}S_i s_0(\tau) + {}^{\phi}S_i n_0(\tau) \quad . \qquad \text{(A-10)}$$

Given that the input signal and input noise are uncorrelated, it is easy to show that the input signal and output noise are also uncorrelated, i.e.,

$${}^{\phi}S_i n_0(\tau) = \int_{-\infty}^{\infty} S_i(t) n_0(t + \tau) dt = 0 \quad . \qquad \text{(A-11)}$$

To do this we use the superposition integral on (A-11)

$${}^{\phi}S_i n_0(\tau) = \int_{-\infty}^{\infty} S_i(t) dt \int_{-\infty}^{\infty} h(v) n_i(t + \tau - v) dv \quad . \qquad \text{(A-12)}$$

After interchanging the order of integration

$${}^{\phi}S_i n_0(\tau) = \int_{-\infty}^{\infty} h(v) dv \int_{-\infty}^{\infty} S_i(t) n_i(t + \tau - v) dt \; . \qquad \text{(A-13)}$$

Since

$${}^{\phi}S_i n_0 \; (\tau - v) = \int_{-\infty}^{\infty} S_i(t) n_i(t + \tau - v) dt \qquad \text{(A-14)}$$

then

$${}^{\phi}S_i n_0(\tau) = \int_{-\infty}^{\infty} h(v) {}^{\phi}S_i n_i(\tau - v) dv \qquad \text{(A-15)}$$

but, we assumed that the input signal and input noise are uncorrelated, i.e.,

$$\phi_{S_i n_i}(\tau - v) = 0 \quad ; \tag{A-16}$$

therefore, from (A-16) in (A-15)

$$\phi_{S_i n_0}(\tau) = 0 \tag{A-17}$$

and (A-9) becomes

$$\phi_{i0}(\tau) = \phi_{S_i S_0}(\tau) \quad . \tag{A-18}$$

Hence, the crosscorrelation between the input signal, $S_i(t)$, and the total output response, $S_0(t) + n_0(t)$, is just the crosscorrelation between the input signal and the output signal. As shown in Section 6.3, the computation of $\phi_{i0}(\tau)$ can be an important key to the determination of gain-phase information in certain linear and non-linear systems in the presence of noise.

APPENDIX B

Figure 4.5 shows diagrammatically how the transfer function for a system can be extracted by computing the ratio of the input-output cross power density spectrum to the input power density spectrum. This method was mentioned in the methods section of Chapter VIII and Chapter IX

To justify the process mathematically, consider the linear system in Figure B.1:

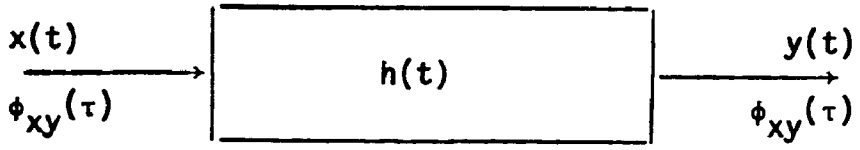

FIGURE B.1

First, we shall write the input-output crosscorrelation function $\phi_{xy}(\tau)$ for a linear system with input x(t) and output y(t) according to definition[1]

$$\phi_{xy}(\tau) = \lim_{T \to \infty} \frac{1}{2T} \int_{-T}^{T} x(t)y(t + \tau)dt \quad . \tag{B-1}$$

[1] See Y. W. Lee (36).

To bring the system unit-impulse response into the expression, we use the superposition integral to replace $y(t + \tau)$ in Equation (B-1). Accordingly,

$$\phi_{xy}(\tau) = \lim_{T \to \infty} \frac{1}{2T} \int_{-T}^{T} x(t)dt \int_{-\infty}^{\infty} h(\gamma) \times (t + \tau - \gamma)d\gamma \quad . \tag{B-2}$$

By interchanging the order of intergration, we get

$$\phi_{xy}(\tau) = \int_{-\infty}^{\infty} h(\gamma)d\gamma \lim_{T \to \infty} \frac{1}{2T} \int_{-T}^{T} x(t) \times (t + \tau - \gamma)d\gamma \quad . \tag{B-3}$$

However ,

$$\phi_{xx}(\tau - \gamma) = \lim_{T \to \infty} \frac{1}{2T} \int_{-T}^{T} x(t) \times (t + \tau - \gamma)dt \quad . \tag{B-4}$$

Therefore (B-2) becomes

$$\phi_{xy}(\tau) = \int_{-\infty}^{\infty} h(\gamma)\phi_{ii}(\tau - \gamma)d\gamma \quad . \tag{B-5}$$

This important relationship shows that the input-output cross-correlation function for a linear system is the convolution of the unit-impulse response and the input autocorrelation.

Equation (B-5) can be expressed in the frequency domain by taking the Fourier transform of both sides of (B-5)

$$\frac{1}{2\pi} \int_{-\infty}^{\infty} \phi_{xy}(\tau)\, e^{-j\omega\tau} d\tau = \frac{1}{2\pi} \int_{-\infty}^{\infty} e^{-j\omega\tau} d\tau \int_{-\infty}^{\infty} h(\gamma) \phi_{xx}(\tau - \gamma)d\gamma \quad . \tag{B-6}$$

With the change of variable, $\delta = \tau - \gamma$, Equation (B-6) becomes

$$\Phi_{xy}(\omega) = \frac{1}{2\pi} \int_{-\infty}^{\infty} e^{-j\omega(\delta - \gamma)} d\delta \int_{-\infty}^{\infty} h(\gamma)\phi_{xx}(\delta)d\gamma$$

$$= \frac{1}{2\pi} \int_{-\infty}^{\infty} h(\partial)\, e^{-j\omega\partial} d\partial \int_{-\infty}^{\infty} \phi_{xx}(\delta)\, e^{-j\omega\delta} d\delta$$

$$= H(\omega)\Phi_{xx}(\omega) \quad , \tag{B-7}$$

or,

$$H(\omega) = \Phi_{xy}(\omega)/\Phi_{xx}(\omega) \quad .$$

$\Phi_{xx}(\omega)$ and $\Phi_{xy}(\omega)$ can be computed by use of an A to D sampler and suitable FFT software; hence, $H(\omega)$ can be extracted by this technique.

APPENDIX C

In this Appendix, the relationship between open loop data and the closed loop data will be explored. The system is assumed to have the unity feedback configuration given in Figure 9.1. With reference to Figure 9.1, some of the important terminology used in the block diagrams of feedback control systems is defined as follows:

$\theta_i(S)$ = reference input signal

$\theta_0(S)$ = output signal

$E(S)$ = actuating signal or error signal

$G_\alpha(S) = \theta_0(S)/\theta_i(S)$ = closed loop transfer function

$C_\alpha(S)$ = oculomotor controller

$P(S)$ = oculomotor plant

$g_\alpha(S) = C_\alpha(S)\ P(S)$ = open loop transfer function

The closed-loop transfer function, $G_\alpha(S) = \theta_0(S)/\theta_i(S)$, can be expressed as a function of $C_\alpha(S)$ and $P(S)$. From Figure 9.1, we have

$$\theta_0(S) = E(S)C_\alpha(S)P(S) \qquad \text{(C-1)}$$

and

$$E(S) = \theta_i(S) - \theta_0(S) \quad . \tag{C-2}$$

Substituting Equation (C-2) into Equation (C-1), we have

$$\theta_0(S) = \theta_i(S)C_\alpha(S)P(S) - \theta_0(S)C_\alpha(S)P(S) \tag{C-3}$$

or

$$\theta_0(S) + \theta_0(S)C_\alpha(S)P(S) = \theta_i(S)C_\alpha(S)P(S) \tag{C-4}$$

and

$$\theta_0(S)[1 + C_\alpha(S)P(S)] = \theta_i(S)C_\alpha(S)P(S) \tag{C-5}$$

from which, the closed-loop transfer function is given by

$$G_\alpha(S) = \theta_0(S)/\theta_i(S) = \frac{C_\alpha(S)P(S)}{1 + C_\alpha(S)P(S)} \quad . \tag{C-6}$$

Likewise, the open-loop transfer function, g_α $g_\alpha(S) = C_\alpha(S)P(S)$ can be expressed as a function of $G_\alpha(S)$. Substituting $G_\alpha(S)$ for $C_\alpha(S)P(S)$ in Equation (C-6), we have

$$G_\alpha(S) = \frac{g_\alpha(S)}{1 + g_\alpha(S)} \tag{C-7}$$

or solving for $g_\alpha(S)$, we obtain

$$g_\alpha(S) = \frac{G_\alpha(S)}{1 - G_\alpha(S)} \quad . \tag{C-8}$$

For a fundamental justification of the above manipulations, one should consult textbooks on automatic feedback control system theory.[1]

In this study, linear systems analysis techniques are used to characterize changes in the oculomotor control system that result from changes in the degree of predictability present in the input tracked signal. The use of linear transfer functions to represent an adapative physiological system has many precedents in the literature.[2] Even for systems displaying obvious nonlinearities, it is customary to treat the system in terms of the nearest linear approximation.[3] Fortunately, the only salient nonlinearity of the oculomotor control system appears to be its adaptive quality.

---

[1]For example, see B. C. Kuo (1967). Automatic Control Systems (2nd ed.), Prentice-Hall, Inc.

[2]Birmingham, H. P. and Taylor, F. V. (1954). A Design Philosophy for Man-machine Control Systems. Proc. IRE. 42:1748-1758; McRuer, D. T., Graham, D. and Krendal, E.S. Manual Control of Single Loop Systems, J. Franklin Institute, 283, (January 1967), pp. 1-29; Ibid., (February 1967), pp. 145-168; McRuer, D. T., and Krendel, E. S. (1957). A Dynamic Response of Human Operators. USAF WADC tech. Rep. No. 56-524.

[3]Birmingham and Taylor (1954).

APPENDIX D

EXTRAOCULAR MUSCLE-EYEBALL DYNAMICS FOR HORIZONTAL EYE MOVEMENTS

In order to understand how the CNS controls movement of the eye in response to target movement, it is necessary to study the dynamics of the mechanical system made up of the extraocular muscles, the eyeball, and the surrounding connective tissue. It is the purpose of this Section to derive a mathematical transfer function of the oculomotor plant from net active state muscle tension to globe rotation, i.e., the torque-angle transfer function of the plant.

The mechanical scheme [from Robinson (48, 50)] describing the mechanical properties of the eyeball, restraining orbital tissues, and the extraocular muscles is given in Figure D.1 along with a table of component values. The muscles properties are represented by a series elastic component of stiffness K_e and contractile component with a force-velocity relation of mean slope R_m g.sec/deg through which active-state tension F_0 is applied. Passive orbital tissues such as Tenon's capsule, sarcolemma, suspensory ligaments, orbital fat, etc., are lumped together and represented by three visco-elastic Voigt elements with spring constants K_1, K_2 and K_3 g/deg associated

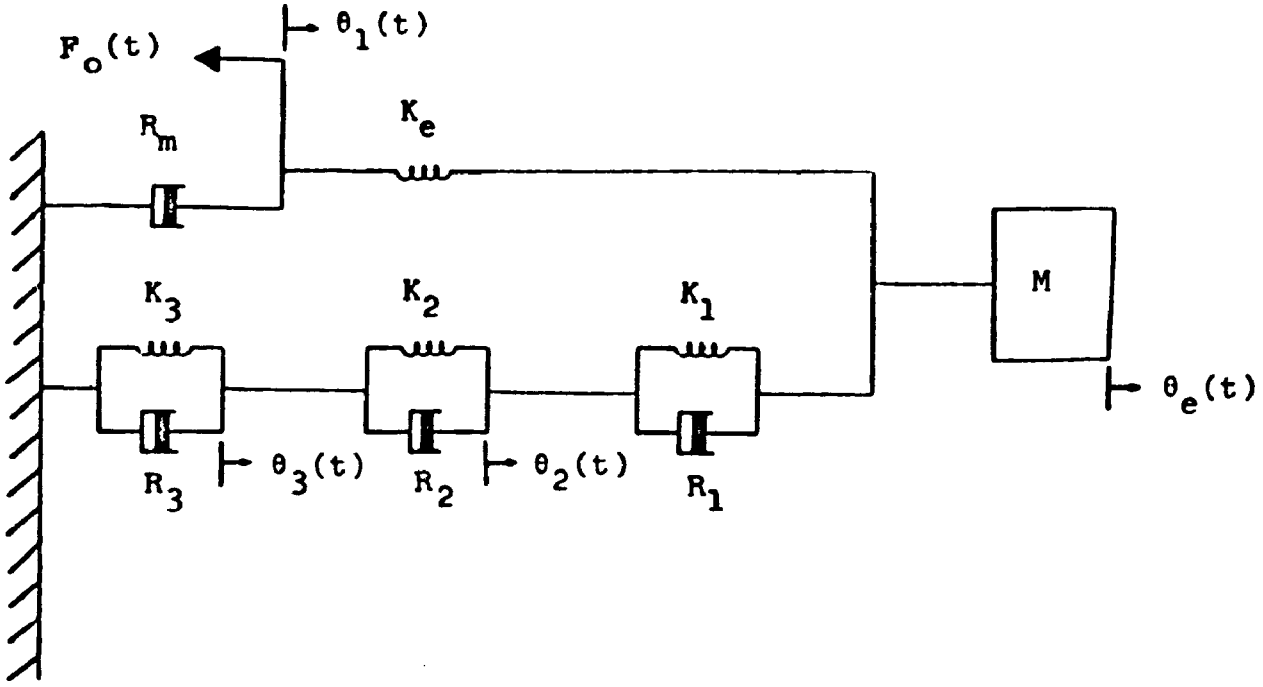

K_e = 3.2 g/deg

R_m = 0.072 g.sec/deg

K_1 = 3.00 g/deg

R_1 = 0.025 g.sec/deg

K_2 = 6.36 g/deg

R_2 = 1.81 g.sec/deg

K_3 = 2.86 g/deg

R_3 = 1.43 g.sec/deg

M = 0.677×10^{-4} g.sec^2/deg

FIGURE D.1. Mechanical Schema of the Oculomotor Plant.

with damping elements of viscosities R_1, R_2 and R_3 g. sec/deg. The moment of inertia of the globe is M g.sec^2/deg.

Exact values for the parameters of Figure D.1 were determined by iterative analog computer trials that provided the best match with experimental data (51, 50). To obtain these data, Robinson (1964) measured normal saccades, high inertia saccades, and the force produced on the globe during an attempted saccade while the globe was held isometrically. He also abducted the eye (vision in unencumbered eye only) and measured quick release responses. Later (1965) he extended his work to include pure smooth pursuit responses to Rashbass type step-ramp stimuli. He measured isometric force in one eye and the movement of the other eye. This resulting mechanical model of the plant was thus derived from data from both smooth pursuit and saccadic eye movements.

Robinson claims that the mechanical schema of Figure D.1 has the advantage of being the simplest system consistent with the known physiology of the mechanics of muscle and passive tissue that agrees quantitatively as well as qualitatively with his extensive experimental data. It is significant that the schema is consistent for both saccadic and smooth pursuit horizontal eye movements.

The following differential equations describe mathematically the properties of Robinson's mechanical schema:

$$F_0 = R_m\dot{\theta}_1 + K_e(\theta_1 - \theta_e)$$

$$0 = M\ddot{\theta}_e + R_1(\dot{\theta}_e - \dot{\theta}_2) + K_e(\theta_e - \theta_1) + K_1(\theta_e - \theta_2)$$

$$0 = R_1(\dot{\theta}_2 - \dot{\theta}_e) + R_2(\dot{\theta}_2 - \dot{\theta}_3) + K_1(\theta_2 - \theta_e) + K_2(\theta_2 - \theta_3)$$

$$0 = R_3\dot{\theta}_3 + R_2(\dot{\theta}_3 - \dot{\theta}_2) + K_2(\theta_3 - \theta_2) + K_3\theta_3 \quad . \qquad \text{(D-1)}$$

Using Laplace transform notation, the above equations become:

$$F_0(S) = (R_m S + K_e)\theta_1(S) - K_e\theta_e(S)$$

$$0 = - K_e\theta_1(S) + (MS^2 + R_1S + K_1 + K_e)\theta_e(S)$$

$$- (R_1^S + K_1)\theta_2(S)$$

$$0 = - (R_1S + K_1)\theta_e(S) + (R_1S + R_2S + K_1 + K_2)\theta_2(S)$$

$$- (R_2S + K_2)\theta_3(S)$$

$$0 = - (R_2S + K_2)\theta_2(S) + (R_3S + R_2S + K_2 + K_3)\theta_3(S) \quad . \qquad \text{(D-2)}$$

It is possible to solve for the torque-angle transfer function $\frac{\theta_e(S)}{F_0(S)}$ using Cramer's rule:

$$\frac{\theta_e(S)}{F_0(S)} = \frac{\begin{vmatrix} A_{11}(S)F_0(S)A_{13}(S)A_{14}(S) \\ A_{21}(S) \quad 0 \quad A_{23}(S)A_{24}(S) \\ A_{31}(S) \quad 0 \quad A_{33}(S)A_{34}(S) \\ A_{41}(S) \quad 0 \quad A_{43}(S)A_{44}(S) \end{vmatrix}}{\begin{vmatrix} A_{11}(S)A_{12}(S)A_{13}(S)A_{14}(S) \\ A_{21}(S)A_{22}(S)A_{23}(S)A_{24}(S) \\ A_{31}(S)A_{32}(S)A_{33}(S)A_{34}(S) \\ A_{41}(S)A_{42}(S)A_{43}(S)A_{44}(A) \end{vmatrix}} \qquad \text{(D-3)}$$

where

$$A_{11}(S) = R_m S + K_3$$

$$A_{22}(S) = MS + R_1 S + K_1 + K_e$$

$$A_{33}(S) = R_1 S + R_2 S + K_1 + K_2$$

$$A_{44}(S) = R_2 S + R_3 S + K_2 + K_3$$

$$A_{12}(S) = A_{21}(S) = -K_e$$

$$A_{23}(S) = A_{32}(S) = - R_1 S - K_1$$

$$A_{34}(S) = A_{43}(S) = - R_2 S - K_2$$

$$A_{13}(S) = A_{31}(S) = A_{14}(S) = A_{41}(S) = A_{24}(S) = A_{42}(S) = 0 \quad .$$

When $S = j\omega$, Equation (D-3) was solved for different values of ω and a normalized Bode plot of the torque-angle transfer function was drawn (Figure 3.2). The transfer function as

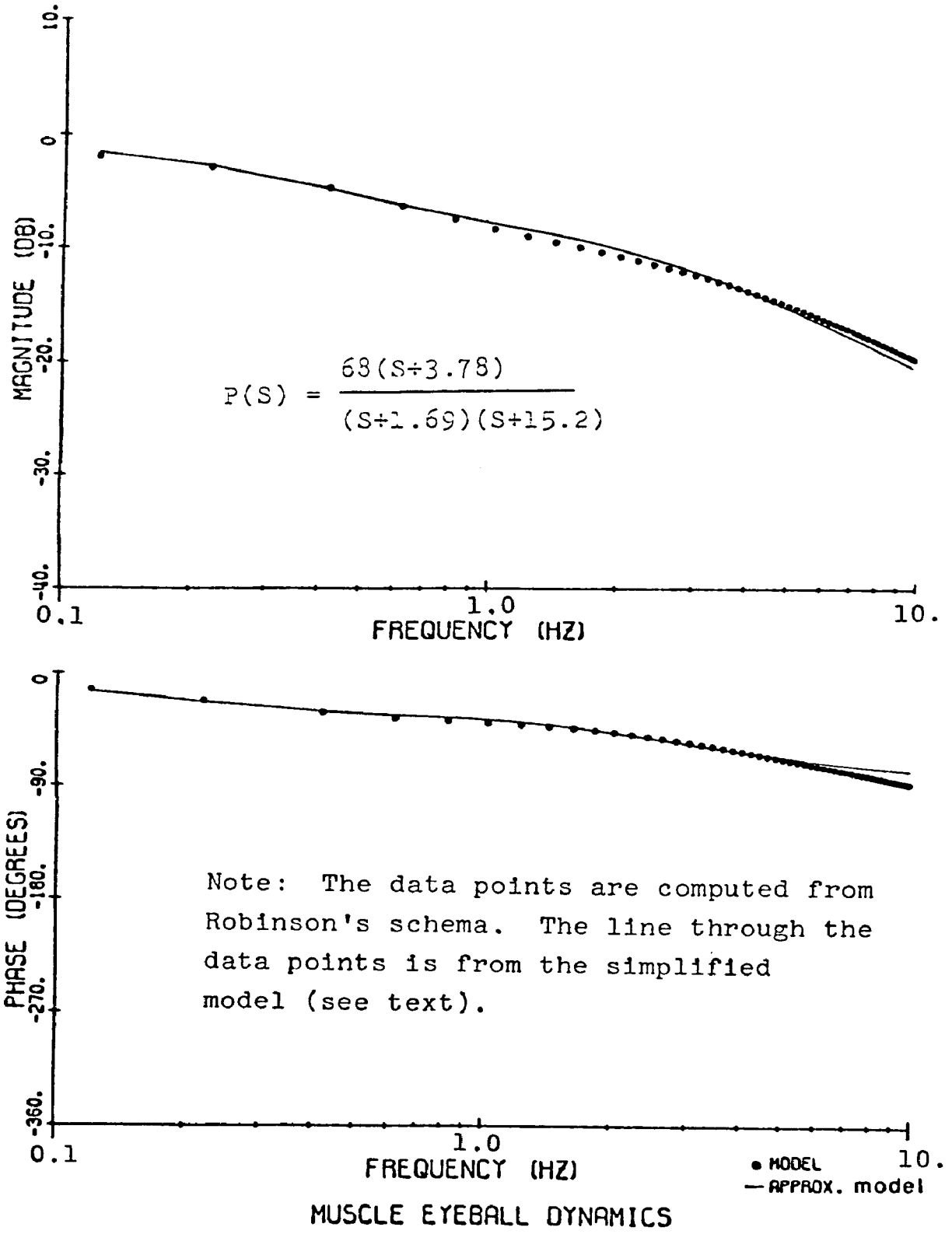

FIGURE D.2. Normalized Bode Plot of the Torque Angle Transfer Function of the Oculomotor Plant.

represented by Equation (D-3) is a fifth order system. However, over the frequency range of the experiments described in this thesis (less than 5 Hz), the system can be approximated closely by a second order system of the form:

$$\frac{\theta_e(S)}{F_0(S)} = \frac{68(S + 3.78)}{(S + 1.69)(S + 15.2)} \qquad \text{(D-4)}$$

This approximation to the data was obtained by a computer routine based on the conjugate gradient optimization technique. Figure D.2 shows how closely Equation (D-4) approximates the normalized Bode plot of the torque-angle transfer function. For the remainder of this study, Equation (D-4) will be used as the mathematical representation of the oculomotor plant.

From Figure D.2, it is obvious that the oculomotor plant is a highly damped relatively low bandwidth system. This observation is corroborated by some interesting experiments performed by Reinhart and Zuber (47). These investigators stimulated the abducens nerve with a sinusoidally modulated stimulus and measured the corresponding eye movements cause by contraction of the lateral rectus muscle. They obtained a transfer function best represented by a single pole (first order) system. It should be noted that Robinson's (50) heavily damped

mechanical schemma is also in good agreement with the mechanics of the oculomotor plant determined by Childress (7, 8). Childress evaluated the mechanical properties of the oculomotor plant by observing transient responses to forces applied to the human eye.

APPENDIX E

The following tables are a listing of the data used to draw Figures 7.4 to 7.6. They list the average phase angle at the appropriate signal frequency and S/N ratio. The standard deviation is listed below each average value. Each data point is the average of five runs.

TABLE E-1

Phase Vs. S/N Ratio : Subject W.W.

FREQUENCY (HZ)	S/N RATIO: ∞	121.6184	19.0546	4.8417	2.1184	1.4289	1.2106
0.25	-0.7633 0.8927	-4.1346 0.3417	-6.4448 1.5739	-7.5414 1.9638	-9.4020 4.6330	-9.1032 2.8797	-9.5135 7.3018
0.50	-2.6942 0.5253	-9.5460 1.8562	-18.6508 2.8797	-28.7698 5.6750	-29.2500 7.8779	-30.1160 3.4171	-32.1158 2.4613
0.75	-6.2612 1.2145	-14.1566 3.6094	-20.5420 3.9153	-32.8552 10.2587	-33.7800 4.1536	-40.8310 14.8195	-44.0676 18.1253
1.00	-10.9604 0.9190	-19.0880 1.7852	-27.7224 4.2544	-36.6038 9.9773	-38.7336 10.0933	-46.0402 10.8762	-47.9702 3.6923
1.50	-27.2342 3.8036	-28.6290 5.1482	-33.4234 6.5928	-41.7222 6.7876	-56.5724 9.2472	-58.0788 6.4652	-63.5556 10.0999

TABLE E-2

Phase Vs. S/N Ratio : Subject M.F.

FREQUENCY (HZ)	S/N RATIO						
	∞	121.6164	19.0546	4.8417	2.1184	1.4289	1.2106
0.25	-0.9805 1.1398	-3.6194 1.8465	-6.9276 2.3665	-10.1831 3.9661	-8.6346 6.9943	-6.6432 5.8842	-8.1678 7.6651
0.50	-3.3851 0.7838	-10.0438 1.2883	-18.3884 2.7192	-29.1274 2.2052	-30.4574 6.1148	-30.9978 11.4784	-25.0768 11.0326
0.75	-9.0230 0.7082	-15.0659 2.4306	-25.8836 5.3041	-35.4556 12.5501	-46.3156 11.4975	-45.7598 7.2808	-50.2980 14.5305
1.00	-12.5394 0.7334	-19.6562 1.3052	-26.4700 3.9114	-42.5026 9.6274	-54.8126 10.5451	-54.6752 8.3660	-57.1402 11.4083

TABLE E-3

Phase Vs. S/N Ratio : Subject T.Y.

FREQUENCY (HZ)	S/N RATIO						
	∞	121.6184	19.0546	4.8417	2.1184	1.4289	1.2106
0.25	0.3230 0.5690	-0.6430 1.2600	-7.8600 3.2550	-19.2380 0.6830	-25.1500 9.1910	-27.4060 8.0610	-28.0600 6.0326
0.50	-2.3880 0.4758	-9.2250 5.8400	-12.4450 2.8213	-24.7500 10.3700	-39.3500 2.7500	-38.2000 3.9500	-37.7750 8.2370
0.75	-6.7090 0.7212	-11.3350 3.0300	-16.8500 1.0800	-26.4300 1.7400	-42.6900 8.4400	-49.0600 6.4820	-52.3000 17.9600
1.00	-7.6200 0.5374	-17.5000 1.5556	-25.9600 1.8526	-33.4000 6.7880	-40.4500 2.1900	-60.5000 12.1600	-65.1000 3.6770

APPENDIX F

The following tables are a listing of the data used to draw Figures 7.7 to 7.9. They list the average normalized signal magnitude at the appropriate signal frequency and S/N ratio. The standard deviation is listed below each average value. Each data point is the average of five runs.

TABLE F-1

Magnitude Vs. S/N Ratio : Subject W.W.

FREQUENCY (HZ)	S/N RATIO ∞	121.6184	19.0546	4.8417	2.1184	1.4289	1.2106
0.25	0.0	-1.0489	-1.4572	-2.3739	-3.0270	-4.1512	-4.4363
	0.0	0.9825	1.0155	0.9763	1.2260	0.7710	0.8383
0.50	0.0	-1.0840	-1.1738	-2.3374	-3.4480	-4.2882	-7.0200
	0.0	0.6739	0.7237	1.5422	2.1483	1.5695	1.6067
0.75	0.0	-1.8066	-2.2769	-3.1715	-4.6532	-5.1819	-7.5000
	0.0	1.6343	1.2229	0.8874	0.9100	0.9485	2.6796
1.00	0.0	-1.4260	-2.1798	-3.2820	-5.6144	-6.6670	-7.9180
	0.0	0.9215	0.8864	1.2418	1.1459	1.0260	1.3420
1.50	0.0	-0.9414	-1.8900	-4.1284	-5.2772	-6.2954	-7.5020
	0.0	0.5774	0.6442	1.2790	0.6687	1.5890	1.5528

TABLE F-2

Magnitude Vs. S/N Ratio : Subject M.F.

S/N RATIO

FREQUENCY (HZ)		∞	121.6184	19.0546	4.8417	2.1184	1.4289	1.2106
0.25	0.0		-1.3088	-0.8385	-1.6900	-3.9516	-4.3760	-3.8916
	0.0		0.8951	0.9322	1.2234	2.1360	2.3390	2.8540
0.50	0.0		-0.0952	-0.9694	-1.1015	-3.8112	-3.0840	-2.4112
	0.0		1.3016	0.9007	2.8500	2.5590	2.5900	2.6700
0.75	0.0		-0.8420	-3.8240	-5.3390	-6.7892	-7.0247	-9.1120
	0.0		0.4730	0.7630	1.0710	1.2167	2.7750	1.5080
1.00	0.0		-0.8398	-3.3400	-6.0030	-9.4890	-10.8640	-11.0200
	0.0		0.1291	1.0400	1.2490	1.7650	1.5990	2.3000

TABLE F-3

Magnitude Vs. S/N Ratio : Subject T.Y.

FREQUENCY (HZ)	S/N RATIO	∞	121.6184	19.0546	4.8417	2.1184	1.4289	1.2106
0.25	0.0		-0.2783	-1.9343	-3.9244	-4.3400	-5.7750	-6.3950
	0.0		0.0602	0.0165	1.2366	0.9617	0.4455	0.9263
0.50	0.0		-0.7074	-3.0250	-6.1250	-7.2250	-11.0000	-7.6520
	0.0		0.3711	1.2230	3.7830	1.4213	3.3941	4.8831
0.75	0.0		-0.6245	-2.9800	-6.2370	-9.0737	-11.2000	-13.1500
	0.0		0.0870	1.3150	0.2234	1.4800	2.1950	4.9620
1.00	0.0		-1.2750	-5.3200	-6.9650	-8.5300	-11.9567	-13.0000
	0.0		0.9479	0.9192	1.1102	0.7721	1.6779	2.6800

APPENDIX G

The complete data for the closed loop Bode plots of Figures 9.2 to 9.6 are given in the five tables in this Appendix. These data are the results of averaging six different runs. The appropriate standard deviations are included in the tables.

TABLE G-1

CLOSED LOOP BODE PLOT DATA - SUBJECT W.W.

INPUT WAVEFORM : 0% NOISE - 100% SWEPT

NUMBER OF RUNS AVERAGED - 6

AVERAGE GAIN (db)	AVERAGE PHASE (DEG.)	FREQUENCY (HZ)	GAIN STANDARD DEVIATION (db)	PHASE STANDARD DEVIATION (DEG.)
-.44992E 00	-.17985E 01	0.15625E 00	0.11860E 01	0.13586E 01
-.46768E 00	-.27428E 01	0.31250E 00	0.10795E 01	0.13244E 01
-.55437E 00	-.36204E 01	0.46875E 00	0.94377E 00	0.10664E 01
-.73672E 00	-.49597E 01	0.62500E 00	0.78625E 00	0.10663E 01
-.10347E 01	-.68873E 01	0.78125E 00	0.64377E 00	0.10207E 01
-.14210E 01	-.91257E 01	0.93750E 00	0.59371E 00	0.95124E 00
-.18537E 01	-.11439E 02	0.10937E 01	0.68871E 00	0.10120E 01
-.23565E 01	-.14305E 02	0.12500E 01	0.83392E 00	0.11417E 01
-.29966E 01	-.18446E 02	0.14062E 01	0.92803E 00	0.14033E 01
-.38155E 01	-.23823E 02	0.15625E 01	0.98511E 00	0.17132E 01
-.48474E 01	-.29551E 02	0.17187E 01	0.10810E 01	0.21553E 01
-.62025E 01	-.35455E 02	0.18750E 01	0.11938E 01	0.29024E 01
-.79866E 01	-.42130E 02	0.20312E 01	0.12479E 01	0.40015E 01
-.10024E 02	-.47589E 02	0.21875E 01	0.13327E 01	0.53604E 01
-.11790E 02	-.50987E 02	0.23437E 01	0.15667E 01	0.57431E 01
-.13165E 02	-.54387E 02	0.25000E 01	0.16816E 01	0.61260E 01
-.14619E 02	-.57785E 02	0.26562E 01	0.18248E 01	0.65089E 01
-.16073E 02	-.61186E 02	0.28125E 01	0.20310E 01	0.68920E 01
-.17527E 02	-.64584E 02	0.29687E 01	0.22832E 01	0.72748E 01
-.18982E 02	-.67984E 02	0.31250E 01	0.25681E 01	0.76576E 01
-.20435E 02	-.71382E 02	0.32812E 01	0.28756E 01	0.80405E 01
-.21890E 02	-.74783E 02	0.34375E 01	0.31997E 01	0.84236E 01

TABLE G-2

CLOSED LOOP BODE PLOT DATA - SUBJECT W.W.

INPUT WAVEFORM : 25% NOISE - 75% SWEPT

NUMBER OF RUNS AVERAGED - 6

AVERAGE GAIN (db)	AVERAGE PHASE (DEG.)	FREQUENCY (HZ)	GAIN STANDARD DEVIATION (db)	PHASE STANDARD DEVIATION (DEG.)
-.21754E 01	-.10426E 02	0.15625E 00	0.94057E 00	0.21535E 01
-.21135E 01	-.12914E 02	0.31250E 00	0.90331E 00	0.22777E 01
-.22265E 01	-.13107E 02	0.46875E 00	0.91784E 00	0.19720E 01
-.24631E 01	-.14016E 02	0.62500E 00	0.98839E 00	0.19088E 01
-.28277E 01	-.16389E 02	0.78125E 00	0.11101E 01	0.17436E 01
-.32606E 01	-.19652E 02	0.93750E 00	0.12515E 01	0.13451E 01
-.36692E 01	-.22618E 02	0.10937E 01	0.13784E 01	0.14071E 01
-.40680E 01	-.25382E 02	0.12500E 01	0.14531E 01	0.15198E 01
-.45574E 01	-.29121E 02	0.14062E 01	0.14587E 01	0.13250E 01
-.52323E 01	-.34676E 02	0.15625E 01	0.14023E 01	0.14428E 01
-.61471E 01	-.42036E 02	0.17187E 01	0.13094E 01	0.25697E 01
-.73533E 01	-.50783E 02	0.18750E 01	0.12529E 01	0.48010E 01
-.89049E 01	-.60004E 02	0.20312E 01	0.13465E 01	0.81439E 01
-.10854E 02	-.67139E 02	0.21875E 01	0.16608E 01	0.10842E 02
-.13110E 02	-.71103E 02	0.23437E 01	0.19797E 01	0.11830E 02
-.15279E 02	-.76226E 02	0.25000E 01	0.20927E 01	0.12164E 02
-.16973E 02	-.83609E 02	0.26562E 01	0.21763E 01	0.11149E 02
-.18285E 02	-.88248E 02	0.28125E 01	0.23544E 01	0.12174E 02
-.19596E 02	-.93147E 02	0.29687E 01	0.26797E 01	0.12848E 02
-.20908E 02	-.98051E 02	0.31250E 01	0.31069E 01	0.13525E 02
-.22219E 02	-.10295E 03	0.32812E 01	0.35990E 01	0.14201E 02
-.23530E 02	-.10786E 03	0.34375E 01	0.41337E 01	0.14878E 02

TABLE G-3

CLOSED LOOP BODE PLOT DATA - SUBJECT W.W.

INPUT WAVEFORM : 50% NOISE - 50% SWEPT

NUMBER OF RUNS AVERAGED - 6

AVERAGE GAIN (db)	AVERAGE PHASE (DEG.)	FREQUENCY (HZ)	GAIN STANDARD DEVIATION (db)	PHASE STANDARD DEVIATION (DEG.)
-.47511E 01	-.16900E 02	0.15625E 00	0.15024E 01	0.34320E 01
-.45120E 01	-.21886E 02	0.31250E 00	0.15065E 01	0.34339E 01
-.46156E 01	-.24066E 02	0.46875E 00	0.14215E 01	0.26226E 01
-.49084E 01	-.27907E 02	0.62500E 00	0.13393E 01	0.23252E 01
-.53467E 01	-.34735E 02	0.78125E 00	0.13144E 01	0.27162E 01
-.57936E 01	-.43412E 02	0.93750E 00	0.13908E 01	0.29768E 01
-.61311E 01	-.51142E 02	0.10937E 01	0.14935E 01	0.36127E 01
-.64018E 01	-.57473E 02	0.12500E 01	0.15481E 01	0.54262E 01
-.67171E 01	-.64137E 02	0.14062E 01	0.15622E 01	0.64697E 01
-.71428E 01	-.72832E 02	0.15625E 01	0.15716E 01	0.62716E 01
-.75846E 01	-.84279E 02	0.17187E 01	0.16259E 01	0.56617E 01
-.78578E 01	-.97266E 02	0.18750E 01	0.16766E 01	0.52865E 01
-.81186E 01	-.10873E 03	0.20312E 01	0.16639E 01	0.48277E 01
-.88501E 01	-.11715E 03	0.21875E 01	0.16422E 01	0.44335E 01
-.10018E 02	-.12420E 03	0.23437E 01	0.16432E 01	0.51533E 01
-.10940E 02	-.13217E 03	0.25000E 01	0.16105E 01	0.66092E 01
-.11221E 02	-.14006E 03	0.26562E 01	0.14790E 01	0.70744E 01
-.11603E 02	-.14541E 03	0.28125E 01	0.15415E 01	0.75096E 01
-.13208E 02	-.14908E 03	0.29687E 01	0.17299E 01	0.11490E 02
-.15413E 02	-.15474E 03	0.31250E 01	0.19669E 01	0.17961E 02
-.16655E 02	-.16272E 03	0.32812E 01	0.18629E 01	0.18332E 02
-.18261E 02	-.17314E 03	0.34375E 01	0.26405E 01	0.15761E 02

TABLE G-4

CLOSED LOOP BODE PLOT DATA - SUBJECT W.W.

INPUT WAVEFORM : 75% NOISE - 25% SWEPT

NUMBER OF RUNS AVERAGED - 6

AVERAGE GAIN (db)	AVERAGE PHASE (DEG.)	FREQUENCY (HZ)	GAIN STANDARD DEVIATION (db)	PHASE STANDARD DEVIATION (DEG.)
-.64855E 01	-.21519E 02	0.15625E 00	0.17963E 01	0.28324E 01
-.61167E 01	-.28503E 02	0.31250E 00	0.17884E 01	0.25781E 01
-.61646E 01	-.32688E 02	0.46875E 00	0.17336E 01	0.17450E 01
-.63394E 01	-.39320E 02	0.62500E 00	0.16820E 01	0.16158E 01
-.65401E 01	-.49133E 02	0.78125E 00	0.16903E 01	0.17811E 01
-.67375E 01	-.59755E 02	0.93750E 00	0.17696E 01	0.22633E 01
-.69535E 01	-.68512E 02	0.10937E 01	0.18202E 01	0.32314E 01
-.71213E 01	-.75928E 02	0.12500E 01	0.17904E 01	0.35997E 01
-.71729E 01	-.83564E 02	0.14062E 01	0.16950E 01	0.34134E 01
-.72198E 01	-.91481E 02	0.15625E 01	0.16333E 01	0.35757E 01
-.74108E 01	-.99168E 02	0.17187E 01	0.17159E 01	0.47461E 01
-.76457E 01	-.10687E 03	0.18750E 01	0.18861E 01	0.59435E 01
-.78011E 01	-.11481E 03	0.20312E 01	0.19914E 01	0.60805E 01
-.81849E 01	-.12250E 03	0.21875E 01	0.19766E 01	0.58888E 01
-.91378E 01	-.13041E 03	0.23437E 01	0.19792E 01	0.56847E 01
-.10291E 02	-.14022E 03	0.25000E 01	0.21616E 01	0.42979E 01
-.10905E 02	-.15086E 03	0.26562E 01	0.24242E 01	0.37508E 01
-.11263E 02	-.15788E 03	0.28125E 01	0.25431E 01	0.58277E 01
-.12420E 02	-.16263E 03	0.29687E 01	0.26685E 01	0.96776E 01
-.13981E 02	-.16803E 03	0.31250E 01	0.27357E 01	0.14229E 02
-.15021E 02	-.17671E 03	0.32812E 01	0.28523E 01	0.15957E 02
-.16220E 02	-.18604E 03	0.34375E 01	0.29506E 01	0.15669E 02

TABLE G-5

CLOSED LOOP BODE PLOT DATA - SUBJECT W.W.

INPUT WAVEFORM : 100% NOISE - 0% SWEPT

NUMBER OF RUNS AVERAGED - 6

AVERAGE GAIN (db)	AVERAGE PHASE (DEG.)	FREQUENCY (HZ)	GAIN STANDARD DEVIATION (db)	PHASE STANDARD DEVIATION (DEG.)
-.78355E 01	-.21313E 02	0.15625E 00	0.19624E 01	0.30837E 01
-.74285E 01	-.28618E 02	0.31250E 00	0.18311E 01	0.37548E 01
-.74145E 01	-.33070E 02	0.46875E 00	0.17794E 01	0.44755E 01
-.75224E 01	-.39617E 02	0.62500E 00	0.17555E 01	0.52620E 01
-.76728E 01	-.48724E 02	0.78125E 00	0.18103E 01	0.53967E 01
-.78550E 01	-.58378E 02	0.93750E 00	0.19419E 01	0.47275E 01
-.80192E 01	-.67108E 02	0.10937E 01	0.19890E 01	0.44948E 01
-.80224E 01	-.75853E 02	0.12500E 01	0.19200E 01	0.48934E 01
-.78528E 01	-.85304E 02	0.14062E 01	0.18535E 01	0.49565E 01
-.77877E 01	-.94015E 02	0.15625E 01	0.18363E 01	0.51874E 01
-.80993E 01	-.10063E 03	0.17187E 01	0.18745E 01	0.58948E 01
-.85730E 01	-.10617E 03	0.18750E 01	0.18874E 01	0.68625E 01
-.88672E 01	-.11245E 03	0.20312E 01	0.17157E 01	0.74404E 01
-.91927E 01	-.11999E 03	0.21875E 01	0.13688E 01	0.68691E 01
-.99624E 01	-.12867E 03	0.23437E 01	0.12402E 01	0.61588E 01
-.10881E 02	-.13870E 03	0.25000E 01	0.16989E 01	0.63799E 01
-.11400E 02	-.14902E 03	0.26562E 01	0.22980E 01	0.61573E 01
-.11966E 02	-.15726E 03	0.28125E 01	0.24596E 01	0.85250E 01
-.13711E 02	-.16266E 03	0.29687E 01	0.25195E 01	0.13001E 02
-.16020E 02	-.16979E 03	0.31250E 01	0.25660E 01	0.16119E 02
-.17878E 02	-.18116E 03	0.32812E 01	0.31701E 01	0.10107E 02
-.19123E 02	-.18979E 03	0.34375E 01	0.39079E 01	0.10589E 02

APPENDIX H

PROFILE ON SUBJECTS

The subjects used in the experiments described in this dissertation ranged in age from 21-35 years. Subjects M. C. and M. F. were female subjects. Subjects T. Y., M. E., and W. W. were male. All subjects were unpaid volunteers recruited from personnel of the Bioelectrical Sciences Laboratory of The University of Michigan. All subjects except T. Y. had normal vision (20/20 visual acuity in both eyes). Subject T.Y. wore contact lenses during the experiments. T.Y.'s corrected visual acuity was 20/20 in both eyes.

Additional Details of the Experimental Methodology

The following procedure was followed for all subjects in all the experiments. Upon entering the darkened eye tracking booth, the subject was asked to sit in the chair while the bite bar was adjusted until judged comfortable by the subject. The subject was asked to fixate the eyes on a stationary spot in the center of the screen. The eye movement monitor was then placed on the subject's head and an initial adjustment was made on the light-slit projectors and photodiodes (see Figure 4.1). The subject was then instructed to "follow the spot as closely as possible." The spot was then moved by a 0.2 Hz triangular waveform (±5° peak to peak amplitude). The subject's response to this waveform was observed on a strip chart

recorder. Minor adjustments on the eye movement monitor were then made to obtain a linear response trace on the strip chart recorder. The infrared filters were then placed over the light-slit projectors.

To calibrate the eye monitor amplifier gain, the subject was asked to fixate carefully on a ±5° calibration square wave. The square wave was of low frequency (0.2 Hz) giving the subject time to obtain good fixation. Calibration procedures are discussed in Chapter IV.

After the above calibration procedure, the subject was instructed not to move the eye monitor frame or to release the grip on the bite bar. The subject was then given a rest period while the investigator arranged the equipment for presentation of the first stimulus waveform of the experiment. This period was approximately three minutes.

Additional details of the experimental methodology are given in the following paragraphs. Each experiment is discussed individually.

Experiment 1

Subjects: M. C. and W. W.

Methodology: Each subject was asked to track ten sinusoids, each one minute in duration. The sinusoids ranged in frequency from 0.2 Hz to 2.5 Hz. The order of presentation of the sinusoids (by frequency) was random. The rest period between each input waveform was determined by the subject but was a minimum of two mintues. An experimental run (presentation of all ten sinusoids) was never repeated on the same day. The data consist of an average of five separate runs taken on five different days.

Experiment 2a

Subject: M.C.

Methodology: The subject was asked to track two different random noise sequences. Each sequence had a duration of two minutes. One sequence had an RMS amplitude of 3.5° while the other had an amplitude of 1.75°. The only difference between the sequences was the amplitude. The order of presentation of the sequences was random. The rest period between each input waveform was determined by the subject but was a minimum of two minutes. An experimental run (presentation of the two sequences) was never repeated on the same day. The data consist of an average of five separate runs taken on five different days.

Experiment 2b

Subjects: M. F., W. W. and T.Y.

Methodology: One experimental run consists of having the subject track seven waveforms, each 90 sec. in duration. The amplitude of the sinusoidal part of each input waveform remains unchanged. Only the amplitude of the "noise" component of the waveform changes. A complete experiment consists of five runs, each with a different frequency of the sinusoidal signal.

Each experimental run occurred on separate days. The S/N ratio of each 90 sec. waveform on a given run was presented randomly. The rest period between waveforms was

determined by the subject but was a minimum of two minutes. A complete experiment was repeated five times to obtain data for averaging.

Experiment 3 and Experiment 4

Subjects: M. C., M. E. and W. W.

Methodology: The data for Experiments 3 and 4 were taken during the same experimental trials. The subjects were asked to track a set of five different waveforms. Each member of the set had a different ratio of random noise amplitude to swept sinusoid amplitude. The duration of each waveform was two minutes. The rest period between waveforms was determined by the subject but was a minimum of two minutes. The order of presentation of the waveforms was random. The subjects were never asked to track the five waveform set more than once on a given day.

BIBLIOGRAPHY

1. Adler, F. H. (1969). Physiology of the Eye. (4th ed.), St. Louis, Missouri: The C. V. Mosby Co.

2. Alpern, M. (1962), "Movement of the Eyes," in The Eye, Hugh Davson, ed., Vol. 3, New York: Academic Press, Inc.

3. Becker, E. and Fuchs, A. F. (1961). Further properties of the human saccadic system: Eye movements and correction saccades with and without visual fixation point, Vision Res. 9:1247-1258.

4. Bender, M. B. (1964). The Oculomotor System. New York: Harper and Row Co.

5. Brown, K. T. (1958). The electroretinogram: Its components and their origin. Vision Res. 8:633-677.

6. Byford, G. H. (1964). Anomalies of the human corneo-retinal potential. DDC Report #FRPC/1223.

7. Childress, D. S. (1967). A study of the mechanics of horizontal movements of the human eye. Ph.D. Thesis, Northwestern University.

8. Childress, D. S. and Jones, R. W. (1967). Mechanics of horizontal movement of the eye. J. Physiol. 188:273-284.

9. Christman, E. H. and Kupfer. C. (1963). Proprioception in extraocular muscles, Arch. Ophth. 69:824.

10. Cooper, S. and Daniel, P. (1949). Muscle spindles in human extrinsic eye muscles, Brain 72:1.

11. Cornsweet, T. N. (1956). Determination of the stimuli for involuntary eye movements. J.O.S.A. 46:987.

12. Cornsweet, T. N. (1958). New technique for the measurement of small eye movements. J.O.S.A. 48:808-811.

13. Delabarre, E. B. (1968). A method of recording eye movements. Am. J. Psychol. 9:572-574.

14. Dallos, P. J. (1962). A small signal analysis of the human eye fixation mechanism. Ph.D. Dissertation, Northwestern University.

15. Dallos, P. J. and Jones, R. W. (1963). Learning behavior of the eye fixation control system. IEEE Trans. Automatic control AC-8:218-227.

16. Daniel, P. (1946). Spiral nerve endings in the extrinsic eye muscles of man, J. Anat. 80:189.

17. Davson, H. (1963). The Physiology of the Eye (2nd. ed.), Boston: Little Brown and Co.

18. Deckert, G. H. (1963). Pursuit eye movements in the absence of moving visual stimulus. Science 143:1192-1193.

19. Ditchburn, R. W., Fender, D. H., and Mayne, S. (1959). Vision with controlled movements of the retinal image, J. Physiol. 145:98.

20. Ditchburn, R., and Foley-Fisher, J. (1967). Assembled data in eye movements. Optica Acta 14:113-118.

21. Ditchburn, R. W. and Ginsborg, B. L. (1953). Involuntary eye movements during fixation. J. Physiol. 119:1-17.

22. Dodge, R. (1903). Five types of eye movements in the horizontal meridian plane of the field of regard, Amer. J. Physiol. 8:307-329.

23. Dodge, R. and Cline, T. S. (1901). The angle velocity of eye movements. Psychol. Rev. 8:145-157.

24. Feinstein, R. (1970). Interactions of the horizontal and vertical eye movement systems. Ph.D. thesis, The University of Michigan.

25. Fender, D. H. and Nye, P. W. (1961). An investigation of the mechanisms of eye Movement control. Kybernetik 1:81-88.

26. Hubel, D. H. (1963). Integrative processes in central visual pathways of the cat. J.O.S.A. 53:58-65.

27. Hubel, D. H. (1963). Single unit activity in lateral geniculate body and optic tract of unrestrained cats. J. Physiol. 150:91-104.

28. Hubel, D. H., and Wiesel, T. N. (1959). Receptive fields of single neurones in the cat's striate cortex. J. Physiol. 148:574-591.

29. Hubel, D. H., and Wiesel, T. N. (1961). Receptive fields, binocular interaction and functional architecture of the cat's visual center. J. Physiol. 160:106-154.

30. Hubel, D. H., and Wiesel, T. N. (1963). Shape and arrangement of columns in cat's striate cortex. J. Physiol. 165:559-568.

31. Hubel, D. H., and Wiesel, T. N. (1965). Receptive fields and functional architecture in two nonstriate visual areas (18 and 19) of the cat. J. Neurophysiol. 28:229-289.

32. Huey, E. B. (1899). On the psychology and physiology of reading. Am. J. Psychol. 11:283-302.

33. Kris, E. C. (1958). A technique for electrically recording eye position. WADC Technical Report #58-660, RLE, Mass. Institute of Technology.

34. Kronfeld, P. C. (1962). "The Gross Anatomy and Embryology of the Eye," in The Eye, Hugh Davson, ed., Vol. 1, New York: Academic Press, Inc.

35. Latour, P. L. (1962). Visual threshold during movements, Vision Res. 2:261.

36. Lee, Y. W. (1960). Statistical Theory of Communication. New York: John Wylie and Sons, Inc.

37. Lehmann, D., Beeler, G. W., and Fender, D. H. (1965). Changes in patterns of the human electroencephalogram during fluctuations of perception of stabilized images, Electroenceph. Clin. Neurophsyiol. 18:527.

38. Marriott, F. H. C. (1962). "Colour Vision: Theories," in The Eye, Hugh Davson, ed., Vol. 2, New York: Academic Press. Inc.

39. McMullen, C. W. (1968). Communication Theory Principles. New York: MacMillan Co.

40. Noback, C. R. (1967). The Human Nervous System. New York: McGraw-Hill.

41. Pirenne, M. (1945). Vision and the Eye. London: The Pilot Press.

42. Polyak, S. (1941). The Retina. Chicago: University of Chicago Press.

43. Puckett, J., and Steinman, R. M. (1969). Tracking eye movements with and without saccadic correction. Vision Res. 9:695-703.

44. Rashbass, C. (1961). The relationship between saccadic and smooth tracking eye movements. J. Physiol. 159:326-338.

45. Rashbass, C., and Westheimer, G. (1961). Disjunctive eye movements. J. Physiol. 159:339-360.

46. Ratliff, F., and Riggs, L. A. (1950). Involuntary motions of the eye during monocular fixation. J. Exp. Psych. 40:687-698.

47. Reinhart, R. J., and Zuber, B. L. (1970). Horizontal eye movements from abducens nerve stimulation in the cat. IEEE Trans. on Bio-Medical Engineering. BME-17, #1:11-14.

48. Robinson, D. A. (1964). The mechanics of human saccadic eye movement. J. Physiol. 174:245-264.

49. Robinson, D. A. (1968). The oculomotor control systems: A review. Proc. IEEE. 56:1032-1049.

50. Robinson, D. A. (1965). The mechanics of human smooth pursuit eye movements. J. Physiol. 180:569-591.

51. Smith, W. M., and Warter, P. J. (1960). Eye movement and stimulus movement; new photoelectric electro-mechanical system for recording and measuring motions of the eye. J.O.S.A. 50:245-250.

52. Stark, L., Vossius, G., and Young, L. R. (1962). Predictive control of eye tracking movements, I.R.E. Trans. Human Factors Engineering. HFE-3:52-57.

53. St-Cyr, G. J., and Fender, D. H. (1969). Nonlinearities of the human oculomotor system: Gain. Vision Res. 9:1235-1246.

54. St-Cyr, G. J., and Fender, D. H. (1969). The interplay of drifts and flicks in binocular fixation. Vision Res. 9:245-265.

55. St-Cyr, G. J., and Fender, D. H. (1969). Nonlinearities of the human oculomotor control system: Time delays. Vision Res. 9:1491-1503.

56. Sugie, N. (1971). A model of predictive control in visual target tracking. IEEE Trans. on Systems, Man, and Cybernetics. SMC-1:2-7.

57. Volkman, F. C. (1962). Vision during voluntary saccadic eye movements. J. Opt. Soc. Amer. 52:571-578.

58. Von Noorden, G. K., and Preziosi, T. (1966). Eye movement disturbances in neurological disorders. A.M.A. Arch Ophthal. 52:710-717.

59. Watanabe, A. (1966). Control mechanism of eye movement. NHK Gijutsy Kenkyu, vol. 18:94-116.

60. Westheimer, G. (1956). Mechanism of saccadic eye movements. A.M.A. Arch. Ophth. 52:710-724.

61. Wheeless, L. (1965). The effects of intensity on the eye movement control system. Ph.D. dissertation. University of Rochester, New York.

62. Wheeless, L. L., Boynton, R. M., and Cohen, G. H. (1965). Eye movements responses to step and pulse-step stimuli, J.O.S.A. 56, 7:956-960.

63. Wolf, E. (1968). Anatomy of the Eye and Orbit. (6th ed.) Philadelphia and London: W. B. Saunders Co.

64. Wolter, J. (1965). Morphology of the sensory nerve apparatus in striated muscle of the human eye. Arch. Ophth. 55:201-221.

65. Yarbus, A. L. (1968). Eye Movements and Vision. New York: Plenum Press.

66. Young L. R. (1962). A sampled data model for eye tracking movements. Ph.D. dissertation, Massachusetts Institute of Technology.

67. Young L. R., Forster, J. D., and Van Houtte, N. (1968). A revised stochastic sampled data model for eye tracking movements. Fourth Annual NASA-University Conference on Manual Control.

68. Young, L. R., and Stark, L. A discrete model for eye tracking movements. IEEE Trans. on Military Electronics. MIL-7:113-115.

69. Young, L. R., and Stark, L. Variable feedback experiments testing a sampled data model for eye tracking movements. IEEE Trans. on Human Factors in Electronics. HRE-4:38-51.

70. Zuber, B. L., Michael, J. A., and Stark, L. (1964). Visual suppression during voluntary saccadic eye movements. Quarterly Prog. Report 73, Massachusetts Institute of Technology.